PRODUCTION AND CHARACTERIZATION OF ALUMINA FIBER
REINFORCED SQUEEZE CAST ALUMINUM ALLOY MATRIX
COMPOSITES

A THESIS SUBMITTED TO
THE GRADUATE SCHOOL OF NATURAL AND APPLIED SCIENCES
OF
MIDDLE EAST TECHNICAL UNIVERSITY

BY

ÖZGÜR KELEŞ

IN PARTIAL FULFILLMENT OF THE REQUIREMENTS
FOR
THE DEGREE OF MASTER OF SCIENCE
IN
METALLURGICAL AND MATERIALS ENGINEERING

JULY 2008

Approval of the thesis:

PRODUCTION AND CHARACTERIZATION OF ALUMINA FIBER REINFORCED SQUEEZE CAST ALUMINUM ALLOY MATRIX COMPOSITES

Submitted by **ÖZGÜR KELEŞ** in partial fulfillment of the requirements for the degree of **Master of Science in Metallurgical and Materials Engineering Department, Middle East Technical University** by,

Prof. Dr. Canan Özgen   _____
Dean, Graduate School of **Natural and Applied Sciences**

Prof. Dr. Tayfur Öztürk   _____
Head of Department, **Metallurgical and Materials Engineering**

Prof. Dr. Ali Kalkanlı   _____
Supervisor, **Metallurgical and Materials Engineering Dept., METU**

Examining Committee Members:

Prof. Dr. Ekrem Selçuk   _____
Metallurgical and Materials Engineering Dept., METU

Prof. Dr. Kemal İder   _____
Mechanical Engineering Dept., METU

Prof. Dr. Ali Kalkanlı   _____
Metallurgical and Materials Engineering Dept., METU

Prof. Dr. Hakan Gür   _____
Metallurgical and Materials Engineering Dept., METU

Prof. Dr. Cevdet Kaynak   _____
Metallurgical and Materials Engineering Dept., METU

                                             Date: 30.07.2008

I hereby declare that all information in this document has been obtained and presented accordance with the academic rules and ethical conduct. I also declare that, as required by these rules and conduct, I have fully cited and referenced all material and results that are not original to this work.

Name, Last name : Özgür Keleş

Signature   :

ABSTRACT

PRODUCTION AND CHARACTERIZATION OF ALUMINA FIBER REINFORCED SQUEEZE CAST ALUMINUM ALLOY MATRIX COMPOSITES

Keleş, Özgür

M.S., Department of Metallurgical and Materials Engineering

Supervisor: Prof. Dr. Ali Kalkanlı

July 2008, 113 pages

The aim of the present study was to investigate the effects of different levels of Saffil alumina fiber addition, magnesium content in aluminum alloy matrix and casting temperature on the mechanical behavior, microstructure and physical properties of short fiber reinforced aluminum matrix composites. The main alloying element silicon was kept constant at 10 wt%. Magnesium contents were selected as 0.3 wt% and 1 wt%. Saffil alumina fiber preforms varied from 10 to 30 vol%. The casting temperatures were fixed at 750 °C and 800 °C.

Micro porosity was present at the fiber-fiber interactions. Closed porosity of the composites increased when fiber vol% increased, however, variation in casting temperature and magnesium content in matrix did not have influence on porosity. Hardness of the composites was enhanced with increasing fiber vol%, magnesium content in matrix and decreasing casting temperature. Alignment of fibers within the composite had an influence on hardness; when fibers were aligned perpendicular to the surface, composites exhibited higher hardness. The highest hardness values obtained from surfaces parallel and vertical to fiber orientation were 155.6 Brinell hardness and 180.2 Brinell hardness for AlSi10Mg1 matrix 30

vol% alumina fiber reinforced composite cast at 800 °C and at 750 °C, respectively. 30 vol% Saffil alumina fiber reinforced AlSi10Mg0.3 matrix composite cast at 750 °C showed the highest flexural strength which is 548 MPa. Critical fiber content was found as 20 vol% for all composites.

Keywords: Metal Matrix Composites, Saffil Fiber, Alumina Fiber, Pressure Die Casting

ÖZ

ALÜMİNA FİBER TAKVİYELİ ALÜMİNYUM ALAŞIM MATRİS KOMPOZİTLERİNİN SIKIŞTIRMA DÖKÜM İLE ÜRETİMİ VE KARAKTERİZASYONU

Keleş, Özgür

Yüksek Lisans, Metalurji ve Malzeme Mühendisliği Bölümü

Tez Yöneticisi: Prof. Dr. Ali Kalkanlı

Temmuz 2008, 113 sayfa

Bu çalışmanın amacı farklı miktarlardaki Saffil alümina fiber katkısı, alüminyum alaşım matrisindeki magnezyum içeriği ve döküm sıcaklığının kısa fiber takviyeli alüminyum matris kompozitlerin mekanik davranış, iç yapı ve fiziksel özelliklerine etkisini incelemektir. Ana alaşım elementi silikon ağırlıkça % 10'da sabit tutulmuştur. Magnezyum içeriği ağırlıkça % 0.3 ve % 1 olarak seçilmiştir. Saffil alümina fiber preformları hacimce % 10'dan 30'a değişmiştir. Döküm sıcaklığı 750 °C ve 800 °C'de sabitlenmiştir.

Fiber-fiber kesişmelerinde mikro boşluklar bulunmaktadır. Kompozitlerin kapalı boşlukları fiber hacim yüzdesi arttığında artmıştır, fakat, döküm sıcaklığı ve matristeki magnezyum içeriğinin boşluğa etkisi olmamıştır. Kompozitlerin sertliği artan fiber hacim yüzdesi, matristeki magnezyum içeriği ve azalan döküm sıcaklığı ile iyileşmiştir. Kompozit içindeki fiber hizalanmasının sertliğe etkisi olmuştur; fiberler yüzeye dik olarak hizalandığı zaman, kompozitler daha yüksek sertlik göstermiştir. Fiber yönlenmesine paralel ve dik yüzeylerden elde edilen en yüksek sertlik değerleri 800 °C ve 750 °C'de dökülmüş AlSi10Mg1 matris hacimce % 30 alümina fiber takviyeli kompozitler için sırasıyla 155.6 Brinell sertlik ve 180.2 Brinell sertliktir. Hacimce % 30 Saffil alümina takviyeli 750 °C'de dökülmüş

AlSi10Mg0.3 matris kompozit 548 MPa olan en yüksek bükme dayancını göstermiştir. Bütün kompozitler için kritik fiber içeriği hacimce % 20 olarak bulunmuştur.

Anahtar Kelimeler: Metal Matris Kompozit, Saffil Fiber, Alümina Fiber, Basınçlı Döküm.

To my mother and father,

ACKNOWLEDGEMENTS

TABLE OF CONTENTS

LIST OF TABLES

xiii

LIST OF FIGURES

xvi

CHAPTER 1

INTRODUCTION

Composite materials are obtained by artificial combination of two or more phases where the resulting properties cannot be attained by the components individually [1, 2]. Generally composites are composed of a reinforcing material and a matrix material. The reinforcing phase is embedded and dispersed in the matrix to increase strength, stiffness, fatigue, creep and other material properties [3, 4]. Composites can be divided into three main groups according to their matrixes:

1. Polymer matrix composites: These materials consist of a polymer based resin as the matrix material and glass, carbon, aramid, boron, etc. as reinforcing material. Polymer matrix composites are relatively easy to fabricate due to low temperatures required during manufacturing [2].

2. Metal matrix composites: In these materials aluminum, magnesium, titanium, copper, etc. alloys are generally used as the continuous matrix and carbon, boron, ceramic oxides and carbides in the form of fiber, particulate or whisker are used as the reinforcement [1].

3. Ceramic matrix composites: These composites gained attention due to their good oxidation resistance and used at high temperature applications like aerospace and engine components. Fibers and whiskers are mainly used to increase toughness and strength of these composites [2].

Composites can be used for structural, electronic, thermal, biomedical, etc. applications because of their higher elastic modulus, tensile strength, high temperature stability, fatigue, wear resistance, electrical conductivity and lower

thermal expansion compared to unreinforced materials [2, 5]. The increase in stiffness, yield strength, tensile strength and/or decrease in density of material accounts for reduction in structural weight. Accordingly, the combination of low density, high stiffness and strength led the aerospace and automotive industry to research and develop for new composite materials [6- 9].

Metal matrix composites are used in these industries if there is a reasonable cost-performance relationship in the part production or a specific material property is only achieved by the composite part. Light materials like aluminum and magnesium alloys are generally used as matrix material due to their low density, good castability and high mechanical properties. The improvement of yield strength and tensile strength at room and elevated temperature while maintaining toughness, increase in creep resistance, fatigue strength, corrosion resistance, elastic modulus at high temperatures and decrease in thermal expansion are the main aims in metal matrix composite production [1, 2, 4].

Metal matrix composite reinforcements can be separated into five main categories:

1. Particulates
2. Whiskers
3. Discontinuous fibers
4. Continuous fibers
5. Wires

Wires which can be regarded as metal fibers aren't used in structural applications due to their high density but used as contacts, conductors and superconductors. The first four categories are generally nonmetal inorganic materials like carbon, boron, metal oxides, borides, nitrides and carbides. The use of particulate reinforcements results in slight enhancement in physical properties but the composite cost is low and show isotropic properties. Continuous fiber reinforced composites have high strength and elastic modulus but the properties are anisotropic and the cost is high due to expensive fibers. The short fiber or whisker reinforced composites show properties between continuous fiber and particulate reinforced ones. The production

costs can be lowered due to cheaper short fibers and isotropic profile can be changed. Some properties of particulate, whisker, short and continuous fiber reinforcements are seen in Tables 1.1, 1.2 and 1.3 [4, 7].

Table 1.1 Various properties for continuous fiber reinforcements of metals [4].

Fiber Name	Manufacturer	Chemical comp.	Fiber Diameter (μm)	Density (g cm^{-3})	Young's Modulus (GPa)	Tensile Strength (MPa)
Saffil	Saffil	96 Al_2O_3 4 SiO_2	3.0	3.3-3.5	300-330	2000
Nextel 440	3M	70 Al_2O_3 28 SiO_2 2 B_2O_3	10-12	3.05	190	2000
Nextel 610	3M	> 99 Al_2O_3	12	3.9	373	3100
Almax	Mitsumi Mining	99.5 Al_2O_3	10	3.6	330	1800
Saphikon	Saphikon	100 Al_2O_3	125	3.98	460	3500
Sumica	Saphikon	85 Al_2O_3 15 SiO_2	9	3.2	250	7000
Altex	Sumitomo	85 Al_2O_3 15 SiO_2	15	3.3	210	2000

Table 1.2 Various properties of short fiber and whisker reinforcements [4].

Fiber Name	Manufacturer	Chemical comp.	Fiber Diameter (μm)	Density (g cm^{-3})	Young's Modulus (GPa)	Tensile Strength (MPa)
Saffil RF	Saffil	δ-Al_2O_3	1-5	3.3	300	2000
Nextel 312	3M	62 Al_2O_3 24 SiO_2 14 B_2O_3	10-12	2.7	150	17
SCW #1	Tateho Silicon	β-$SiC_{(w)}$	0.5-1.5	3.18	481	2600
Fiberfrax HP	Unifrax	50 Al_2O_3 50 SiO_2	1.5-2.5	2.73	105	1000
Kaowool	Thermal Cer.	50 Al_2O_3 50 SiO_2	2.5	2.6	80-120	1200
Tismo	Otsuka Chem.	$K_2O \times$ $6TiO_{2\,(w)}$	0.2-0.5	3.2	280	7000

Table 1.3 Various properties for particle reinforcements [4].

Types of Particle	SiC	Al_2O_3	AlN	B_4C	TiB_2	TiC
Type of Crystal	Hex.	Hex.	Hex.	Rhomb.	Hex.	Cubic
Melting point (°C)	2300	2050	2300	2450	2900	3140
Young's Modulus (GPa)	480	410	350	450	370	320
Density (g cm^{-3})	3.21	3.9	3.25	2.52	4.5	4.93
Heat conductivity (W m^{-1} K^{-1})	59	25	10	29	27	29
CTE (10^{-6} K^{-1})	4.7-5.0	8.3	6.0	5.0-6.0	7.4	7.4
Mohs-hardness	9.7	6.5	-	9.5	-	-

Numerous metals can be used as matrix material for metal matrix composites some of the examples are given in Table 1.4.

Table 1.4 Examples of matrix alloys used in metal matrix composites [4].

Conventional cast alloys	Conventional wrought alloys	Special alloys
AlSi12CuMgNi	AlMgSiCu (6061)	Al–Cu–Mg–Ni–Fe-alloy (2618)
AlSi9Mg	AlCuSiMn (2014)	Al–Cu–Mg–Li-alloy (8090)
AlSi7 (A356)	AlZnMgCu1.5 (7075)	AZ91Ca
AZ91	TiAl6V4	
AE42		

The determination of suitable matrix alloy is related to specific application of composite material. The conventional light alloys are widely used due to their easy processing and low density. Oversaturated or metastable matrixes can be used by powder metallurgical methods. Moreover, heat treatment can be applied to have optimum properties via dispersion hardening [4].

Aluminum alloys are the most commonly used matrix material due to their low melting point, low cost, low density, excellent strength, toughness and resistance to corrosion. These properties give rise to usage of aluminum matrix composites in aerospace and automotive industries. Aerospace industry have the major research on low density Al-Li alloys where automotive industry conducts research on all kind of aluminum alloys. The common applications consists of the engine parts like piston, piston rod, piston pin, valve train, cylinder head, crankshaft main bearing, cylinder liners, etc. where oscillation and thermal fluctuations are present. Figure 1.1 shows an example of fiber reinforced aluminum piston where recess area is partially reinforced with short Al_2O_3 fibers.

Figure 1.1 Partially short Al$_2$O$_3$ fiber reinforced aluminum diesel piston [4].

The use of such reinforcement increases the thermal shock resistance and high temperature fatigue strength drastically as shown in Figure 1.2 [2, 4].
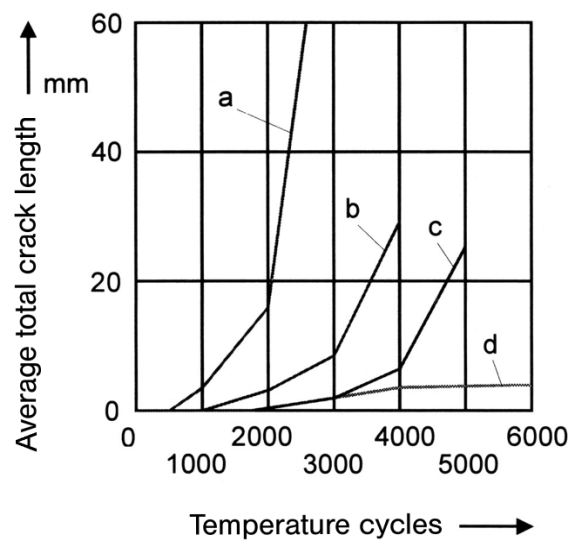
Figure 1.2 Temperature shock resistance of the fiber reinforced piston alloy AlSi12CuMgNi for different fiber contents for a temperature of 350 °C: a) Non-reinforced, b) 12 vol% Al$_2$O$_3$ short fibers, c) 17.5 vol% Al$_2$O$_3$ short fibers and d) 20 vol% Al$_2$O$_3$ short fibers [4].

The problem with the limited commercial use of the fiber reinforced composites not only related to the cost but also to the intricate production routes. One of the

consequential obstacles during alumina fiber reinforced aluminum matrix composite processing is the relatively high temperatures required during infiltration. The roots of the problem may lie in the matrix alloying and casting temperature.

The main objective of the present thesis work was to conduct research on low mould temperature infiltration of various vol% Saffil alumina fiber preforms and was to characterize produced composites. Liquid metal temperature and magnesium content of the alloy was changed to observe the effects on infiltration, mechanical behavior and physical properties of the composites. Five different vol% Saffil alumina short fiber reinforced composites were produced at 190 °C mould temperature. Liquid alloy casting temperature was 750 °C and 800 °C. The magnesium content of the alloy was 0.3 wt% and 1 wt%.

CHAPTER 2

THEORY AND LITERATURE SURVEY

2.1   Processing Techniques of Fiber Reinforced Metal Matrix Composites

Several techniques can be used for metal matrix composite production. The selection of the right process is based on the type, distribution, quantity of the reinforcement, the matrix alloy and the application. In addition, limiting factors like fiber vol% and part geometry should be taken into consideration for different kind of manufacturing processes [4]. These techniques can be divided into three groups [1]:

1. Liquid state processes
2. Solid state processes
3. In situ processes

2.1.1   Liquid State Processes

There are mainly three procedures used in liquid state processes [4]:

1. Melt stirring
2. Gas pressure infiltration
3. Squeeze casting

2.1.1.1 Melt Stirring

In this process particulates or fibers are added to molten metal and intense stirring is applied to avoid agglomeration and contamination films which promote interfacial bonding [10]. It is vital to avoid gas entrapping which can cause porosities or reactions during stirring [4]. There are many approaches for introducing particles and/or fibers to a molten alloy [9]:

   a) Vortex method; particles mixed through the melt by mechanical agitation
   b) Injection method; particles are injected to the melt by an inert gas gun
   c) During mould filling particles are added to molten stream
   d) Particles are mixed into melt by reciprocating rods
   e) Particles are mixed into melt by centrifugal action
   f) Injection of particles to ultra sound irradiated melt [11].

Stirring time and melt temperature must be carefully arranged to avoid excess reactions to occur between reinforcement and melt which can dissolve particles and fibers. Fibers have higher tendency for such reactions due to their high surface to volume ratio than spherical particles.

2.1.1.2 Gas Pressure Infiltration

Infiltration of ceramic preforms is a suitable process for high fiber volume and complex shaped metal matrix composite production [12, 13]. In this method a gas which is inert to matrix material is used to infiltrate molten metal into heated up preform. There are two routes for gas pressure infiltration where the preform can be dipped into a molten bath and gas pressure is applied or the molten metal is pressed to the preform [4]. In the second method vacuum can be applied to assist infiltration which is analogous to low pressure die casting which is shown in Figure 2.1 [14]. As a result, gas entrapment is avoided which is detrimental for mechanical properties [15, 16]. The use of vacuum also decreases the infiltration pressures significantly with respect to squeeze casting method [17]. Moreover, the risk of

inhomogeneous fiber distribution and fiber damage is reduced with the use of lower pressures [18].
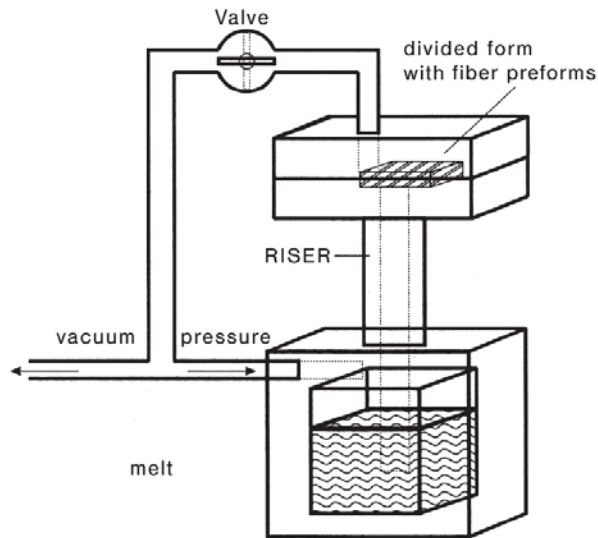
Figure 2.1 Gas pressure infiltration technique analogous to low pressure die casting [4].

2.1.1.3   Squeeze Casting

Squeeze casting is an old and important process which combines casting and forging. Molten metal is poured into a die and pressure is applied to closed die until solidification is completed [19]. This method is the commonly used for metal matrix composite production which has high productivity and near net shape formability [20].

The advantages of this process are elimination of shrinkage and fine grained structure due to the high pressures applied during solidification. In addition, there are no gas inclusions in the parts so thermal treatment can be done safely. Accordingly, the resulting mechanical properties are better than conventional casting methods [4, 20].

Figure 2.2 shows the types of squeeze casting which are direct and indirect squeeze casting. In the first method infiltration of molten metal to prefabricated preforms is done by applying direct pressure to the melt. There is no gate so the tooling is simple in this method. But there are disadvantages like the need to have an exact amount of molten metal and resulting oxide inclusions. In the indirect squeeze casting the molten metal is pressed through a gate system and the oxide inclusions are eliminated. Molten metal flow rate through a gate is less so the turbulent is less during mould filling and gas entrapment is avoided [4].
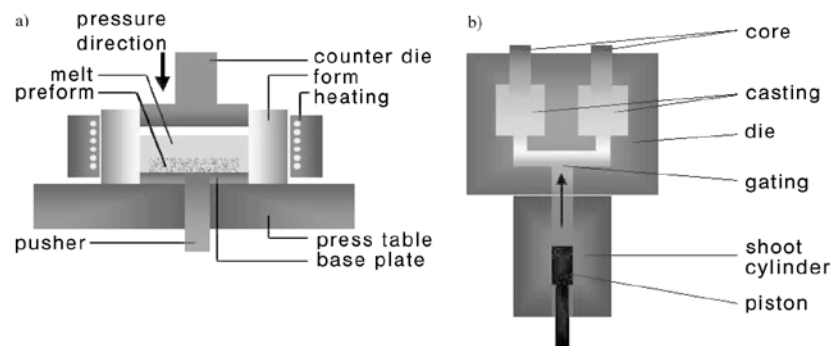
Figure 2.2 a) Direct and b) Indirect squeeze casting [4].

2.1.2 Solid State Processes

2.1.2.1 Powder Metallurgy

Powder metallurgy is used in composite production where rapidly solidified matrix alloy can be in a metastable or oversaturated state without any segregation problem [4]. In figure 2.3 main steps are given for powder metallurgy production of metal matrix composites. First both reinforcement and matrix powders are sieved, than they are blend to have desired composition and compressed to theoretical densities of % 75 and more. In the end degassing and final processes like forging, extrusion, rolling, etc. are done to get the desired composite [7].

11

2.1.2.2 Diffusion Bonding

This process is a solid state welding technique where inter-diffusion of atoms at metal contact points at high temperature result in welding. The important parameters are the pressure and temperature for production of a metal matrix composite which have predetermined order of metal foils and fiber arrays. In diffusion bonding different metals can easily be used and fiber orientation with volume fraction can be controlled. Disadvantage of this process is long process times at high temperature and high pressure which accounts for high cost. In addition, size of the parts produced is limited [1].
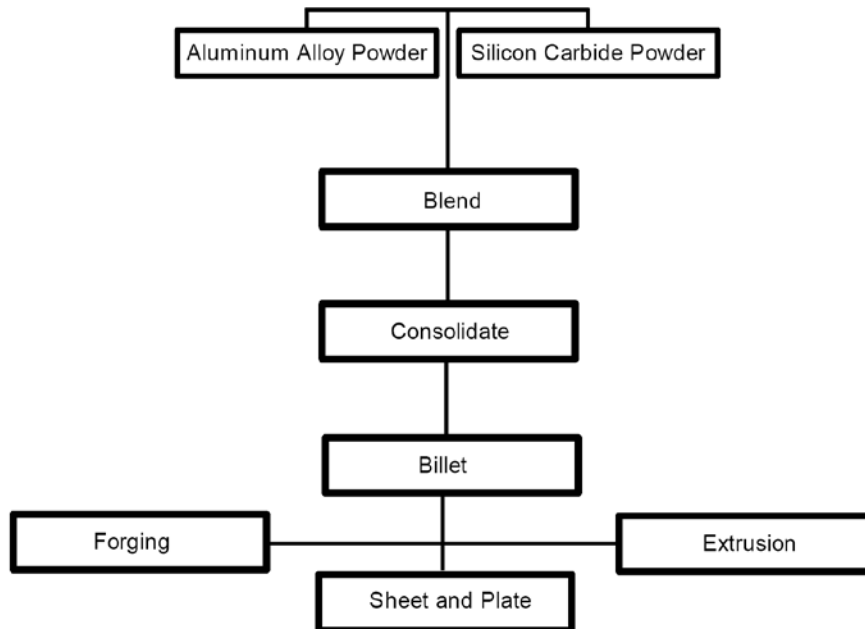
Figure 2.3 Main steps for powder metallurgy production of metal matrix composites [6].

2.1.2.3 Deposition Techniques

In this process, individual fibers are coated in a tow with the desired matrix material and then they are diffusion bonded to get the final metal matrix composite plate or structural materials. Coating of fibers takes long time but control of interfacial

bonding give way to make interfacial diffusion barriers and graded coatings. Immersion plating, electro-plating, chemical vapor deposition and physical vapor deposition are some of the coating techniques [4].

2.1.3 In Situ Processes

In this process the reinforcement phase is formed in situ. A specific alloy is poured and the reinforcement is precipitated during solidification. As a result, the problems occurring while combining two phases are eliminated. By controlling solidification rate and alloy chemistry one can change the type, size and distribution of reinforcing phase. Directional solidification of eutectic alloy is an example of this kind of process [4].

2.2 Short Fiber Preform Production

The most important and gruelling step for production of a locally short fiber reinforced metal matrix composite is preform preparation. To have an effective reinforcement the preform must satisfy some basic requirements [4]:

1. Preform must be extremely clean.
2. Preform must have homogeneous fiber distribution and orientation.
3. Preform must have minimum binder content with homogeneous distribution.
4. Preform must have sufficient strength with high aspect ratio fiber.

In figure 2.4 typical steps for preform production is given. The complexity of the steps depends on the type of the fibers used. There are two main production procedures for discontinuous fibers which are melt spun and spin sinter. In melt spun process generally alumina silicate fibers are produced from a melt. Raw material is melted by electrodes and a temperature above 2000 ℃ is reached. The melt is run out through an orifice at the bottom of the furnace and hit to several fast rotating rollers or is blown by high pressure air. For both case the melt is separated to fine fibers due to centrifugal and drag forces [4].

```
┌─────────────────────────────────────────┐
│      Delivery condition fiber wool       │
└─────────────────────────────────────────┘
                    ↓
        ┌───────────────────────┐
        │       Cleaning        │
        └───────────────────────┘
                    ↓
        ┌───────────────────────┐
        │   Dispersing in water │
        └───────────────────────┘
                    ↓
        ┌───────────────────────┐
        │    Binder addition    │
        └───────────────────────┘
                    ↓
        ┌───────────────────────┐
        │        Shaping        │
        └───────────────────────┘
                    ↓
        ┌───────────────────────┐
        │        Drying         │
        └───────────────────────┘
                    ↓
        ┌───────────────────────┐
        │        Firing         │
        └───────────────────────┘
```
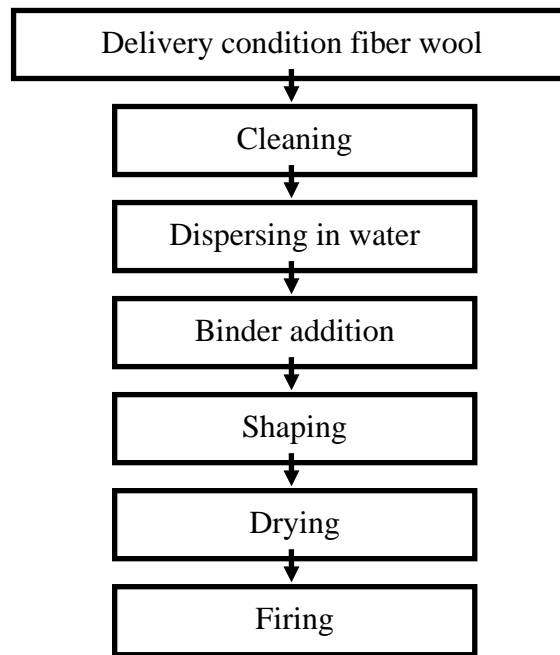
Figure 2.4 Production steps of short fiber preforms.

The production of fibers having % 60 and more Al_2O_3 is not economical by this procedure so spin sinter technique is used. The metal-salt solutions with additives are spun to fine and regular fibers either drawing or blowing. With adequate heat treatment mullite and alumina fibers are produced by this process. The fiber quality and properties are different than melt spun process. The shot particles, which are non-fibrous components, are much higher for melt spun process. The shots in spin sinter produced fibers are due to loose bakings at the spinning device. In table 2.1 some properties of fibers used for preform production can be seen. In this table C fibers don't have shot content because they are chopped or milled from continuous fibers [4].

Shot particles can cause catastrophic failure of metal matrix composites that are stressed by thermal fatigue. Size of the shot particles can be up to 1 mm and at critical size act as crack formation center. The inhomogeneous distribution, size and amount of shot particles must be decreased. The shot particle must be lower than 100 µm to avoid adverse effects [4].

Table 2.1 Properties of fibers used in preform production [4].

Type	Al_2O_3	Al_2O_3-SiO_2	C (PAN)
Name	Saffil, Maftec	Kaowool, Cerafiber	Sigrafil
Chemistry	> 95 % Al_2O_3 < 5 % SiO_2	48 % Al_2O_3 52 % SiO_2	95 % C
Elastic Modulus GPa	270-330	105	240
Strength, MPa	2000	1400	2500
Fiber Diameter, µm	2-3	8	-
Density, g/cm^3	3.3	2.6	1.8
Shot Content, %	> 1	40-60	-

Thermal Ceramics have a procedure where fibers are cleaned from shot particles less than 10 ppm and 75 µm in size. 10 – 40 g fibers are added to a liter of water with colloidal silica as an inorganic binder. Negative charged SiO_2 particles cover the fiber surface and repulsion occur which blocks agglomeration. The addition of a cationic binder which has a long chain molecular structure results in flocculation. By this way strong enough preforms for handling and post processing having less than % 5 binder can be produced. The mechanism of bonding can be seen on Figure 2.5 [4].

Repulsion

Fiber

Silica sol⁻

a)

Agglomeration

Fiber⁻   Starch⁺   Silica sol⁻

b)

Flocculation

c)
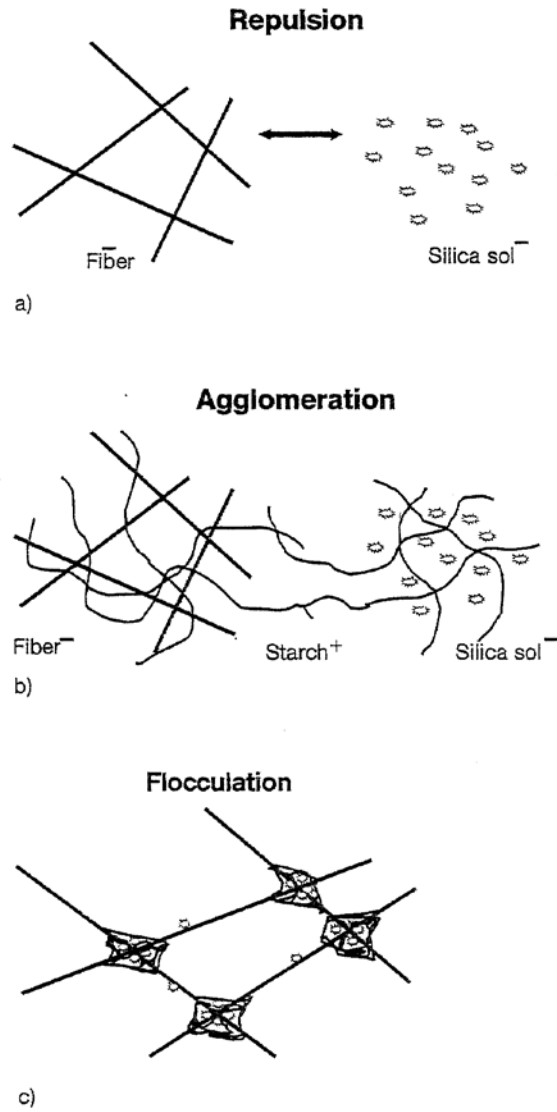
Figure 2.5 Bond mechanism a) repulsion, b) agglomeration and c) flocculation [4].

Figure 2.6 shows the shaping preform where vacuum assisted pressing is applied to fiber suspension. Fibers align themselves perpendicular to pressing direction. With this respect, a planar isotropic fiber structure occurs. After pressing preform is dried at 110 ºC and then fired between 900 ºC and 1100 ºC. At these temperatures organic binder completely burns and SiO_2 binder left [4].

a) Vacuum   b) Vacuum
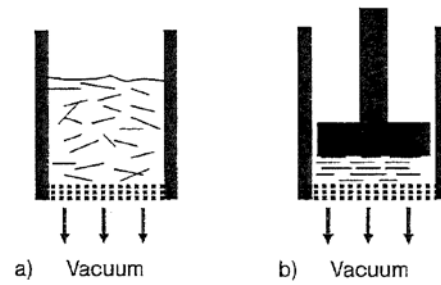
Figure 2.6 Shaping: (a) fiber slurry; (b) pressure and vacuum application [4].

Preforms strengths change with the fiber volume fraction. K. Naplocha et. al. showed that bending strength of Saffil alumina fibers, having volume fractions of 0.10 to 0.22, can change from 2 to 4 MPa which is shown in Figure 2.7 [21]. In addition, compressive strength of Saffil preforms having % 80 porosity is about 2 MPa [22].
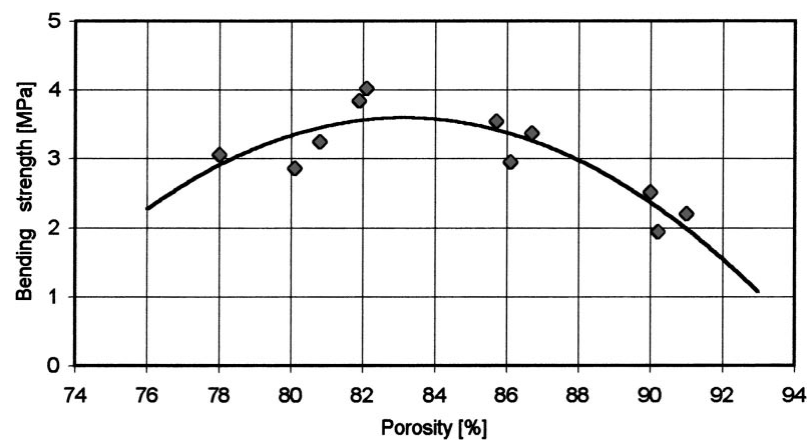
Figure 2.7 Effect of fiber volume fraction on bending strength [21].

17

2.3   Infiltration

2.3.1   Influence of Wetting on Infiltration

Wetting of ceramic reinforcement by liquid metal is a vital issue for metal matrix composite production. Because wetting directly affects kinetics of process and the adhesion between reinforcement and matrix material. However, in technically relevant processes the effect to the process can be less due to the applied external pressure [4].

According to Young, wettability can be shown by the contact angle adjustment of a molten droplet on a solid base,

$$\gamma_{SA} - \gamma_{LS} = \gamma_{LA} \cdot \text{Cos}\theta \tag{2.1}$$

where, γ_{SA} is the surface energy of the solid phase, γ_{LA} is the surface energy of the liquid phase, γ_{LS} is the interface energy between liquid and solid phases and θ is the contact angle. In Figure 2.8 contact angle can be seen for different surface energies and as the contact angle decreases wettability improves [4].
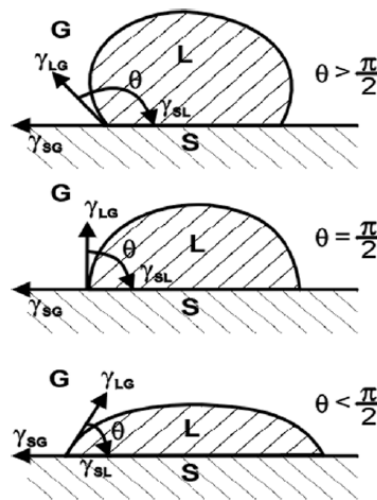
Figure 2.8 Contact angle change for different interface energies [4].

18

2.3.1.1 Influence of Time and Temperature on Wetting

Wetting is a kinetic process, so it depends on temperature and time. Figure 2.9 and 2.10 show the time dependence of SiC plates by aluminum alloys and temperature dependence of wetting between SiC and aluminum alloys, respectively. [23, 24]. The contact angle for Al – Al_2O_3 system changes about 160° to 70° for a temperature change from 670-850°C to 1030 °C [21].
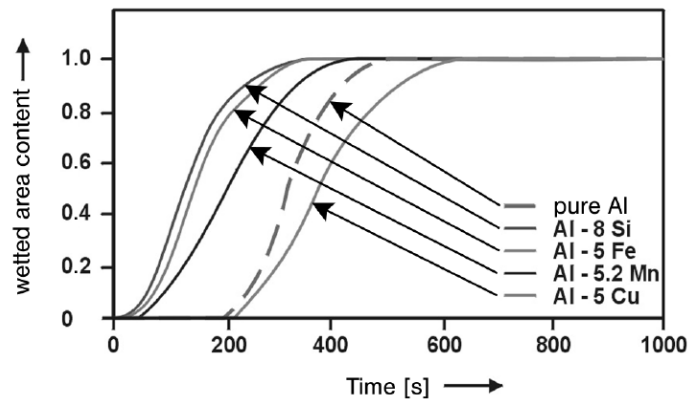
Figure 2.9 Time dependence wetting of SiC plates by different aluminum alloys [23].
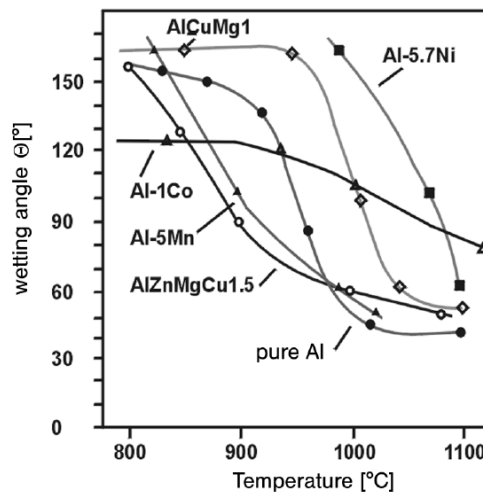
Figure 2.10 Temperature dependence of contact angle between different aluminum alloys and SiC plates [24].

2.3.1.2 Influence of interface reactions on wetting

The alloying elements can change the surface tension of liquid metal or react with the reinforcement which in both cases changes the contact angle. There will be a driving force for magnesium to reduce alumina between an aluminum alloy containing magnesium and alumina system because magnesia is a more stable oxide than alumina [25]. The possible reactions are [26, 27]:

$$Mg\ (l) + 2\ Al\ (l) + O_2 = MgAl_2O_4\ (s) \tag{2.2}$$
$$Mg\ (l) + 4/3\ Al_2O_3\ (s) = MgAl_2O_4\ (s) + 2/3\ Al\ (l) \tag{2.3}$$
$$3\ Mg\ (l) + Al_2O_3\ (s) = 3\ MgO\ (s) + 2\ Al\ (l) \tag{2.4}$$
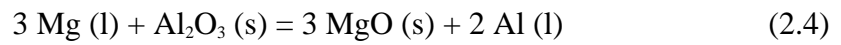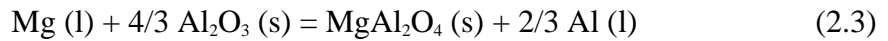
$MgAl_2O_4$ is the main reaction product for magnesium contents lower than 4 wt% where MgO occurs at magnesium contents higher than 4 wt%. Under controlled atmosphere the formation of $MgAl_2O_4$ is favored due to relatively low oxygen partial pressures [26].

These reactions aids wetting but if the reaction degrades the fiber than the mechanical properties decays for composite. But the SiO_2 binder used for preform production is highly reactive and magnesium reacts first with it. Three reactions can occur in Al – Mg - SiO_2 system [28]:

$$2\ SiO_2\ (s) + Al\ (l) + Mg\ (l) = MgAl_2O_4\ (s) + 2\ Si\ (s) \tag{2.5}$$
$$SiO_2\ (s) + 2\ Mg\ (l) = 2\ MgO\ (s) + Si\ (s) \tag{2.6}$$
$$3\ SiO_2\ (s) + 4\ Al\ (l) = 2Al_2O_3\ (s) + 3\ Si\ (s) \tag{2.7}$$
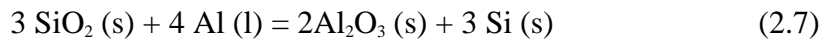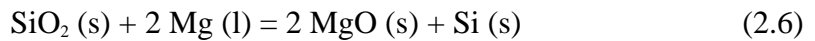
These three reactions are spontaneous, due to lower Gibbs energies of $MgAl_2O_4$, MgO and Al_2O_3 than SiO_2 and the interface is free from silicon initially. As a result, reactions compete with one another. Al_2O_3 will eventually change to $MgAl_2O_4$ or MgO due to high oxygen affinity of magnesium according to process parameters like temperature and magnesium content in alloy [28]. The effect of silica binder on infiltration can be seen in Figure 2.11 [29].
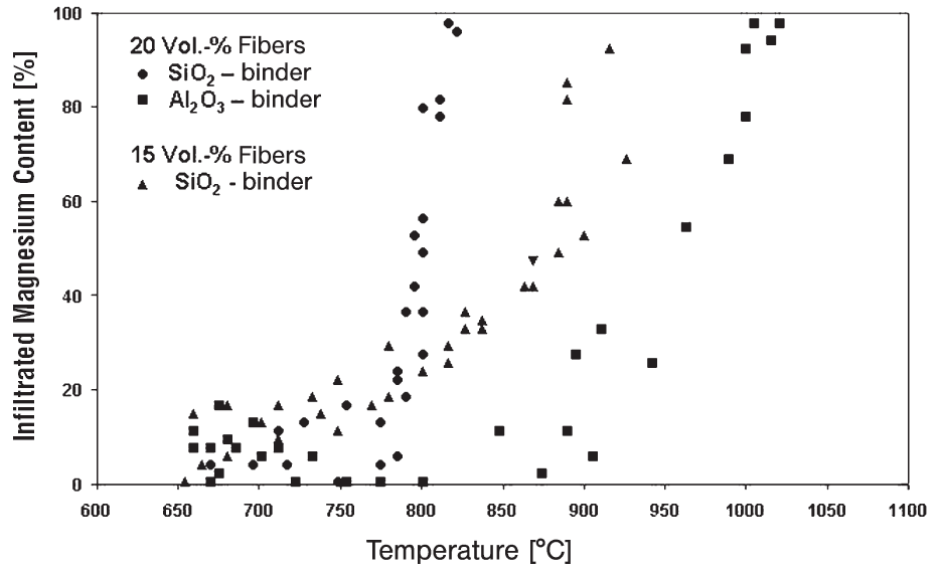
Figure 2.11 The effect of reactive binders on infiltration for pure Mg / Al$_2$O$_3$ fiber
        system [29].

2.3.1.3 Influence of surrounding atmosphere on wetting

The surrounding atmosphere effects wetting by changing the surface energies and
oxygen partial pressure. At high oxygen partial pressure and low temperatures
contact angle is high for Al$_2$O$_3$ / pure aluminum system which is shown in Figure
2.12 [30].
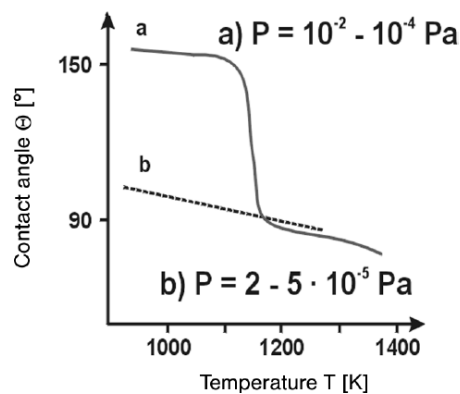
Figure 2.12 Change in contact angle with oxygen partial pressure and temperature
        [30].

2.3.2 Threshold pressure

The infiltration process for the production of metal matrix composites consists of three stages [4]:

1. Formation of a contact between the melt and the reinforcement at the surface of a fiber or particle preform
2. Liquid metal infiltration through the preform
3. Solidification of the composite.

There have to be a minimum pressure for infiltration to start and follow. Pressure-free infiltrations are only possible for thin preforms with reactive systems after long process times. The minimum pressure is called threshold pressure. ΔP, resulting pressure, which is the driving force for the infiltration, can be found by [31]:

$$\Delta P = P_0 - P_a - \Delta P_\gamma \tag{2.8}$$

where, P_0 is the pressure in the melt entering the perform, P_a is the pressure in the melt at the infiltration front, and ΔP_γ is the decrease in pressure due to wetting of surfaces. P_0 and P_a are shown in Figures 2.13 and 2.14, respectively.
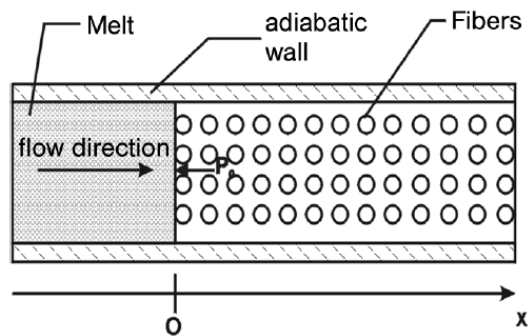
Figure 2.13 Start condition of an adiabatic unidirectional infiltration process [31].

22
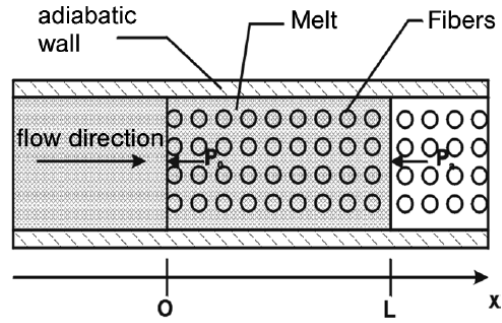
Figure 2.14 Schematic view of an adiabatic unidirectional infiltration process [31].

When P_0 equals P_a the minimum pressure P_{th} (threshold pressure) can be found. P_{th} can be defined as follows [4]:

$$P_{th} = \Delta P_\gamma = S_f (\gamma_{LS} - \gamma_{SA}) \tag{2.9}$$

where, S_f is the surface interface per unit area. S_f can be defined for short fiber preforms as [32];

$$S_f = \frac{4 \, V_f}{d_f (1 - V_f)} \tag{2.10}$$

where, V_f and d_f are fiber volume fraction and fiber diameter. Table 2.2 shows specific surface with increasing Saffil Al_2O_3 fiber volume percent. It is obvious that fiber contents higher than % 20 are significantly decrease permeability [32].

Table 2.2 Specific surface of Saffil Al_2O_3 preforms [33].

Fiber volume fraction of Al_2O_3 preforms	0.10	0.20	0.24	0.25
Specific surface $S_f = 10^6$ fiber surfaces (m^2) / pore volume (m^3)	1.26	3.41	4.39	4.58

Threshold pressure can also be found by,

$$\Delta P_\gamma = \frac{2\gamma_{LA}\cos\theta}{r} \tag{2.11}$$

where r is the hydraulic radius (radius of capillary). If it is assumed that the pores are cylindrical in the preform, the external pressure needed to infiltrate a given pore diameter can be calculated by above equation. The variation of infiltrated pore diameter with infiltration pressure is shown in Figure 2.15 for pure aluminum – alumina system where γ_{LA} is 860 mj/m^2 [34].
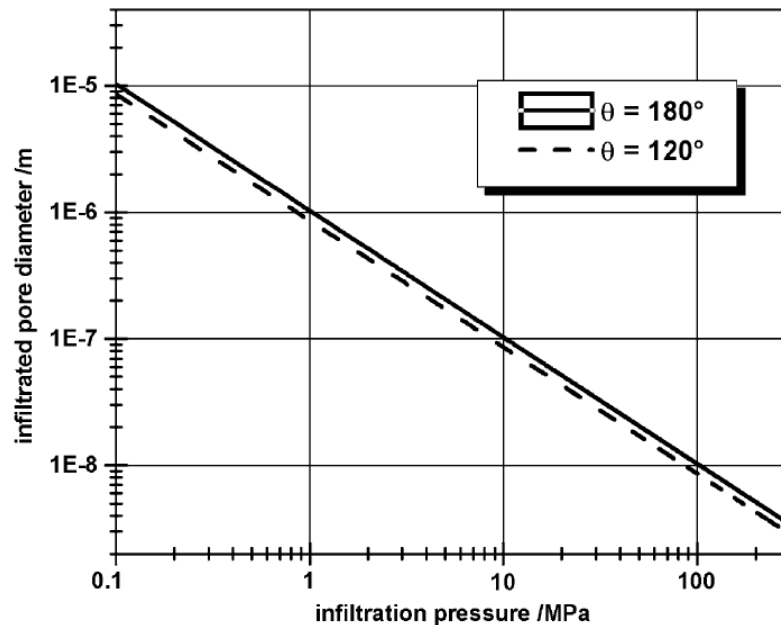
Figure 2.15 Change in pressure with pore diameter [34].

2.3.3 Influence of permeability and viscosity on infiltration

There is an inverse relationship between specific surface and permeability. The results for water permeability of preforms can be seen in Figure 2.16. The even supply of the melt through the preform and pressure for the infiltration is directly

affected by this property. Fiber volume contents higher than 20 % significantly decreases permeability. As a result the importance of viscosity for infiltration increases [33]. The permeability of metal flow perpendicular to the fiber orientation is nearly twice more than for the flow parallel to the fiber orientation [31].
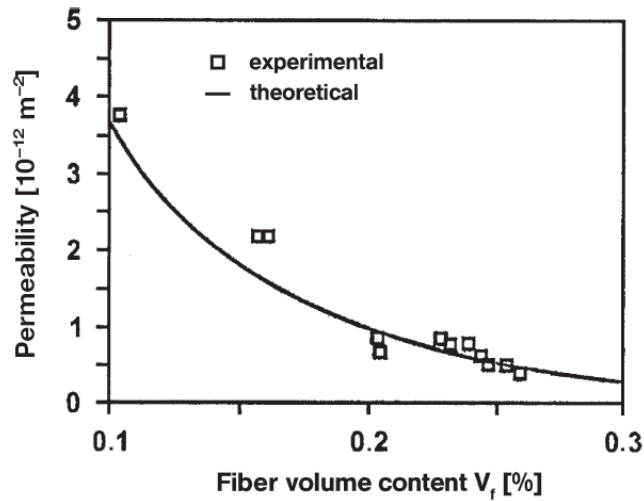
Figure 2.16 Relationship between permeability and fiber volume content for running water [33].

The temperature and composition of the melt have to be optimized to get the ideal viscosity. The effect of temperature on viscosity of unalloyed aluminum and magnesium is given in Figure 2.17. The dependence of the viscosity of aluminum on temperature is higher than the magnesium [4].
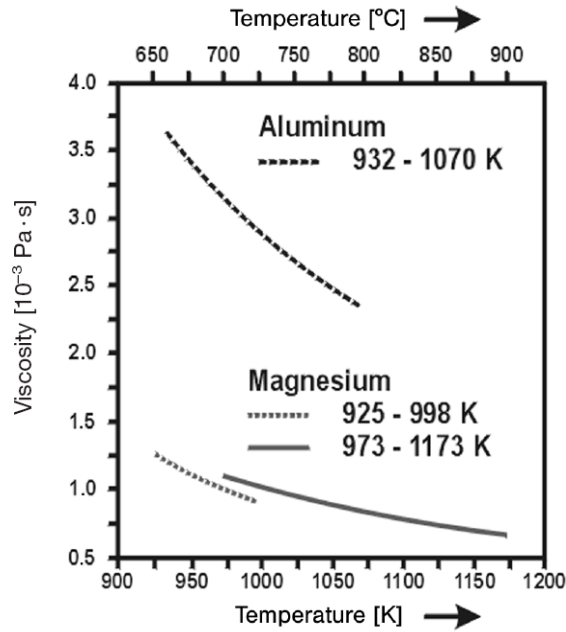
Figure 2.17 Effect of temperature on unalloyed magnesium and aluminum [4].

2.3.4   Infiltration Kinetics

If an infiltration process of liquid metal into a fibrous preform is investigated as shown in Figure 2.18, the dependence of the penetrating velocity of molten metal, U, at a time t on an infiltration depth X, is described by Darcy's law (Assuming that liquid metal is an incompressible homogeneous fluid and metal flow within the preform is laminar) [35],

$$U = \frac{k \cdot \rho}{n \cdot \mu} \cdot \frac{\Delta\varphi}{X} \qquad (2.12)$$

where k and n are the permeability and the porosity of the fiber preform respectively, ρ and μ are the density and the viscosity of the liquid metal respectively, and $\Delta\varphi$ is the energy loss per unit mass of liquid metal during flow through the infiltrated zone [36].

26
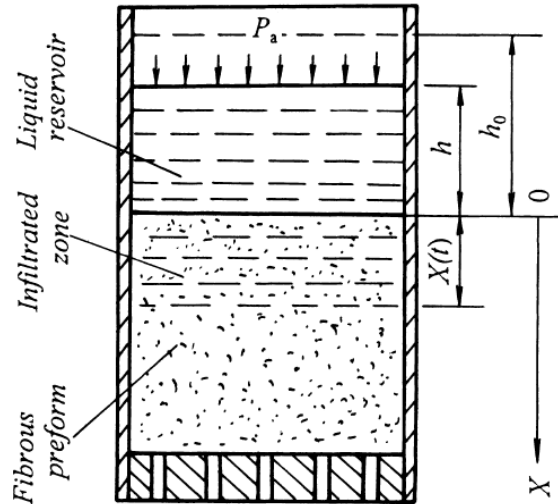
Figure 2.18 Schematic illustration of liquid metal infiltration into a fibrous preform [36].

The permeability term depend only on properties of porous material. There are many analytical models to relate k and properties of porous material where the most common is the capillary model. In this model it is assumed that the porosity is made up of capillaries dispersed in the material [36] and k is expressed as,

$$k = \frac{n \cdot r^2}{24}$$

(2.13)

where, r is the effective capillary tube radius of the preform [35].

The relationship between infiltration depth and time for an Al - 1,5 Mg alloy and alumina fiber system was shown by Hu Lianxi et al [36]. As seen from Figures 2.19 and 2.20, there exists a parabolic relationship between infiltration depth and time. In addition, an incubation time is required for infiltration to start. Darcy's law is basically correct but it must be modified in terms of incubation time .
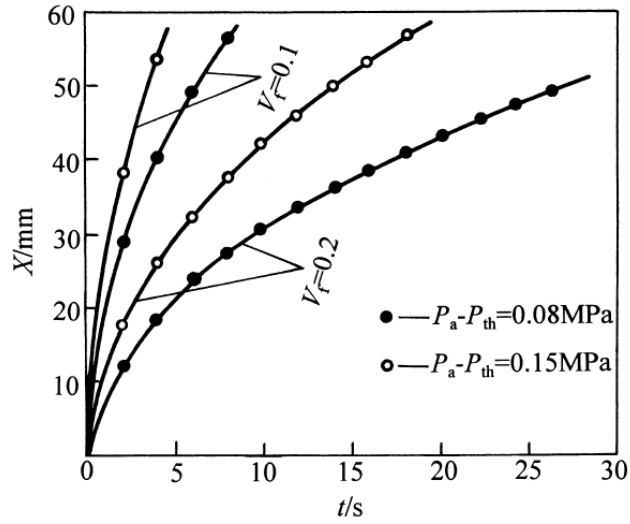
Figure 2.19 Theoretical relationship between infiltration depth and time [36].
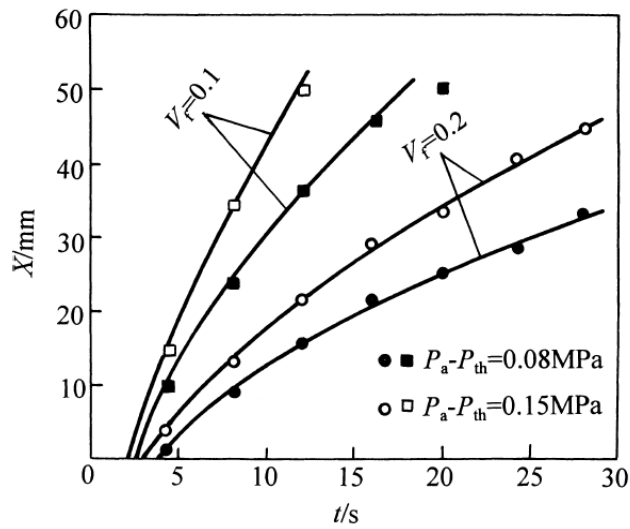
Figure 2.20 Experimental relationship between infiltration depth and time [36].

2.4   Mechanism of fiber reinforcement

2.4.1   Long fiber reinforcement

The linear mixture rule can be used to calculate the strength of a long fiber reinforced composite under stress in the fiber direction if it is assumed that there is

no fiber contact and optimal interface formation [37]:

$$\sigma_C = \varphi_F \cdot \sigma_F + (1 - \varphi_F) \cdot \sigma_M^*$$ (2.14)

where σ is the strength, Φ is the volume fraction; C, F and M subscripts are refer to composite, fiber and matrix respectively; σ_M^* is the matrix yield strength.

To have an effective strengthening effect at least the critical fiber content ($\Phi_{F,crit}$) must be exceeded, which can be determined by [4]:

$$\sigma_M = \varphi_{F,crit} \cdot \sigma_F + (1 - \varphi_{F,crit}) \cdot \sigma_M^*$$

$$\downarrow$$

$$\varphi_{F,crit} = \frac{\sigma_M - \sigma_M^*}{\sigma_F - \sigma_M}$$ (2.15)

2.4.2   Short Fiber Reinforcement

In long fiber reinforced composites the load is carried along the full length of the fibers. Where in short fiber reinforced composites the load is transferred from fiber to fiber by interfacial shear through the matrix. The schematic stress distribution is given in Figure 2.22. The ends of the fibers can carry high shear stress but cannot carry high tensile stress. As the fiber length increases the shear stress and tensile stress balance each other and fiber can be loaded to its full tensile strength. The length at which the fiber is loaded to its full tensile strength is called the critical fiber length l_c and determined by [37]:

$$l_c = \frac{\sigma_F \cdot d_F}{2\tau_{FM}}$$ (2.16)

where, d_F and τ_{FM} are the fiber diameter and matrix shear stress at the fiber/matrix interface respectively.

29
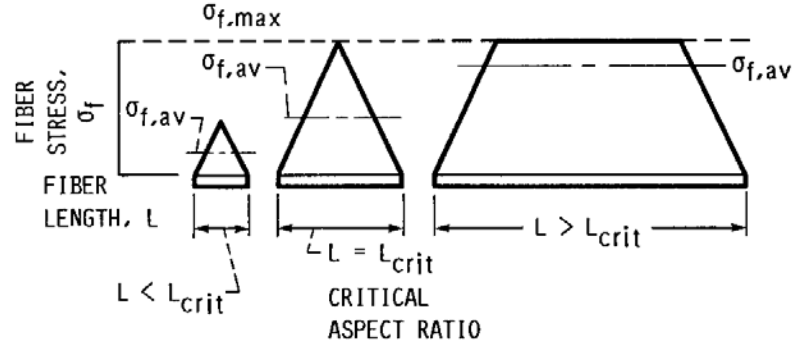
Figure 2.21 Schematic view of tensile stress distribution on fibers of different lengths ($\sigma_{f, av} = \sigma_{F, eff}$) [37].

Shear strength at the fiber/matrix interface can be defined as [4]:

$$\tau_{FM} = 0.5 \cdot \sigma_M^*$$

(2.17)

σ_M^* is the matrix yield point.

The effective fiber strength $\sigma_{F, eff}$, with the dependence of fiber length [4];

$$\sigma_{F, eff} = \eta \cdot \sigma_F \cdot \left(1 - \left(\frac{l_c}{2 \cdot l_m}\right)\right)$$

(2.18)

where, η and l_m are fiber efficiency ($0 < \eta < 1$) and average fiber length respectively.

Accordingly the strength of a short fiber reinforced composite having $l_m > l_c$ can be defined as [4];

$$\sigma_C = \eta \cdot C \cdot \varphi_F \cdot \sigma_F \cdot \left(1 - d_F\left(\frac{\sigma_F}{2 \cdot l_m \cdot \sigma_M^*}\right)\right) + (1 - \varphi_F) \cdot \sigma_M^*$$

(2.19)

where, C is the orientation factor (aligned fiber C=1, irregular C= 0.2, planar isotropic C= 0.375 [38]). In this model it is assumed that the fiber/matrix interface adhesion and distribution of arranged fibers are ideal [4].

30

CHAPTER 3

EXPERIMENTAL PROCEDURE

3.1   Matrix Material

Two aluminum alloys were used as matrix material where the main alloying element is silicon. Magnesium as the second alloying element has a vital effect on wetting of Saffil^{TM} fibers. The difference between the alloys was the magnesium content where the first one has 0.3 wt. % Mg and second has 1 wt. % Mg. The 0.3 wt. % Mg containing alloy was called AlSi10Mg0.3 and the one with 1 wt. % Mg was called AlSi10Mg1. The actual compositions used in our experiments are given in Table 3.1.

Table 3.1 The actual compositions of aluminum alloys used in production of composites. Elements are in wt%.

Alloy	Al	Si	Mg	Fe	Ti	Cu	Cr	Trace Elements
AlSi10Mg0.3	89.82	9.55	0.298	0.197	0.0145	0.006	0.0128	0.01
AlSi10Mg1	89.56	9.16	0.944	0.200	0.0148	0.008	0.0126	0.01

3.2   Reinforcement Material

Saffil^{TM} RF grade (Trade name Saffil Ltd.) fibers were used as the reinforcement

material. Fiber composition and properties are given in Table 3.2 and 3.3. The fibers were bought from Thermal Ceramics as pre-shaped rectangular prism having dimensions of $100 \times 12 \times 7$ mm in x, y and z directions. The preforms have 10, 15, 20, 25 and 30 volume percent Saffil alumina fiber and 5 weight percent silica binder was used during production.

Table 3.2 Composition (wt%) of Saffil RF grade fibers [39].

δ - Al_2O_3	SiO_2	Trace Elements
96 – 97	3 – 4	Ni-Cr-Fe-Ca oxides < 0.5

Table 3.3 Properties of Saffil RF grade fibers [39].

Elastic Modulus, GPa	270-330
Strength, MPa	2000
Average Diameter, µm	3.0-3.5
Density, g/cm^{-3}	3.3
Mohs Hardness	7.0
Maximum Service Temperature, °C	1600

The fibers mainly consist of polycrystalline δ - Al_2O_3 phase. The presence of 3 - 4 percent SiO_2 stabilizes the delta phase and hinders fine grain (50 nm) coarsening at high temperatures [39]. The SEM images of 10, 15, 20, 25, 30 vol% preforms are given in Figures 3.1 through 3.5.
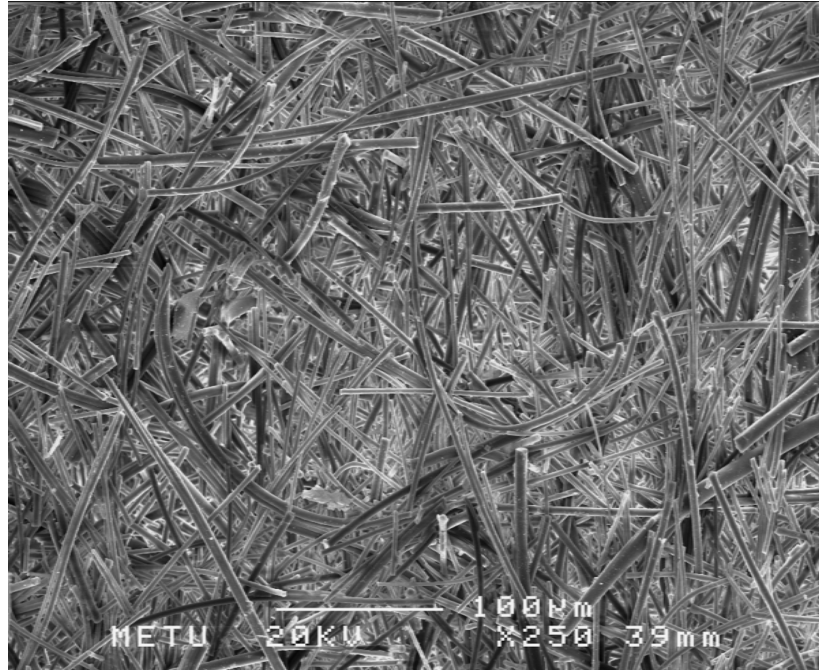
Figure 3.1 SEM image of 10 vol% Saffil fiber preforms vertical to the fiber orientation.
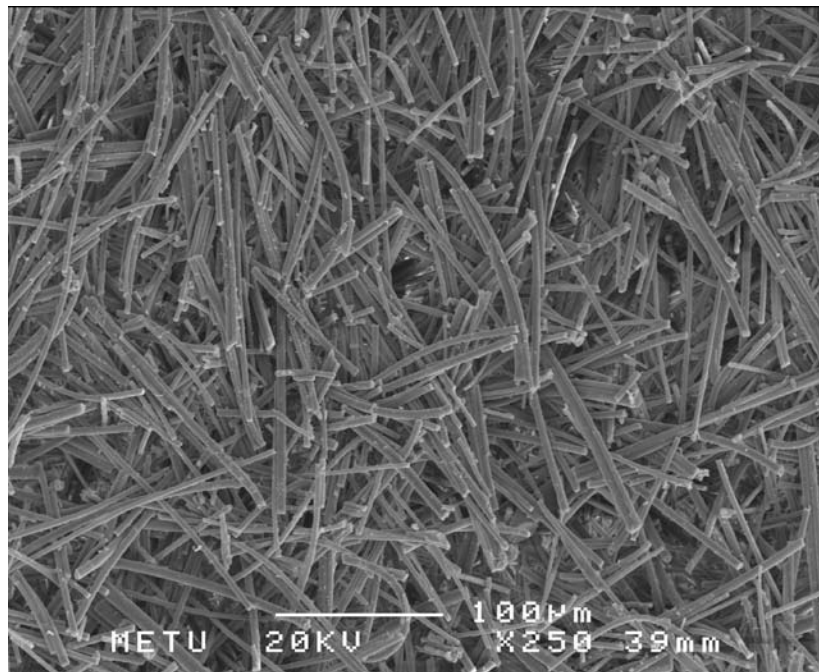
Figure 3.2 SEM image of 15 vol% Saffil fiber preforms vertical to the fiber orientation.
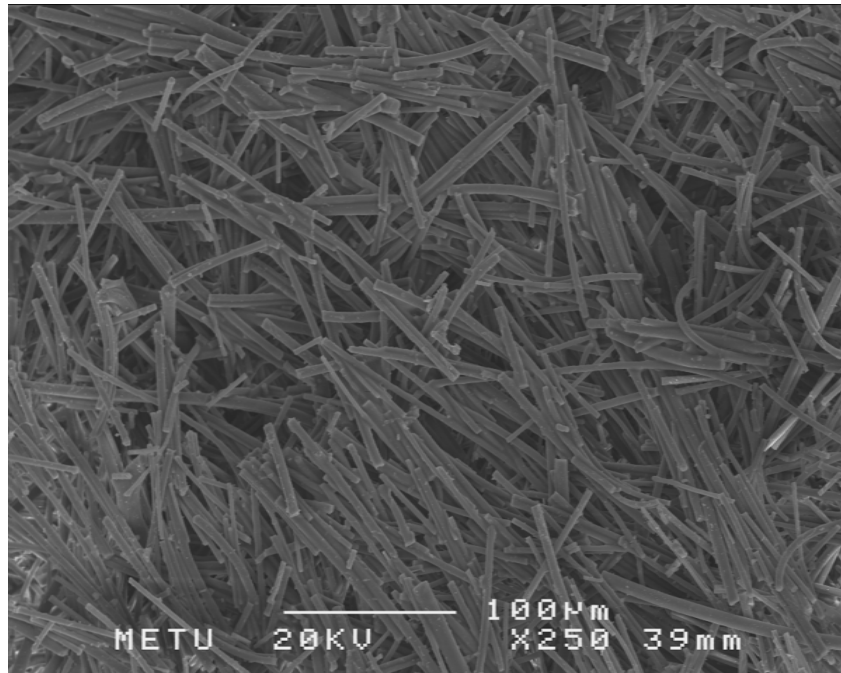
Figure 3.3 SEM image of 20 vol% Saffil fiber preforms vertical to the fiber orientation.
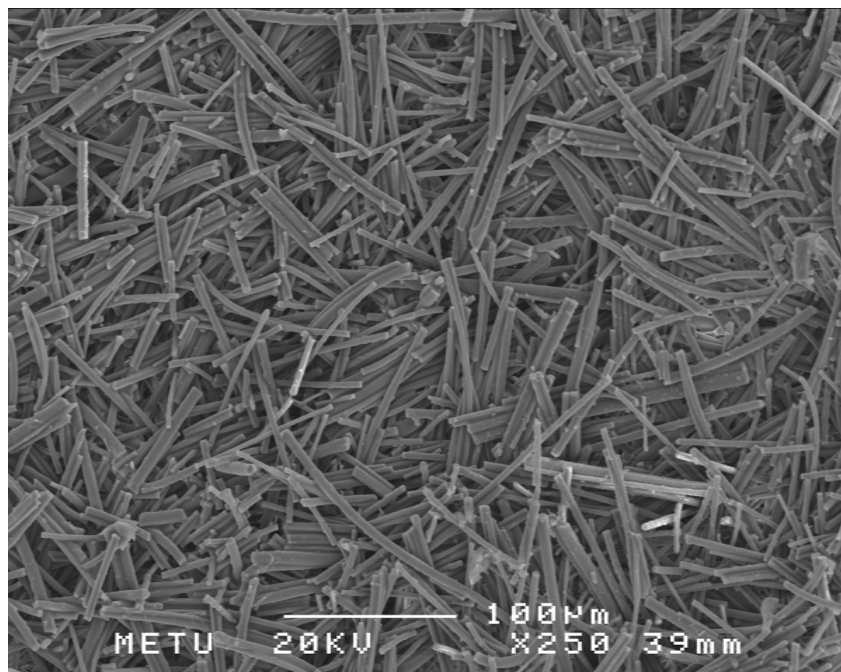
Figure 3.4 SEM image of 25 vol% Saffil fiber preforms vertical to the fiber orientation.
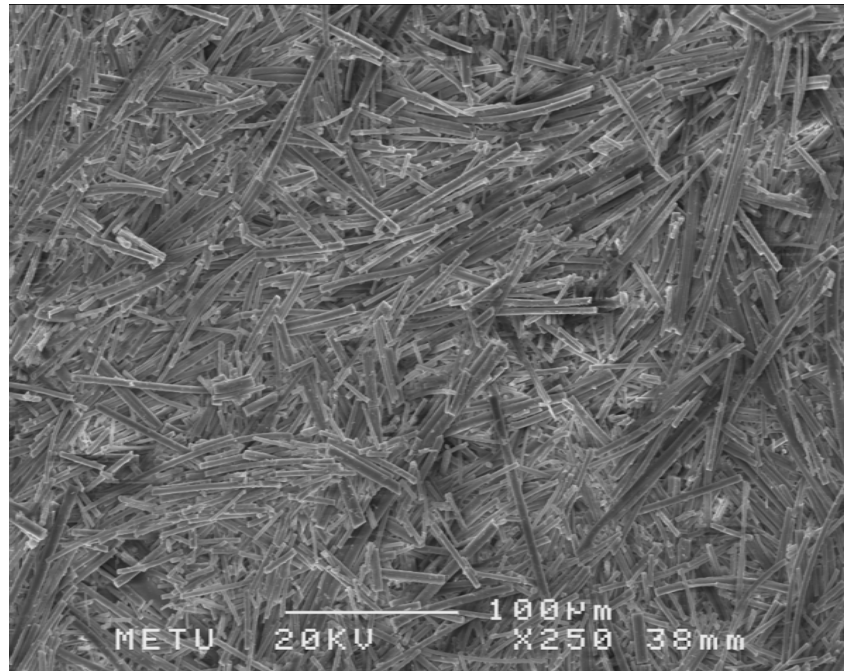
Figure 3.5 SEM image of 30 vol% Saffil fiber preforms vertical to the fiber orientation.

The planar isotropic orientation of fibers which is due to production technique can be observed from the difference of the images taken from parallel and vertical fiber orientation which is shown in Figure 3.6.
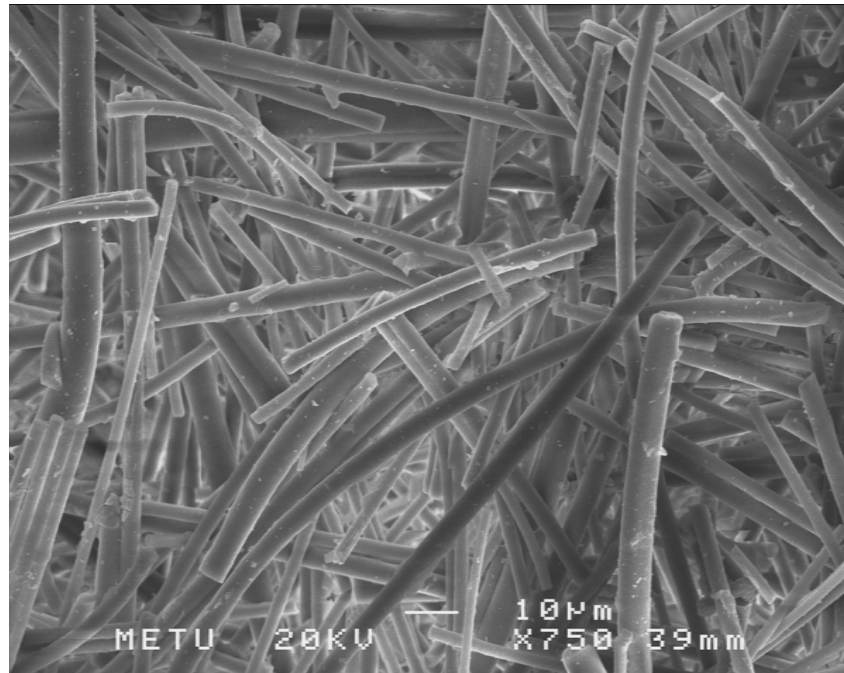
(a)
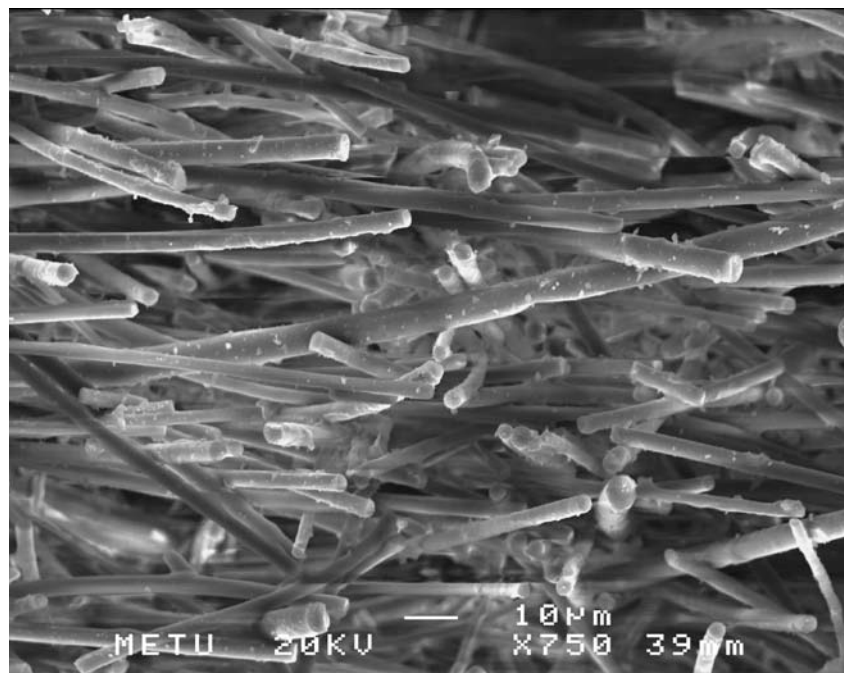
(b)

Figure 3.6 SEM image of 10 vol% Saffil fiber preform a) vertical to the fiber orientation and b) parallel to the fiber orientation.

3.3   Production of Saffil Alumina Fiber Reinforced AlSi10Mg Alloy Matrix Composite:

Vacuum assisted gas pressure infiltration setup was manufactured for Saffil alumina fiber reinforced composite production but the experiments were not successful. Pressure difference required for infiltration was not achieved because isolation between vacuum and gas atmosphere at high temperatures was insufficient. There was pressure leakage from high pressure toward the chamber at vacuum. The picture of the setup is given in Figure 3.7. Production of Saffil alumina fiber reinforced AlSi10Mg matrix composite was done by vertical squeeze casting machine, which is shown in Figure 3.8, through the following steps:

1. Steel mould was manufactured in order to use as a pattern for aluminum moulds and cores.
2. Shell core sand was poured into the steel mould.
3. Shell core sand was baked at 220 °C for 30 minutes to produce cores.
4. Sand mould was produced for aluminum casting.
5. Cores were removed and put into the sand mould.
6. Aluminum sand casting was done to produce aluminum moulds for composite production.
7. Aluminum casting was taken off.
8. Core sand of the aluminum moulds was cleaned.
9. Zirconium silicate dye was painted onto the aluminum moulds in order to avoid sticking of the composites to the die wall.
10. Preforms in the shape of bending specimen were put into the aluminum mould.
11. Preforms and aluminum moulds were heated to 200 °C in a separate furnace.
12. Chemical composition of the AlSi10Mg alloy was adjusted and Inducto-therm induction furnace was used to get the liquid phase. Magnesium addition was done after complete melting.
13. Squeeze casting mould was heated to 190 °C and detailed mould temperatures are given in Appendix A.

14. Aluminum mould having preforms was put into the pressure die casting mould.

15. The liquid alloy was poured into the mould at 750 °C and 800 °C.

16. Squeeze casting process was started. Mould was automatically closed and 108 MPa pressure was applied for 15 seconds.

17. The aluminum mould with excess matrix materials was taken out.

18. The moulds were cut to get the composites.

19. The resulting composites were grinded and polished.

Schematic representation of the composite production steps is given in Figure 3.9. Five types of (10, 15, 20, 25, 30 vol% Saffil fiber) of three point bending test specimens were obtained. Dimensions of the specimens were around 48×12×7 mm in x, y and z directions.
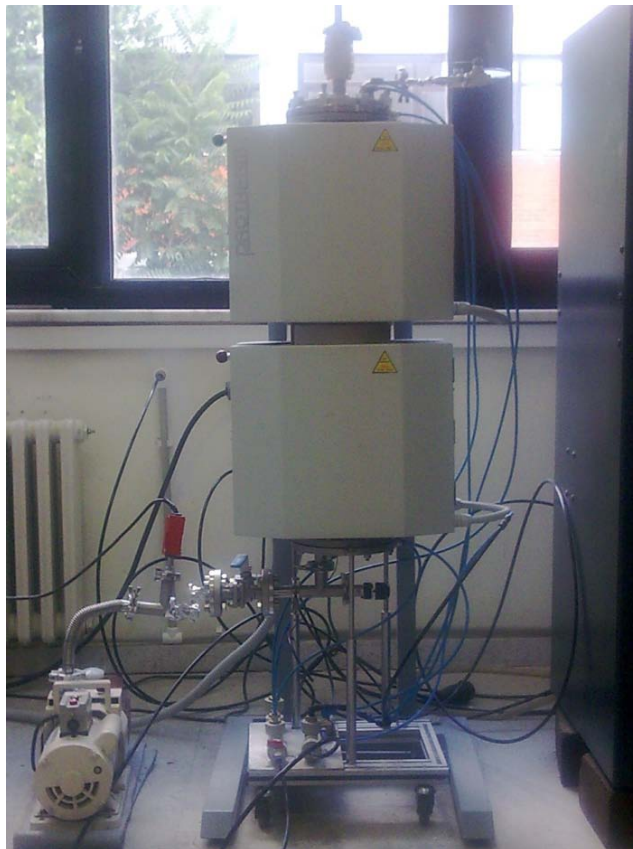
Figure 3.7 Vacuum assisted pressure infiltration furnace.
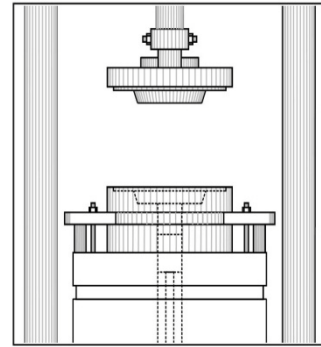
(a)   **(b)**

Figure 3.8 Vertical squeeze casting machine a) Actual view b) Closer view.

1 Steel mould

2 Shell core sand pouring

3 Shell core sand baking

4 Sand mould production

5 Core placing

6 Aluminum casting

7 Aluminum mould

8 Core sand cleaning

9 Zirconium silicate painting

10 Preform placing

11 Preform and mould heating

12 Alloy melting

13-14 Squuze casting die and mould heating

15 Liquid alloy pouring

16 Infiltration by squuze casting

17 Mould and excess alloy removal

18-19 Composite cutting and polishing

Figure 3.9 Schematic representation of composite production steps.

3.4   Density measurement

Density measurements are done according to Archimedes' principle. Composites are dipped into xylol solution and waited for 72 hours. The weight of the composites was measured with a sensitivity of 10^{-4} gr under normal atmosphere. Then the volume of the composite is calculated by finding the difference between the weight of the specimen hanging in a cup of xylol and in air with the xylol film on the specimen. The density which is the ratio of weight of the composite to the volume is calculated. The formulas used for density and porosity calculation are as follows:

$$V = \frac{\left(m_{specimen,air/xylol} - m_{specimen,xylol/xylol} \right)}{\rho_{xylol}} \tag{3.1}$$

$$\rho = \frac{m_{specimen,air}}{V} \tag{3.2}$$

$$P\%(Total) = \left(100 - \left(\frac{\rho}{\rho_{theoretical}} \right) \times 100 \right) \tag{3.3}$$

$$P\%(Open) = \frac{Volume\ of\ xylol\ in\ pores}{V(specimen)} = \frac{\left(\frac{m_{specimen,air/xylol} - m_{specimen,air}}{0.861} \right)}{V(specimen)} \tag{3.4}$$

$$P\%(Closed) = P\%(Total) - P\%(Open) \tag{3.5}$$

Where V is the experimental volume of the matrix and composites, $m_{specimen,air/xylol}$ is the weight of the specimen coated with a thin layer of xylol in air, $m_{specimen,xylol/xylol}$ is the weight of the specimen hanging in a cup of xylol, ρ_{xylol} is the density of the xylol, $m_{specimen,air}$ is the weight of the specimen in air, P%(Total) is the total pore percent, ρ is the experimental density of the matrix and

composites, $\rho_{\text{theoretical}}$ is the theoretical density of the matrix and composites, P%(Open) is the open pore percent and P%(Closed) is the closed pore percent.

3.5   Mechanical Testing and Testing Apparatus

Three point bending tests were done for three specimens of five compositions. Tests were done with Shimadzu test machine according to modified ISO 7438:2005 bend test standard.

Hardness tests were done by Emco Automatic hardness test machine. Brinell 62,5 kg hardness values were acquired. The average of the hardness values are taken from surfaces parallel and vertical to the fiber orientation.

3.6   Calculations

The maximum fracture loads were taken in three-point bending tests. The Newton values of the loads were converted into flexural stress (MPa) values. The flexural stress is defined as:

$$\sigma = \frac{M \cdot y}{I}$$
(3.6)

where σ, M, *y* and I are flexural stress, bending moment, the distance from the natural axis and the moment of inertia respectively. The maximum flexural surface stress occurs in the middle of the specimen and the according equations are valid for rectangular prism shape:

$$M = P \cdot (L/4)$$
(3.7)

$$y = t/2$$
(3.8)

$$I = b \cdot (t^3/12)$$
(3.9)

$$\sigma_{max} = \frac{(3 \cdot P \cdot L)}{(2 \cdot b \cdot t^2)} \tag{3.10}$$

where, P, t, b and L are the load applied by testing machine, the thickness, the width and the span length of the specimen respectively.

3.7   Metallographic Examination

Microstructures of alumina fiber reinforced aluminum composite samples were examined by optical microscopy. Samples are cut and put into bacalite. Automatic polishing was done and etched with Keller solution which contains 1,5% HCl, 2,5% HNO3, 1% HF, 95% H2O. The representative photographs of the resulting samples are taken by an optical microscope.

3.8   X-Ray Study

X-ray studies were made to find out any phase occurred at the matrix-fiber interface. Any other phases that may form during pressure die casting were revealed by x-ray analysis. X-ray analysis was made by Rigaku D MAX 2200 PC diffractometer which uses Cu x-ray tube.

3.9   Scanning Electron Microscope (SEM) Study

The detailed structure of the composite was studied by SEM to see different phases which may form between fiber and in the matrix during infiltration. Chemical analysis was done and according graphs were obtained. SEM studies were done with JSM-6400 Electron Microscope (JEOL), equipped with NORAN System.

CHAPTER 4

RESULTS AND DISCUSSION

In this study the effects of alumina fiber addition, magnesium addition into matrix and temperature of the liquid alloy on the mechanical behavior of aluminum alloy matrix composites was examined. Hardness test and density measurement was also done to reveal the effect of five different vol% of alumina fiber reinforcement which are given in Table 4.1.

Table 4.1 List of Saffil alumina fiber (vol%) reinforced aluminum matrix composites.

% $Al_2O_{3\,(f)}$ addition	Description
Al – 0% $Al_2O_{3\,(f)}$	0 vol% fiber reinforced, pressure die cast Al alloy matrix
Al – 10% $Al_2O_{3\,(f)}$	10 vol% fiber reinforced, pressure die cast Al alloy matrix
Al – 15% $Al_2O_{3\,(f)}$	15 vol% fiber reinforced, pressure die cast Al alloy matrix
Al – 20% $Al_2O_{3\,(f)}$	20 vol% fiber reinforced, pressure die cast Al alloy matrix
Al – 25% $Al_2O_{3\,(f)}$	25 vol% fiber reinforced, pressure die cast Al alloy matrix
Al – 30% $Al_2O_{3\,(f)}$	30 vol% fiber reinforced, pressure die cast Al alloy matrix

4.1 Density Measurement

Density measurement was conducted to find out the closed porosity level of the composites. As seen from Figures 4.1, through 4.4 the difference between experimental and theoretical densities increased with increasing alumina fiber

content. The difference between theoretical and experimental density was highest for 30 vol% alumina fiber addition which was 8.3407 % for AlSi10Mg0.3 matrix cast at 800 °C. This was related to the high pressures needed to infiltrate micro pores between the fibers. A. Mortensen and T. Wong showed that the pressure required to infiltrate micro pores was infinite due to capillary forces [33]. Due to the increased fiber content, the number of fiber cross-links and fiber interactions raised which in turn increased the level of micro porosity. Moreover, due to the movement of the fibers during infiltration, the fiber content locally increased which resulted in high vol% fiber areas which were hard to infiltrate. The shrinkage of the matrix alloy could also cause micro pores but the high pressure used during infiltration prevented this kind of micro pore evolution. The closed porosity values are compared in Figure 4.5.
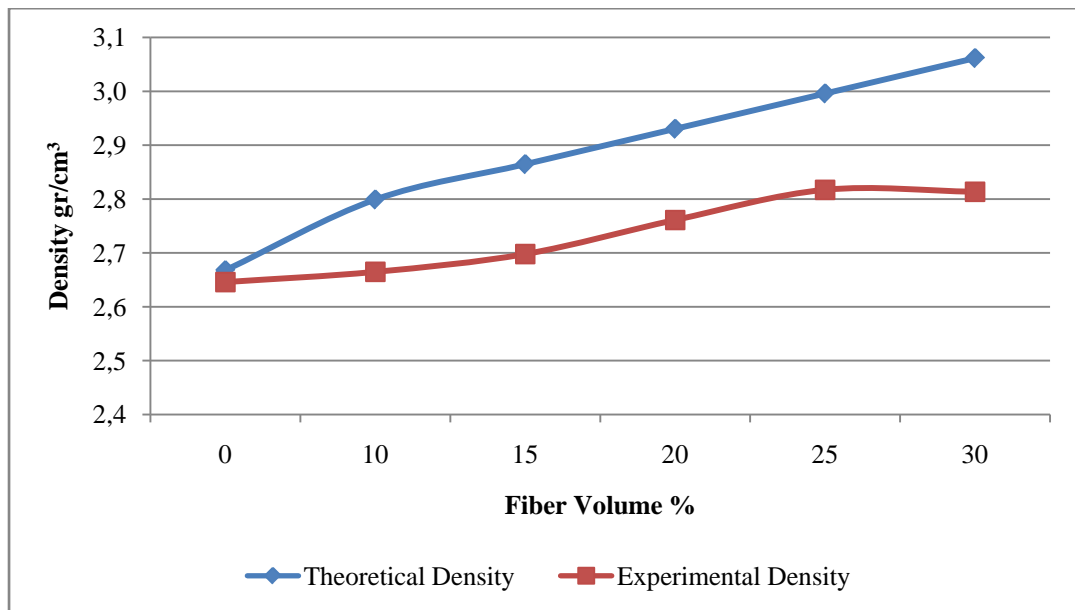
Figure 4.1 Theoretical and experimental density values of AlSi10Mg0.3 matrix composite cast at 750 °C.
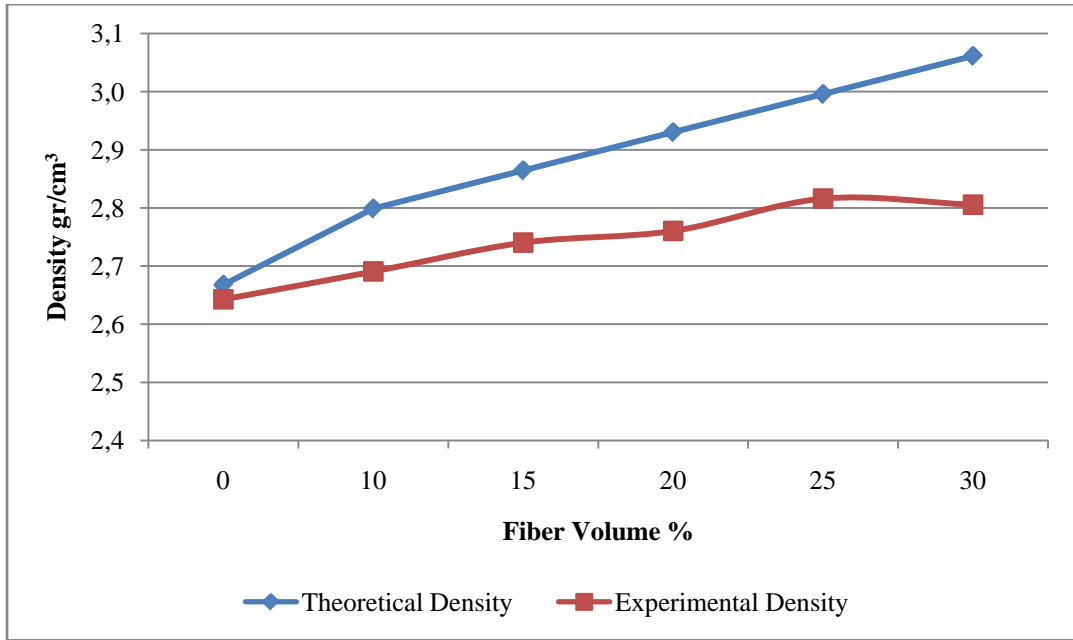
Figure 4.2 Theoretical and experimental density values of AlSi10Mg0.3 matrix composite cast at 800 °C.
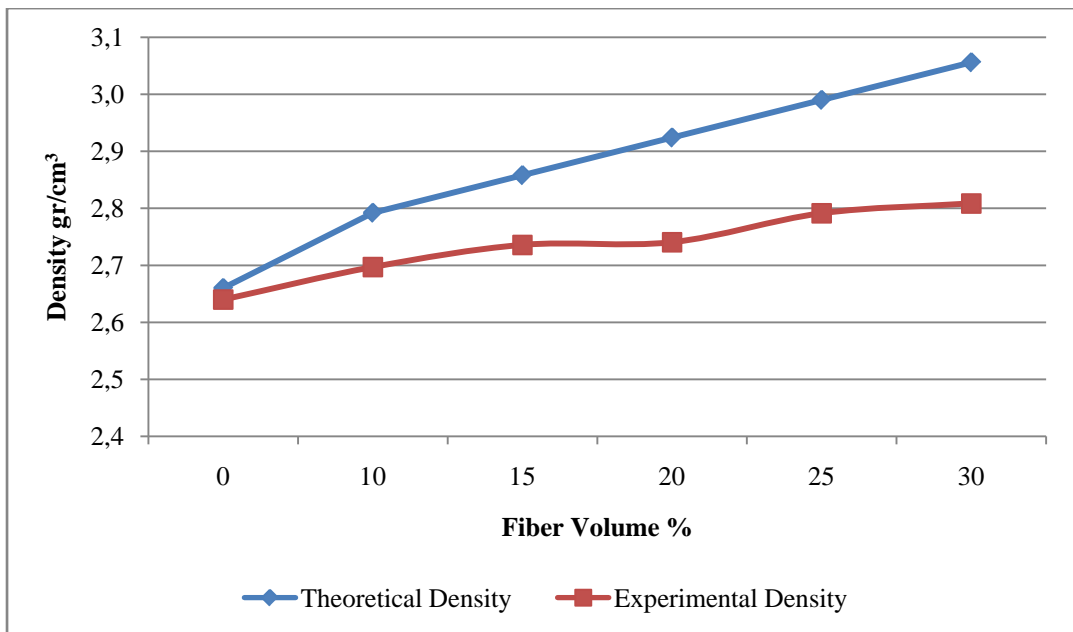
Figure 4.3 Theoretical and experimental density values of AlSi10Mg1 matrix composite cast at 750 °C.
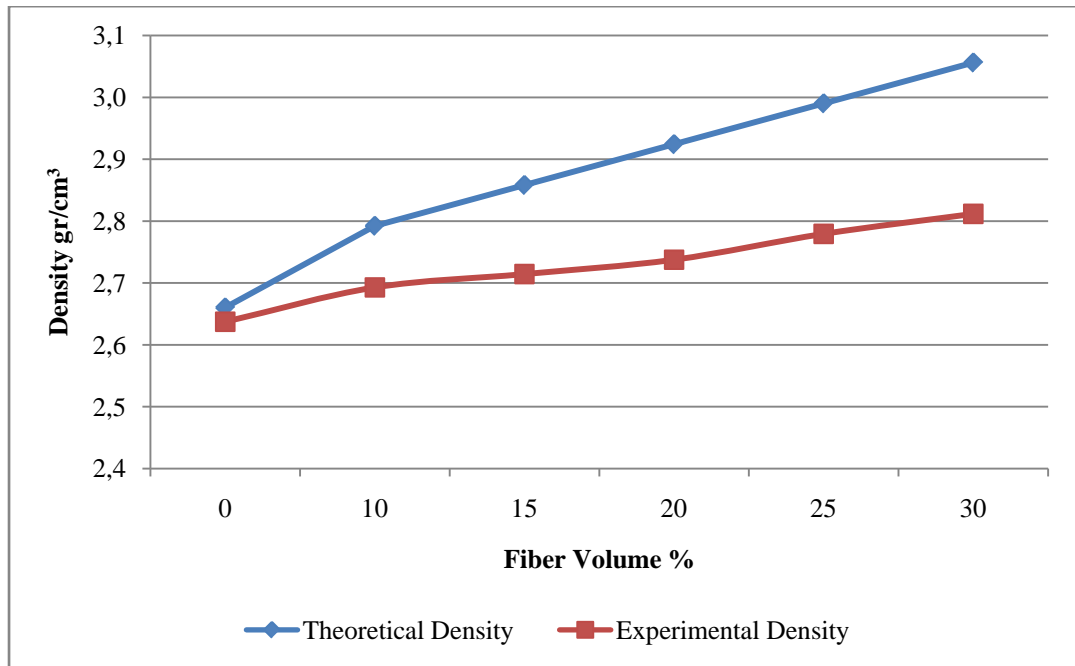
Figure 4.4 Theoretical and experimental density values of AlSi10Mg1 matrix composite cast at 800 °C.
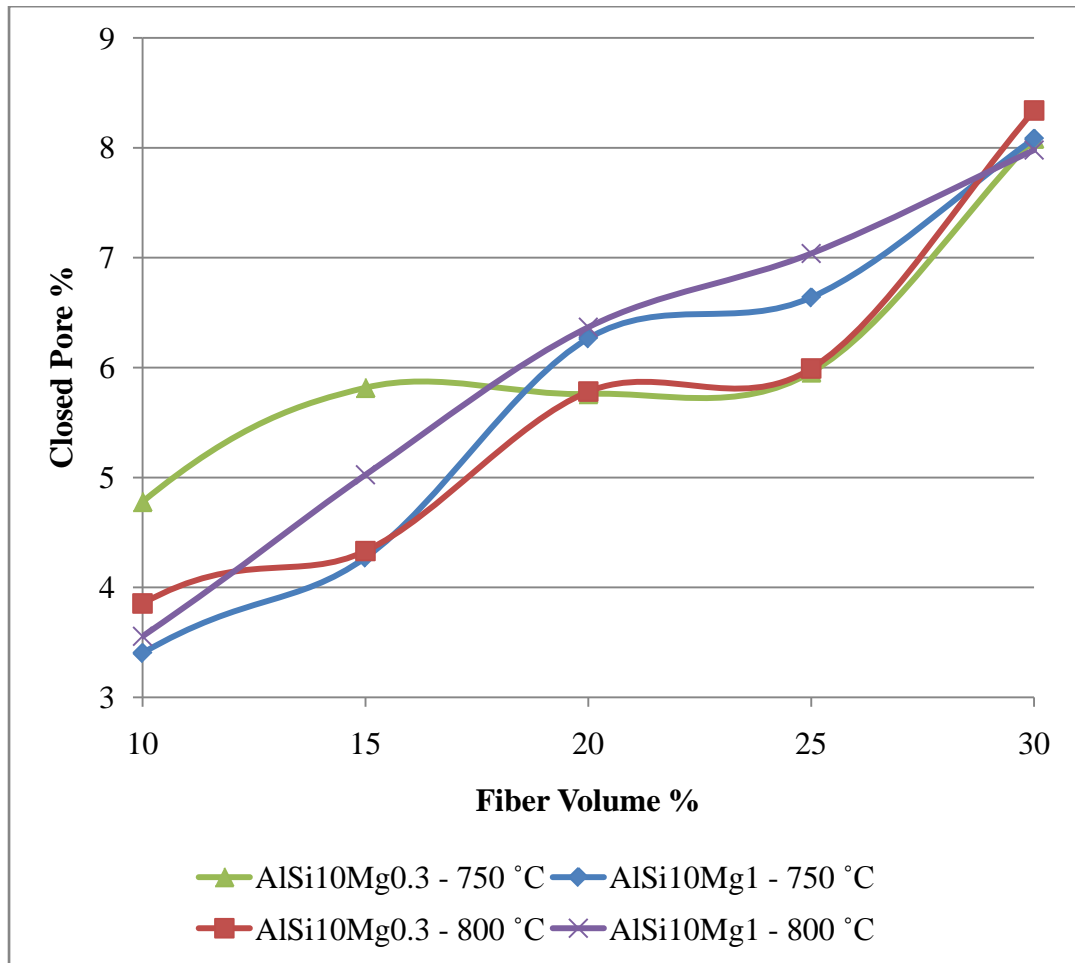
Figure 4.5 Closed pore % comparison of composites.

Data obtained during density measurements are given in Appendix B.

4.2 Hardness Test Results

Hardness tests were done to find out effects of fiber addition on aluminum alloy matrix because hardness is an important indicator of a materials resistance to plastic deformation. Figure 4.6 and 4.7 show the comparison and variation in hardness values with vol% alumina fiber, fiber orientation, casting temperature and magnesium content of matrix. Minimum and maximum values are also shown as bars in the graphs. Detailed hardness test results are given in Appendix C.
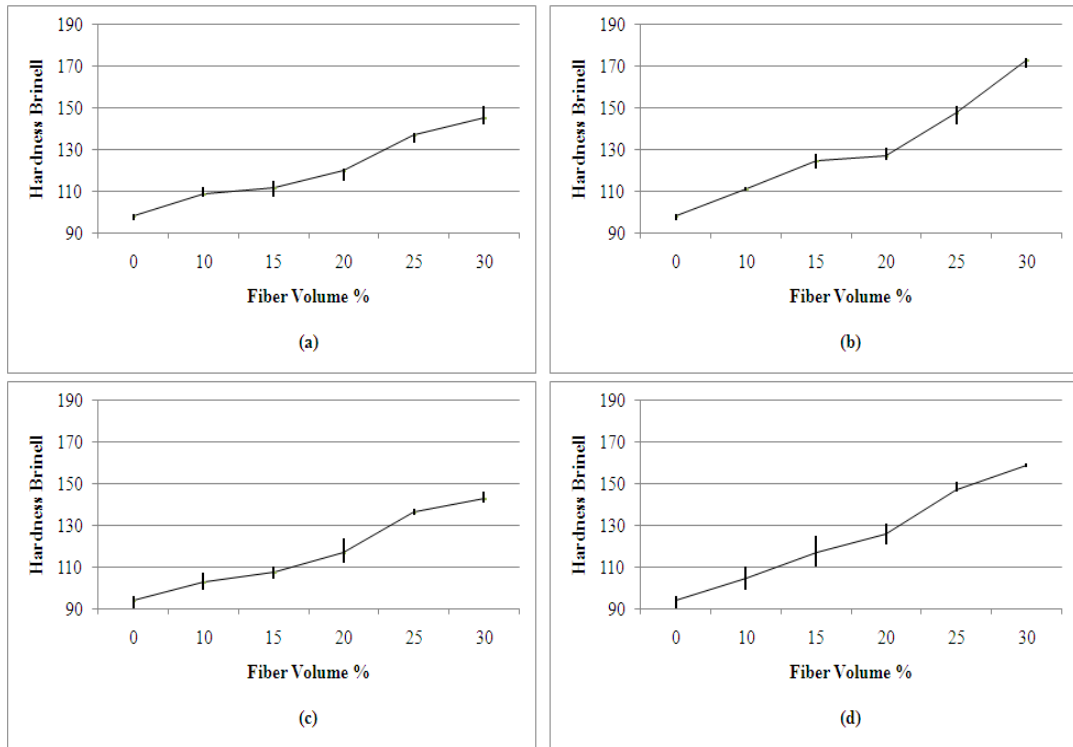
Figure 4.6 Comparison and variation in hardness values taken a) vertical, b) parallel to the fiber orientation of AlSi10Mg0.3 matrix composite cast at 750 °C, c) vertical, d) parallel to the fiber orientation of AlSi10Mg0.3 matrix composite cast at 800 °C.
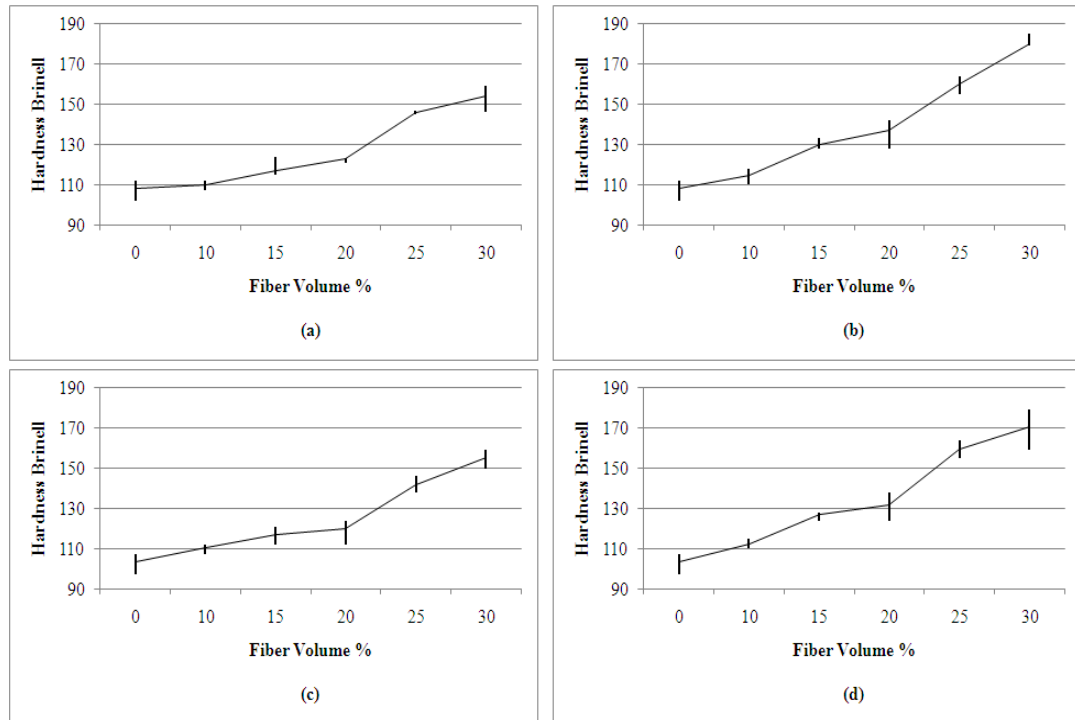
Figure 4.7 Comparison and variation in hardness values taken a) vertical, b) parallel to the fiber orientation of AlSi10Mg1matrix composite cast at 750 °C, c) vertical, d) parallel to the fiber orientation of AlSi10Mg1 matrix composite cast at 800 °C.

It can be observed from Figures 4.6 and 4.7 the hardness values increased with the addition of alumina fiber. Alumina fibers as being the ceramic phase of the composite they are much harder than the aluminum alloy matrix. They hindered the dislocation motion and resulted in a strain hardening. The increased fiber volume also decreases the grain and subgrain size which increases the hardness [40]. The results from the direction parallel to the fiber orientation were higher than the results from the direction vertical to the fiber orientation. Because fibers parallel to the surface did not show as high resistance as the fibers transverse to the surface of the indentation. The highest hardness value vertical and parallel to the fiber orientation was 155.6 and 180.2 for AlSi10Mg1 matrix 30 vol% alumina fiber reinforced composite cast at 800 °C and AlSi10Mg1 matrix 30 vol% alumina fiber reinforced composite cast at 750 °C respectively.

The more the magnesium content the more the hardness was and for 750 °C cast composite the hardness values were higher than the 800 °C cast composites. Magnesium increased the hardness due to the solid solution hardening which is effective especially at low levels < 1 at% [41]. The casting temperature decreased the grain size because the heat needed to be conducted during solidification was less which means faster cooling for the same mould temperature.

4.3 Three Point Bending Test Results

Three point bending tests were performed to observe the flexural strength and fracture behavior of aluminum alloy matrix composites with different percentage additions of alumina fiber. Several three point bending tests were done and their average results are listed in Table 4.2 and details are given in Appendix D. Comparison of the results and standard deviations are given graphically in Figure 4.8 as well.

Table 4.2 Average flexural strength values of AlSi10Mg0.3 and AlSi10Mg1 alloy composites produced at 750 °C and 800 °C.

Composite	Average Flexural Strength AlSi10Mg0.3		Average Flexural Strength AlSi10Mg1	
	750 °C	800 °C	750 °C	800 °C
Al – 0% $Al_2O_{3(f)}$	495.03	475.83	477.24	451.91
Al – 10% $Al_2O_{3(f)}$	370.69	391.30	392.91	368.47
Al – 15% $Al_2O_{3(f)}$	401.56	439.92	435.37	425.93
Al – 20% $Al_2O_{3(f)}$	492.62	479.02	485.37	454.00
Al – 25% $Al_2O_{3(f)}$	512.15	504.59	500.87	497.07
Al – 30% $Al_2O_{3(f)}$	547.84	545.47	520.97	514.65
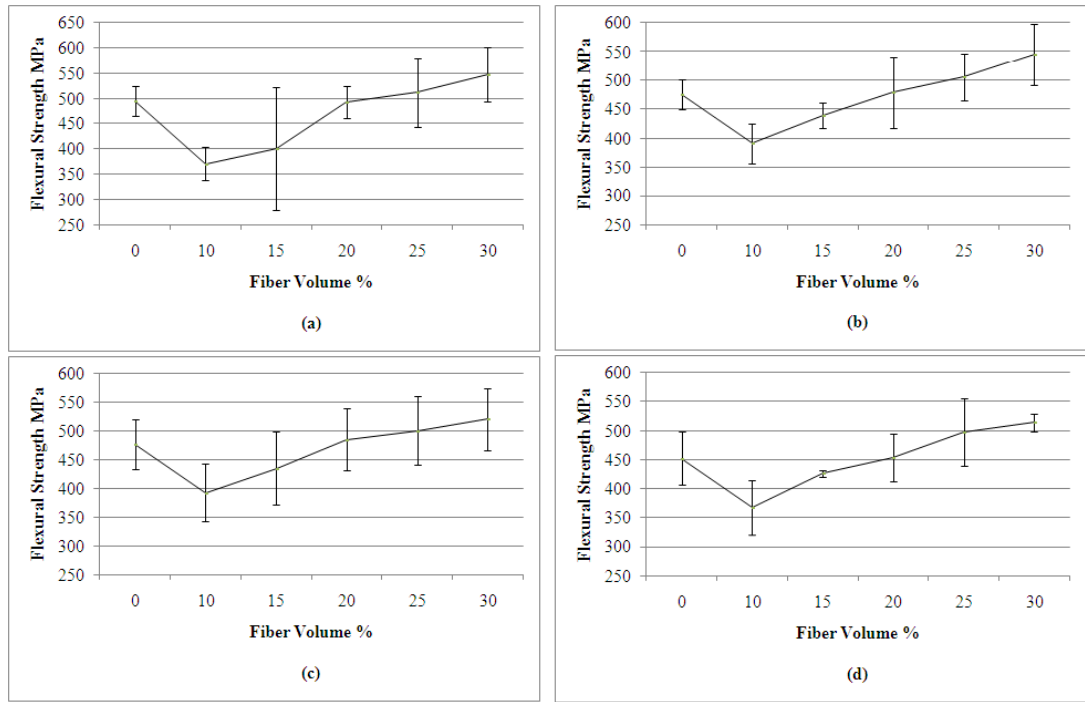
Figure 4.8 Variation in flexural strength of a) AlSi10Mg0.3 matrix composite cast at 750 °C b) AlSi10Mg0.3 matrix composite cast at 800 °C c) AlSi10Mg1matrix composite cast at 750 °C d) AlSi10Mg1 matrix composite cast at 800 °C.

The flexural strength values for the composites increased with the increase in non-reinforced alloys' tensile strengths. The highest value was for AlSi10Mg0.3 alloy cast at 750 °C and the values increased with decreasing magnesium content and decreasing casting temperature for both reinforced and non-reinforced materials. The flexural strength decreased when 10 vol% alumina fiber was present and then started to increase as the alumina fiber content increases which is an expected situation for short fiber reinforced metal matrix composites. All the composites reached unreinforced alloy strength at about 20 vol% alumina fiber addition. This is mainly due to the high critical fiber content needed to have an effective strengthening. From the formula;

$$\sigma_C = \eta \cdot C \cdot \varphi_F \cdot \sigma_F \cdot \left(1 - d_F\left(\frac{\sigma_F}{2 \cdot l_m \cdot \sigma_M^*}\right)\right) + (1 - \varphi_F) \cdot \sigma_M^* \tag{4.1}$$

theoretical critical fiber content ($\varphi_{F,critical}$) was calculated as 16 vol. percent for the AlSiMg0.3 alloy assuming 0.7 fiber efficiency. As a result, the flexural strength values were not to be expected to increase unless there is at least 16 vol. percent alumina fiber was present in the composites under tensile stresses for this alloy. However, the experimental values showed that the critical fiber content is nearly 20 vol. percent for all composites. This is an indication of the lower fiber efficiency and/or the higher critical fiber content needed for bending stresses.

In addition, the fiber lengths were decreased with increasing fiber content which was due to high pressure applied during infiltration and preform production process [42]. Critical fiber lengths for each alloy - casting temperature system were calculated according to tensile strengths from the formula below and are given in Table 4.3.

$$l_C = \frac{\sigma_F \cdot d_F}{2 \cdot \tau_{FM}} \tag{4.2}$$

Table 4.3 Critical fiber lengths for AlSi10Mg0.3 and AlSi10Mg1alloys produced at 750 °C and 800 °C.

Composite	σ_F (MPa)	d_F (µm)	σ_M (MPa)	lc (µm)
AlSi10Mg0.3 750 °C	2000	3	268.5	22.35
AlSi10Mg0.3 800 °C	2000	3	250.75	23.93
AlSi10Mg1 750 °C	2000	3	235.75	25.45
AlSi10Mg1 800 °C	2000	3	215.25	27.87

Critical fiber length was calculated as 27.87 µm for the lowest strength alloy and 22.35 µm for the highest strength alloy. Saffil fiber preforms used in experiments had a decreasing average fiber length with increasing fiber vol% which is given in Table 4.4. As a result there was a decrease in effective fiber strengthening mechanism due to decrease in fiber length. However, the fiber lengths were still at least 4 times higher than the critical fiber length.

Table 4.4 Average fiber length in Saffil short fiber reinforced aluminum composites [42].

Fiber Volume (%)	Fiber Length (µm)
10	154
15	146
20	141
25	134
30	118

The 30 vol% Saffil alumina fiber reinforced AlSi10Mg0.3 matrix composite cast at 750 °C showed the highest flexural strength. The reinforcing effect of the fibers was observed because 30 vol% alumina fiber addition was higher than the critical fiber content. The bonding between fiber and matrix was not degraded with excess reactions because the temperature of the preforms was 190 ℃ which was relatively low for reactions to occur fast. The microstructure of the matrix was changed, dislocation density is increased, grain and sub-grain size was decreased by short fiber reinforcement which all increased the strength of the composite [12, 40].

The flexural strength values did not increased much for 30 vol% alumina fiber reinforced composite compared to 25 vol% alumina fiber reinforced ones which was attributed to increased porosity, local increase in fiber content and fiber breakage. The high porosity levels were evident from the density measurements. There is also a 10 % decrease in fiber length between 25 vol% fiber reinforced composites and 30 vol% fiber reinforced ones. The decrease in fiber length was much higher at high fiber contents which hindered the effective reinforcing. In addition, there was much more fiber-fiber interaction for 30 vol% alumina fiber reinforced composite because of low fiber length and high fiber density. These interactions resulted in fiber breakage during three point bending test and decreased the flexural strength while the test is running [43]. Moreover, high porosity decreased the fiber matrix bonding.

The lowest values among all the composites were observed for 10 and 15 vol% Saffil alumina fiber reinforced AlSi10Mg0.3 matrix composite cast at 750 °C. The relatively low values for these composites were related to the higher closed porosity of these composites.

4.4   X-Ray Study Results

X-Ray analysis of the composites and the Saffil alumina fiber were done. The Saffil alumina fibers are mainly consists of delta alumina and small amount of silica. Composites were analyzed to find out if there was an excess reaction occurred between fiber and matrix. The reaction 2.3 could degrade fiber and lower the composite strength.

The entire XRD pattern showed that aluminum, silicon and alumina were present in the composite. Aluminum gives 2θ peaks at 38º, 44º, 65º, 78º, 82º; silicon gives 2θ peaks at 28º, 47º, 56º, 76º, 88º and delta alumina give 2θ peaks at 36º, 39º, 45º, 46º and 67º. On the XRD patterns, which are given in Figures 4.9 through 4.13. No other phase was observed which is related to the low preform temperature, fast infiltration and solidification. With this respect, any reaction between fiber and matrix were not kinetically favored and no reaction products observed. Any other phase was not revealed by x-ray analysis. As the fiber content increased the strongest peak of alumina was increased for all the composites at around 67º. Detailed XRD patterns of searched phases are given in Appendix E.
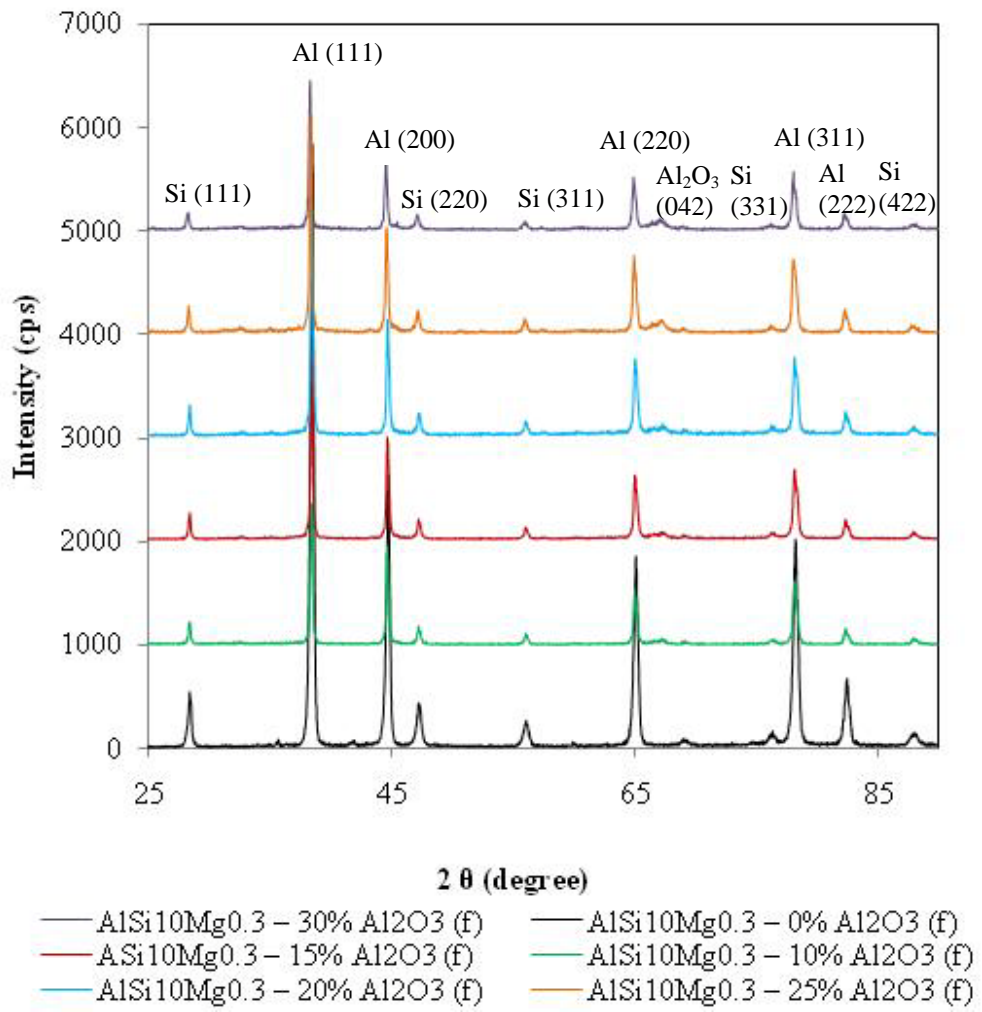
Figure 4.9 XRD pattern of AlSi10Mg0.3 alloy cast at 750 °C.
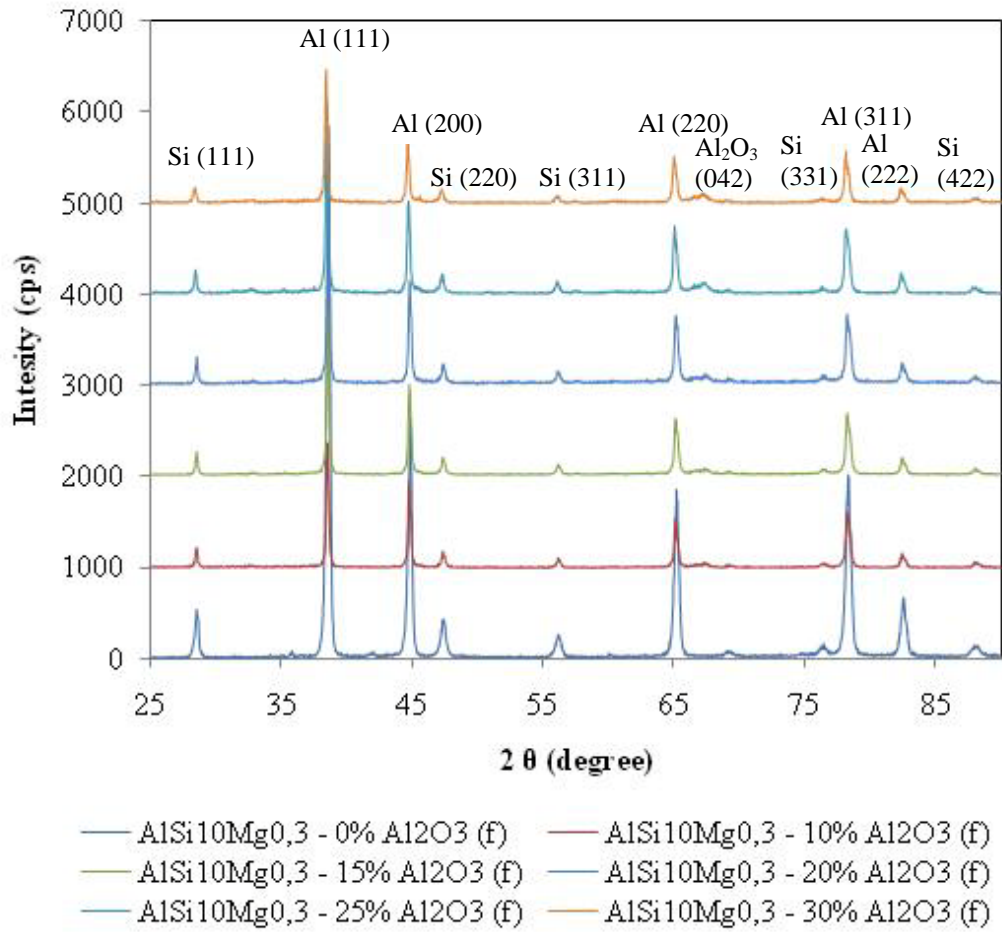
Figure 4.10 XRD pattern of AlSi10Mg0.3 alloy cast at 800 °C.
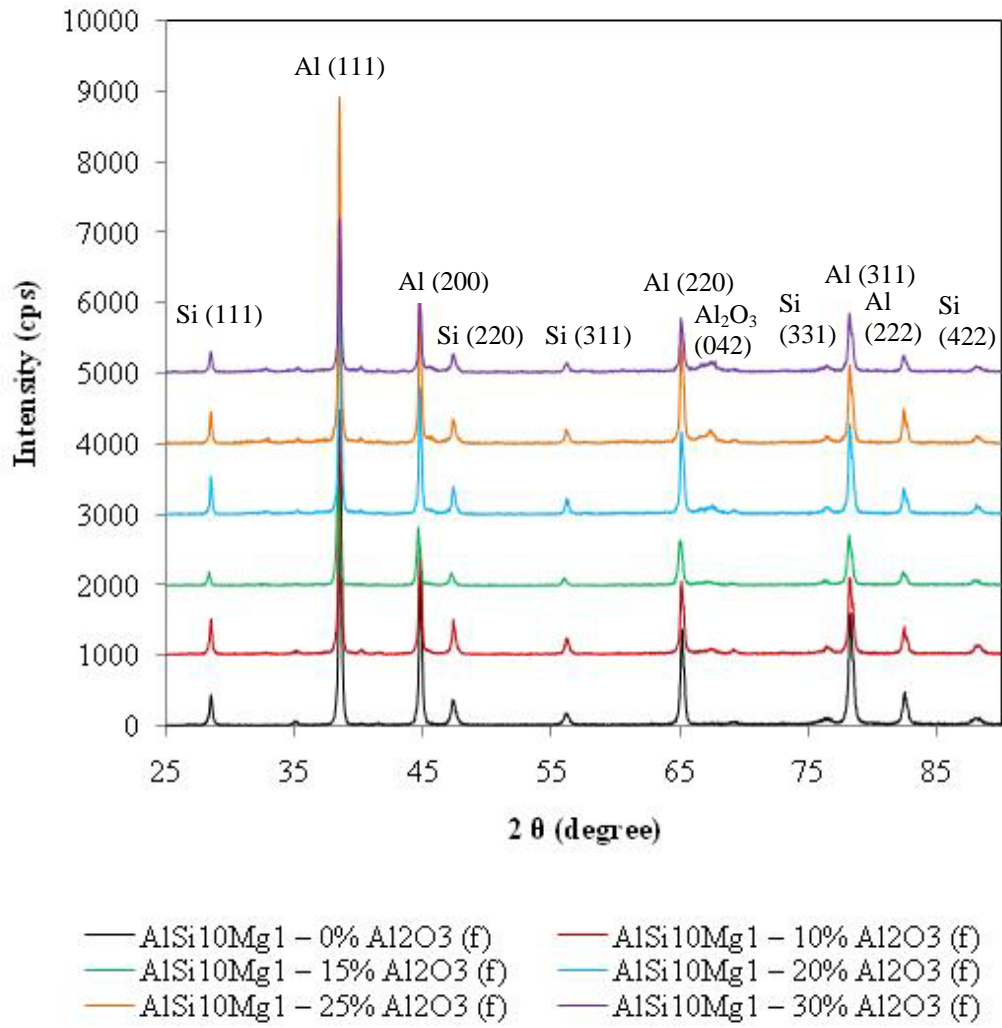
Figure 4.11 XRD pattern of AlSi10Mg1 alloy cast at 750 °C.
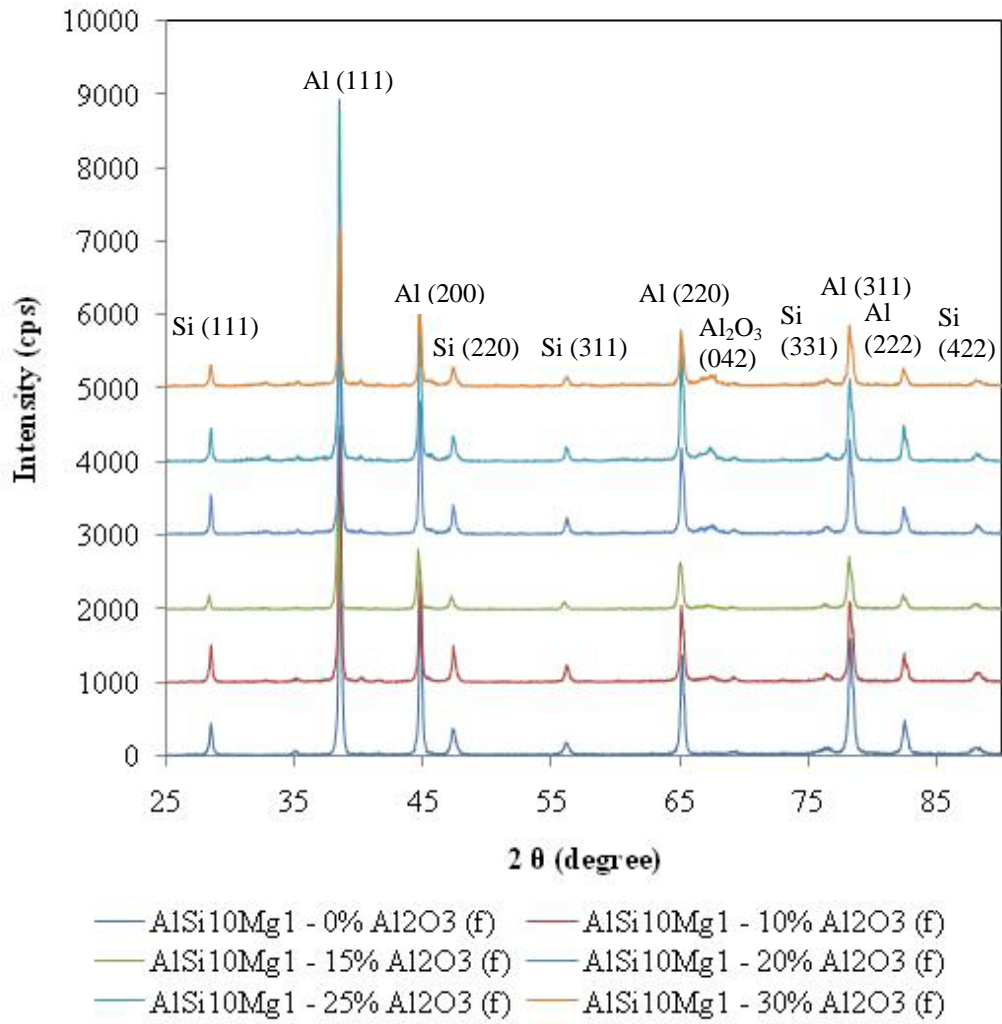
Figure 4.12 XRD pattern of AlSi10Mg1 alloy cast at 800 °C.
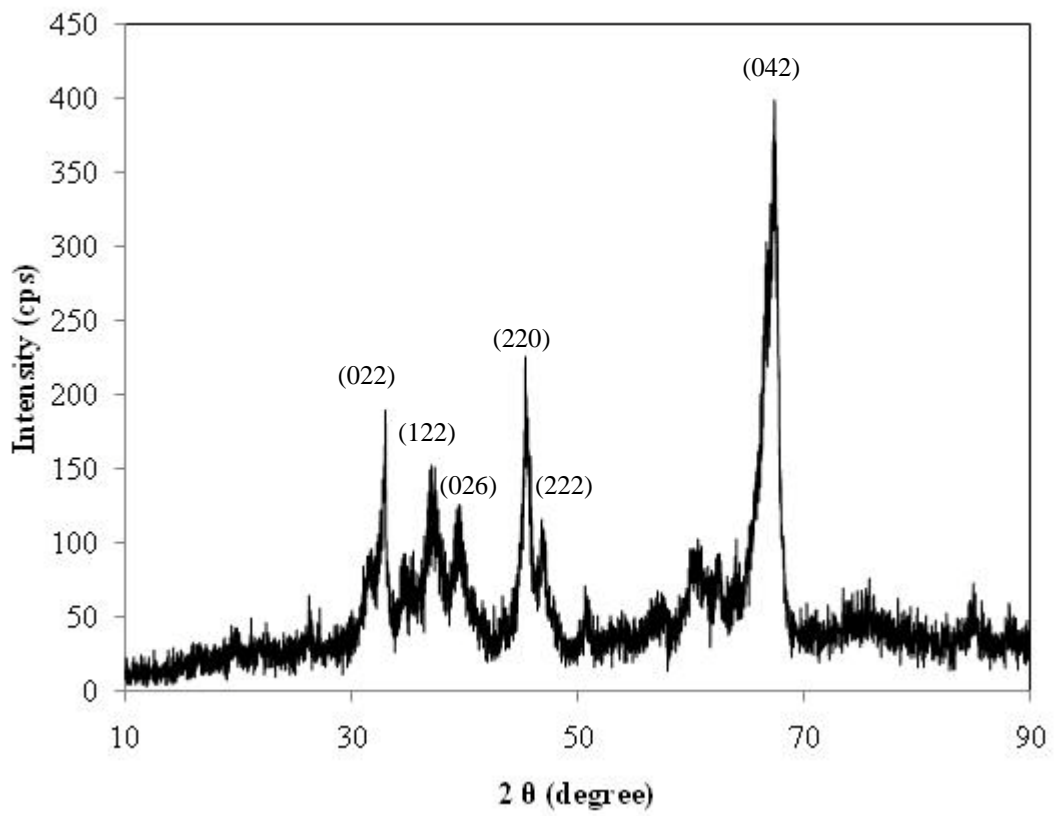
Figure 4.13 XRD pattern of Saffil delta alumina fiber which has tetragonal crystal structure.

4.5 Image Analysis Results

Saffil alumina fiber reinforced AlSi10Mg0.3 and AlSi10Mg1 aluminum alloy composites were examined by Clemex Image Analyzing Program to investigate the vol% of alumina fiber in the matrix. The results were compared with ideal theoretical values where it was assumed that preform vol% was not changed.

Composites were investigated from the surfaces parallel and vertical to the fiber orientation. At the surface parallel to the fiber orientation the fiber density was slightly higher the surface vertical to the orientation which was related to the planar isotropic alignment of the fibers.

The results of the image analyzer were the average of 3 randomly chosen areas at 50X or 200X magnification. The program makes a contrast between two phases and finds the area ratio of these phases. This ratio is than changed into vol%.

The higher vol% fiber reinforced composites were investigated at 200X magnification because at low magnification dark image of the surface resulted in miscalculation of the area ratio by the computer software. The resolution was not enough to reveal the actual contrast between the phases. Accordingly, for higher vol% composites using high magnification images for analysis was meaningful. Also for these composites local change in fiber at surface was less. As a result, increasing magnification gave more accurate data. An example of the image analysis is given in Figure 4.14.
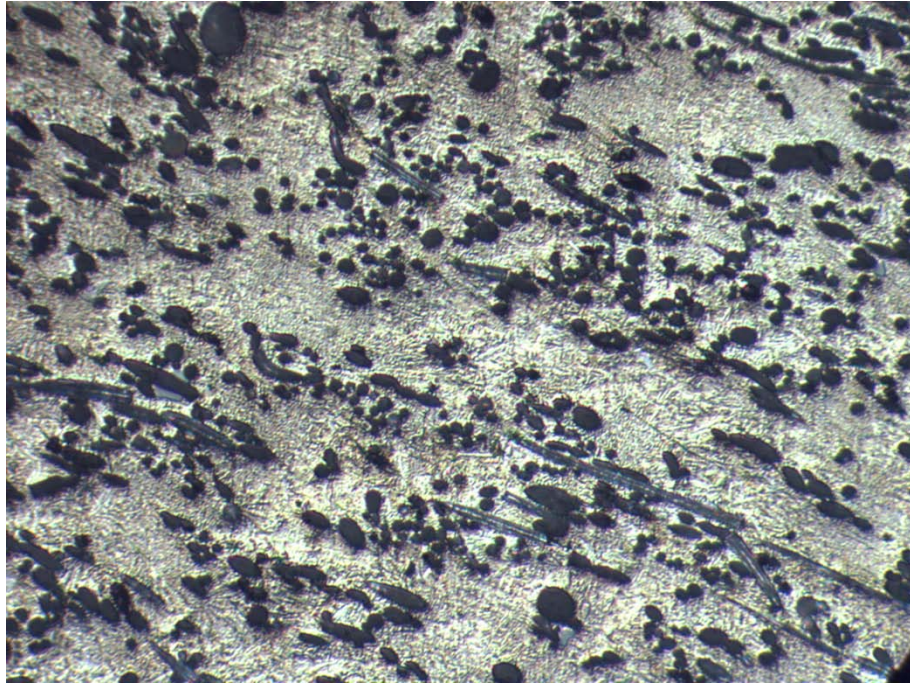
(a)
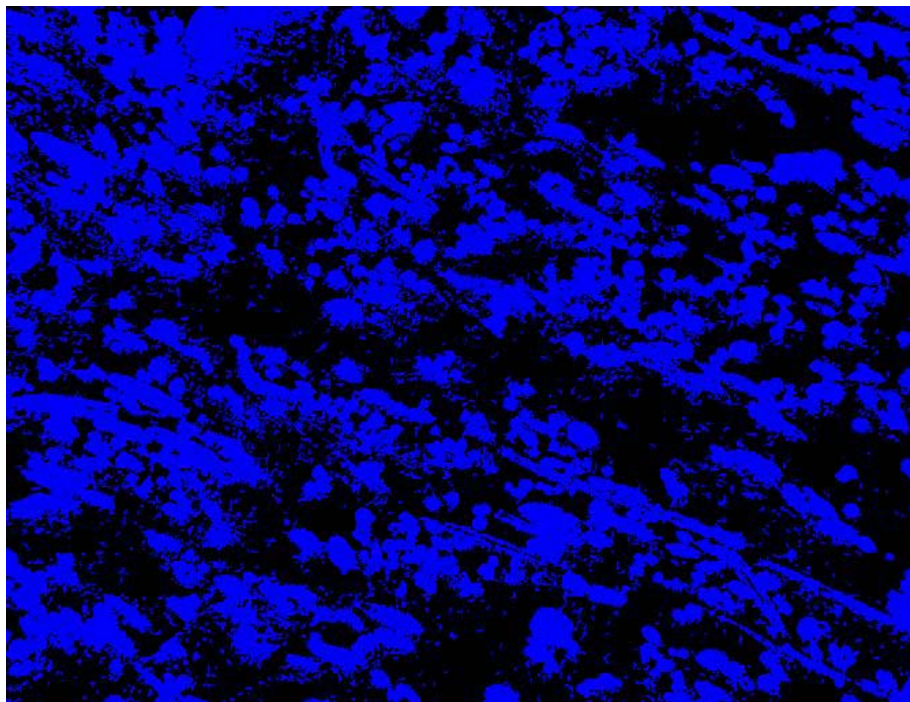
(b)

Figure 4.14 a) The sample image of 20 vol% alumina fiber parallel to the fiber orientation reinforced composite at 200X magnification b) The image after image analyzing.

Table 4.5 Image analyzer results and comparison with theoretical values.

Alumina fiber addition vol%	10	15	20	25	30
Theoretical Volume %	10	15	20	25	30
Image analysis vertical vol%	11.10	16.40	21.10	27.60	33.30
Image analysis parallel vol%	11.20	16.90	22.40	28.50	34.10
Image analysis average vol%	11.15	16.65	21.75	28.05	33.70
Difference Theo. vs. Exp. %	11.50	11.00	8.75	12.20	12.33

Vol%'s calculated by Clemex software are given in Table 4.5. It was seen that all the vol%'s were higher than the theoretical values. Images taken parallel to the fiber orientation accounted for higher vol%'s, which was attributed to more uniform distribution of fiber in this direction. Images taken vertical to the fiber orientation showed inhomogeneous distribution of fibers. 20 vol%, 25 vol% and 30 vol% composites had better uniformity for both parallel and vertical to the fiber orientation. The closest value to the theoretical vol% was for 20 vol% fiber reinforced composite and the highest deviation from theoretical value was for 30 vol% fiber reinforced composite. The highest difference between theoretical and experimental values was 12.33 % for 30 volume % fiber reinforced composites. This was because of local fiber breakages and required high contrast which decreases with increase in magnification.

4.6   Scanning Electron Microscopy Results

The fracture surface and detailed microstructure analysis were done by scanning electron microscope. Back scattered SEM images gave the best contrast between the fibers and matrix which also simplified the investigation of other phases occurred in the composite. But as it can be observed from Figure 4.15 through 4.24, there are only two phases present; matrix and Saffil fibers. Fiber distribution was homogenous and prefoms did not damage during squeeze casting which indicates that high pressure process is suitable for infiltration. The difference between normal and back scattered SEM images can be seen from Figure 4.25.
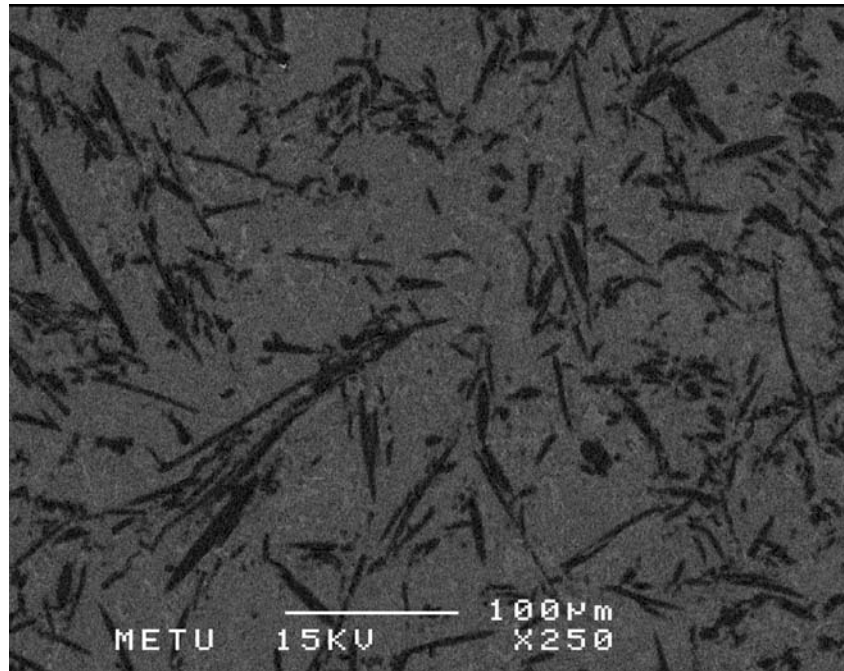
Figure 4.15 Back scattered SEM image of 10 vol% Saffil fiber reinforced AlSi10Mg composite vertical to the fiber orientation.
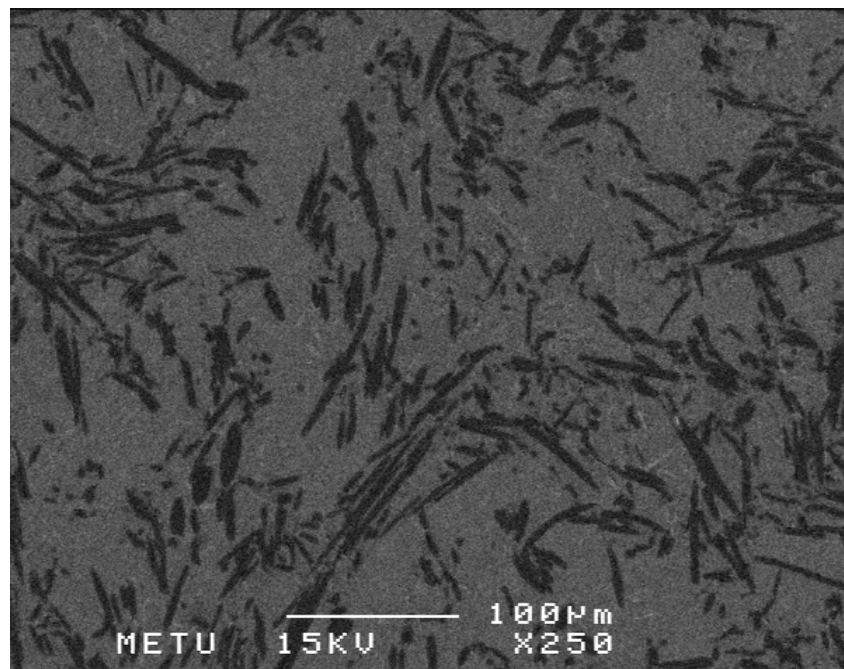
Figure 4.16 Back scattered SEM image of 15 vol% Saffil fiber reinforced AlSi10Mg composite vertical to the fiber orientation.
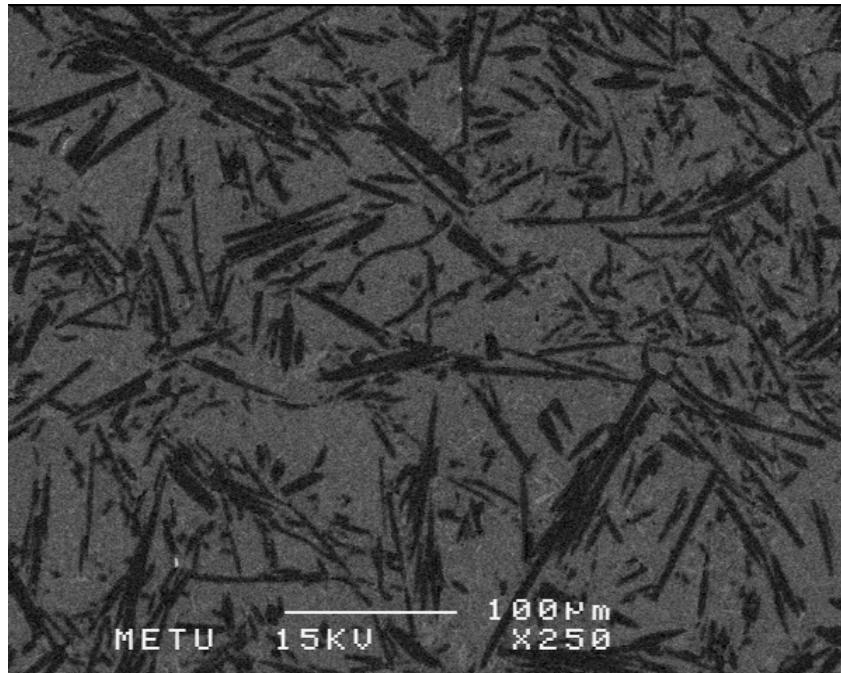
Figure 4.17 Back scattered SEM image of 20 vol% Saffil fiber reinforced AlSi10Mg composite vertical to the fiber orientation.
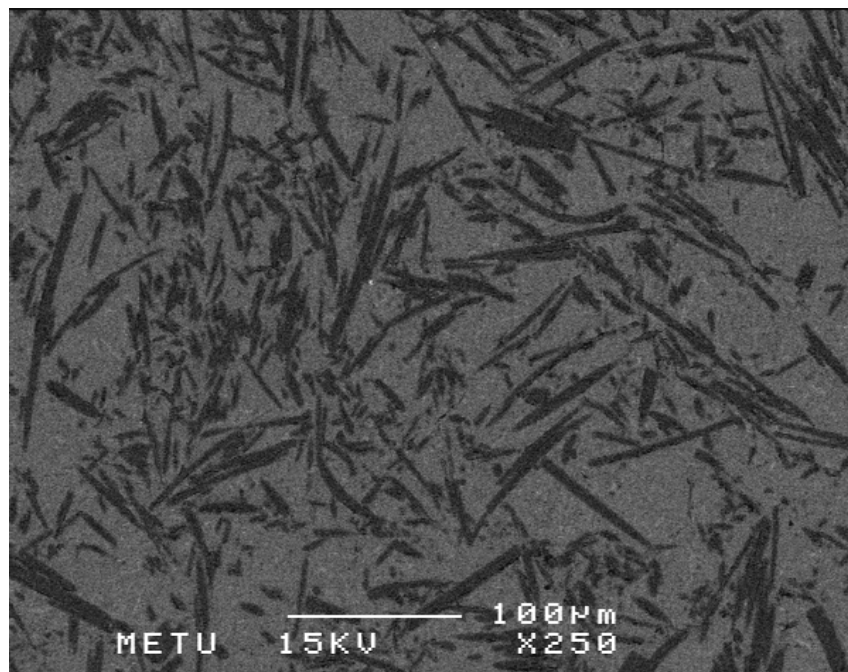
Figure 4.18 Back scattered SEM image of 25 vol% Saffil fiber reinforced AlSi10Mg composite vertical to the fiber orientation.
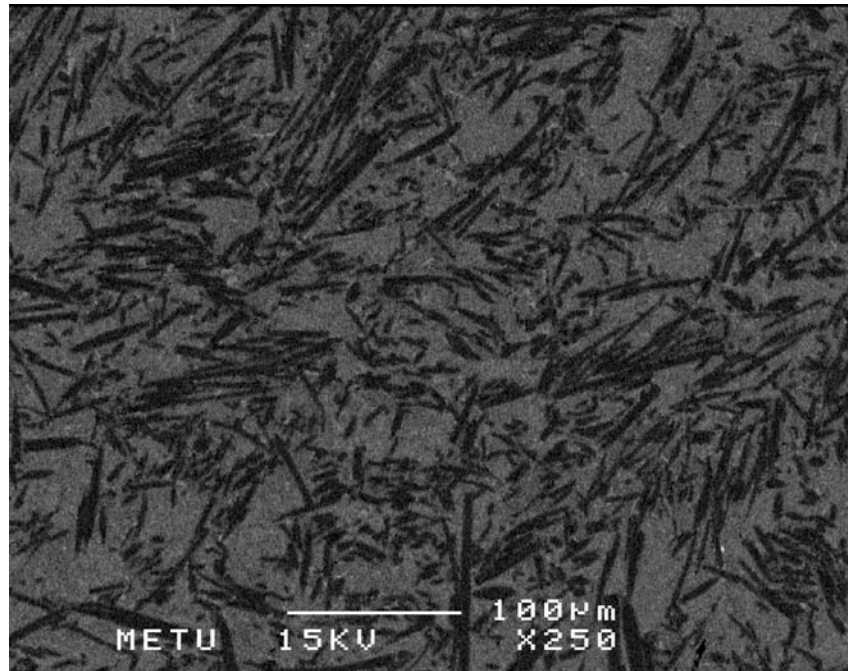
Figure 4.19 Back scattered SEM image of 30 vol% Saffil fiber reinforced AlSi10Mg composite vertical to the fiber orientation.
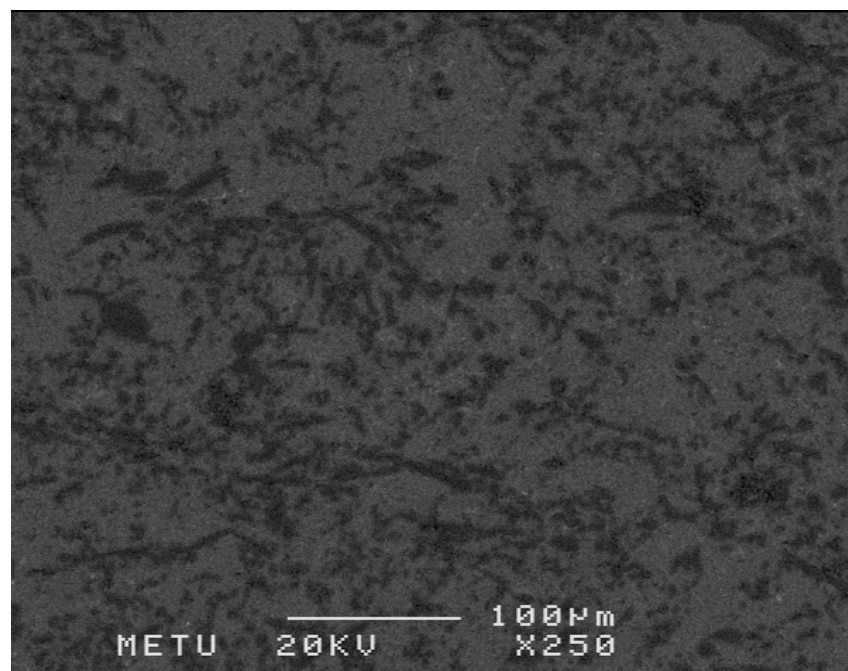
Figure 4.20 Back scattered SEM image of 10 vol% Saffil fiber reinforced AlSi10Mg composite parallel to the fiber orientation.
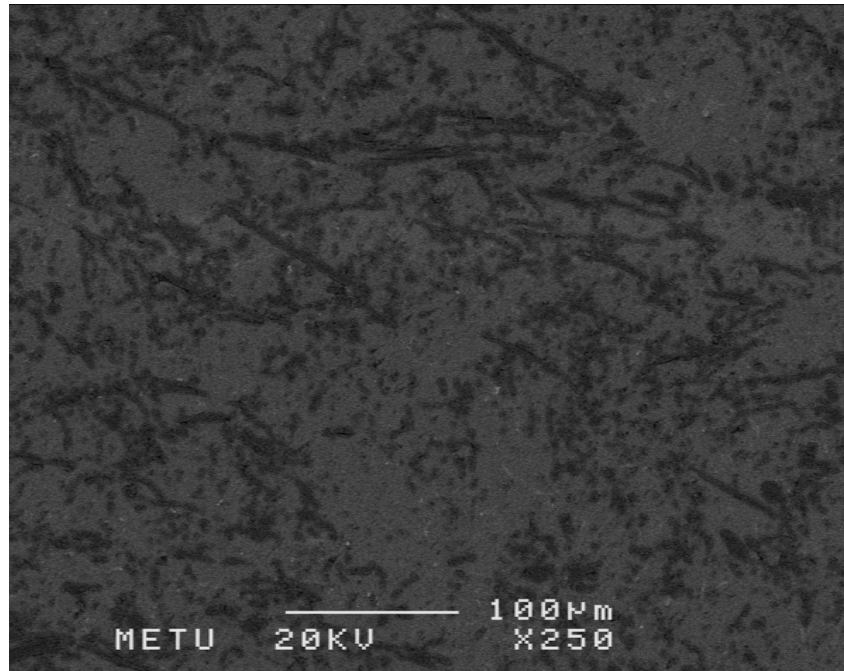
Figure 4.21 Back scattered SEM image of 15 vol% Saffil fiber reinforced AlSi10Mg composite parallel to the fiber orientation.
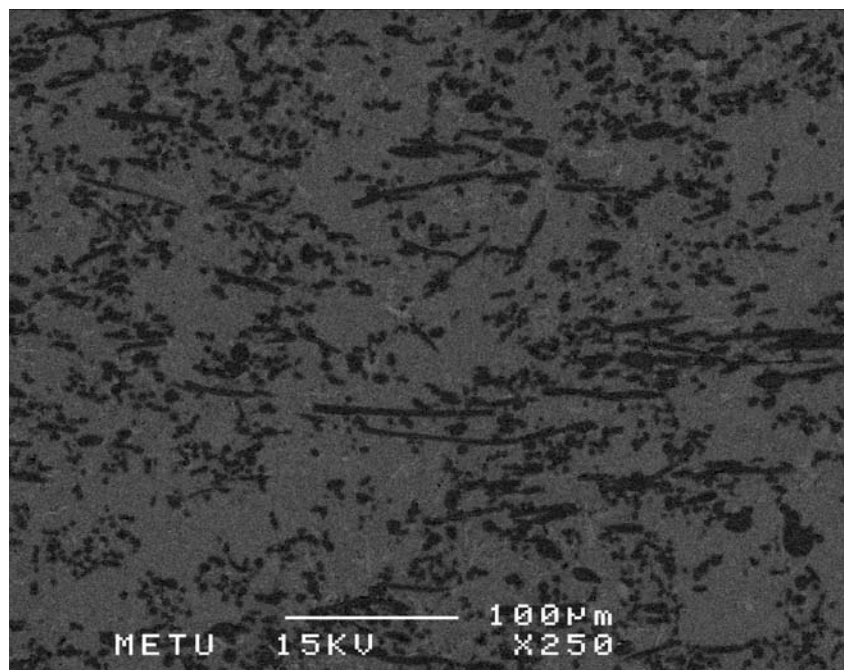
Figure 4.22 Back scattered SEM image of 20 vol% Saffil fiber reinforced AlSi10Mg composite parallel to the fiber orientation.
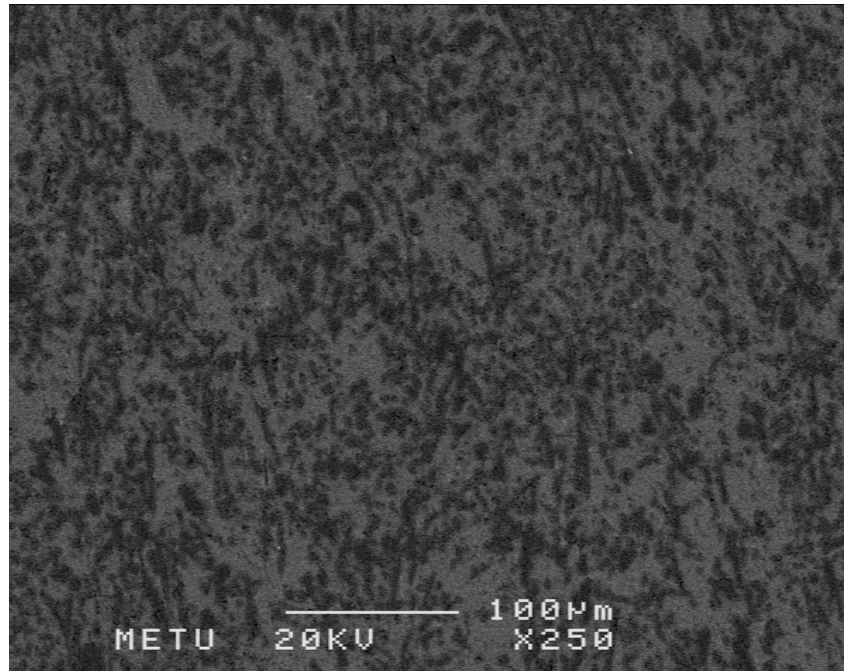
Figure 4.23 Back scattered SEM image of 25 vol% Saffil fiber reinforced AlSi10Mg composite parallel to the fiber orientation.
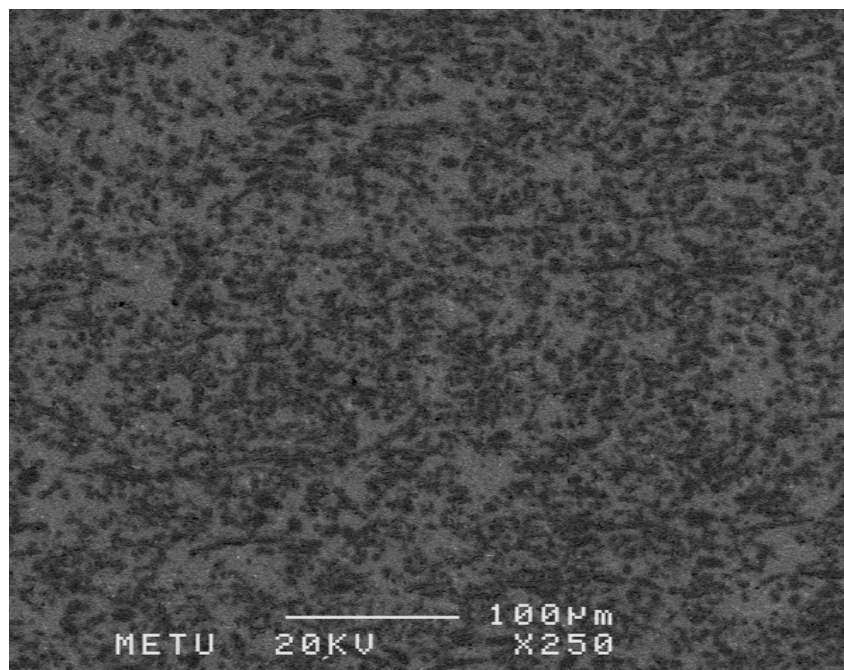
Figure 4.24 Back scattered SEM image of 30 vol% Saffil fiber reinforced AlSi10Mg composite parallel to the fiber orientation.
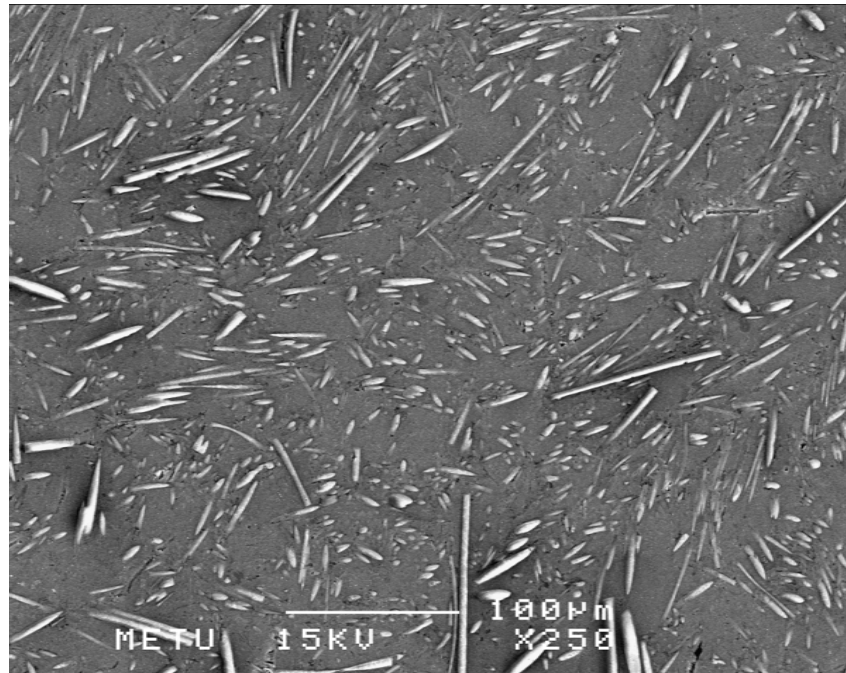
(a)
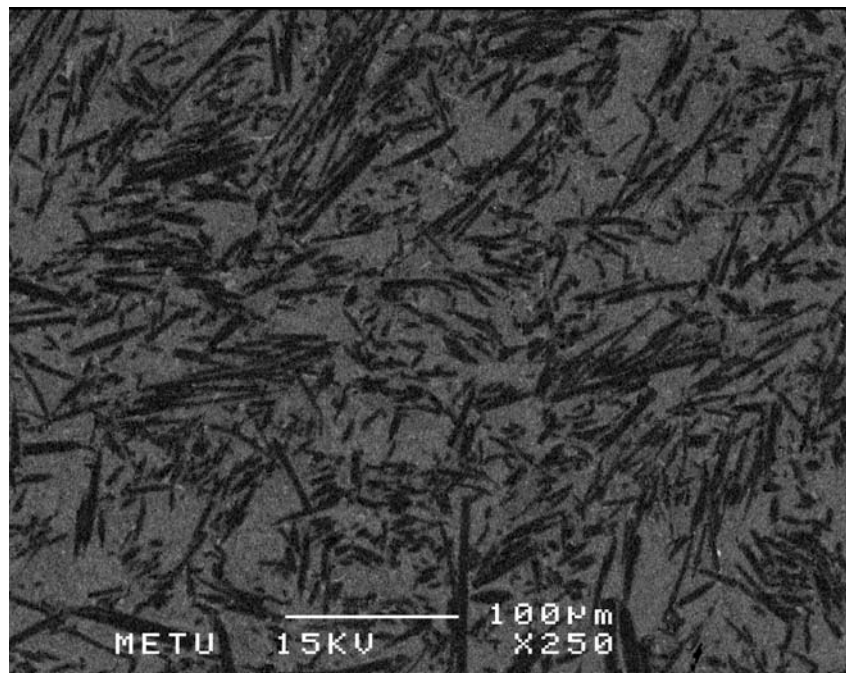
(b)

Figure 4.25 SEM image of 30 vol% Saffil fiber reinforced AlSi10Mg composite vertical to the fiber orientation a) Normal SEM image b) Back scattered image.

All the composites showed brittle fracture and it were seen from the SEM images the bonding between fiber and matrix is good. It is evident from the Figure 4.26 that the fiber pull out was not occurred.
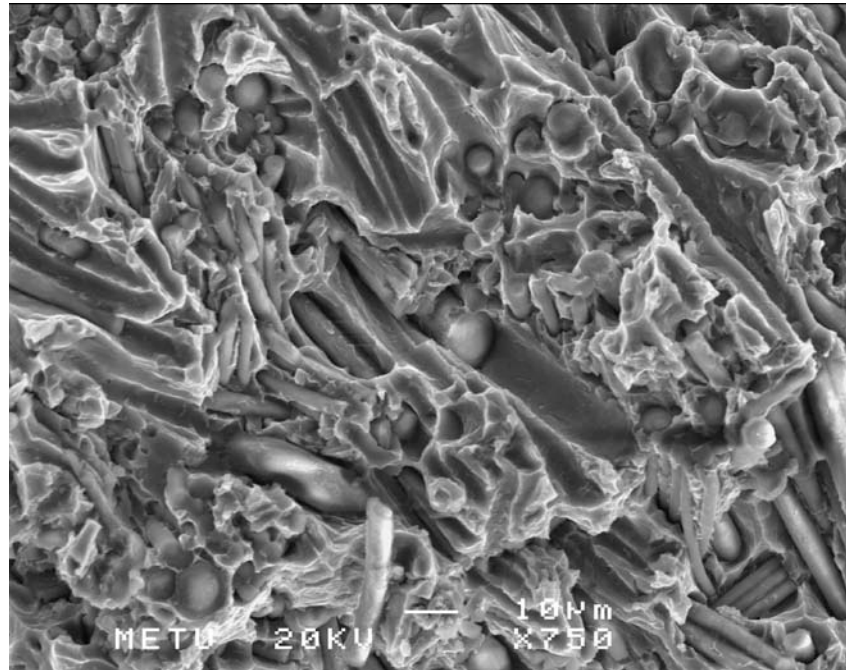
Figure 4.26 SEM image of the fracture surface of 25 vol% Saffil fiber reinforced AlSi10Mg0.3 matrix composite cast at 750 °C.
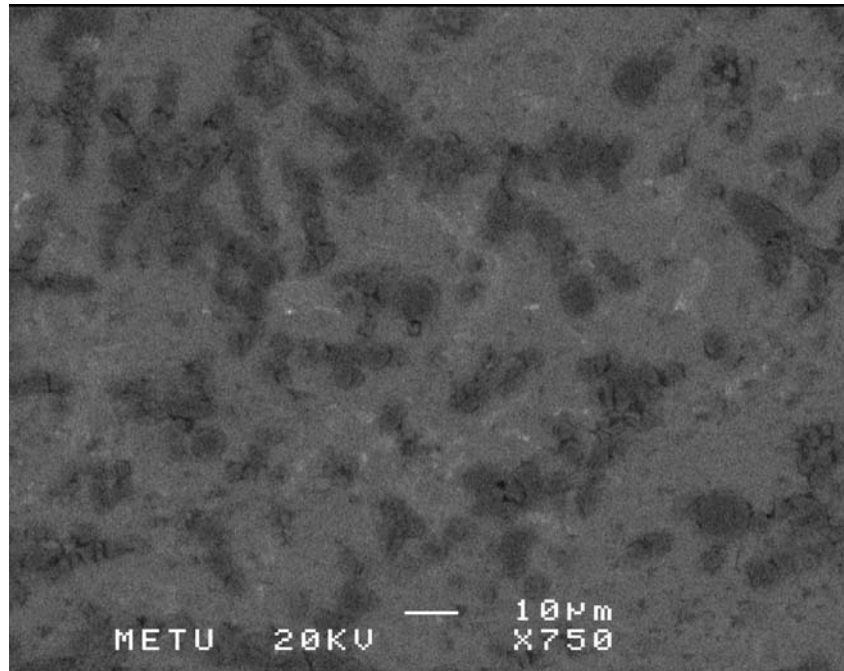
(a)
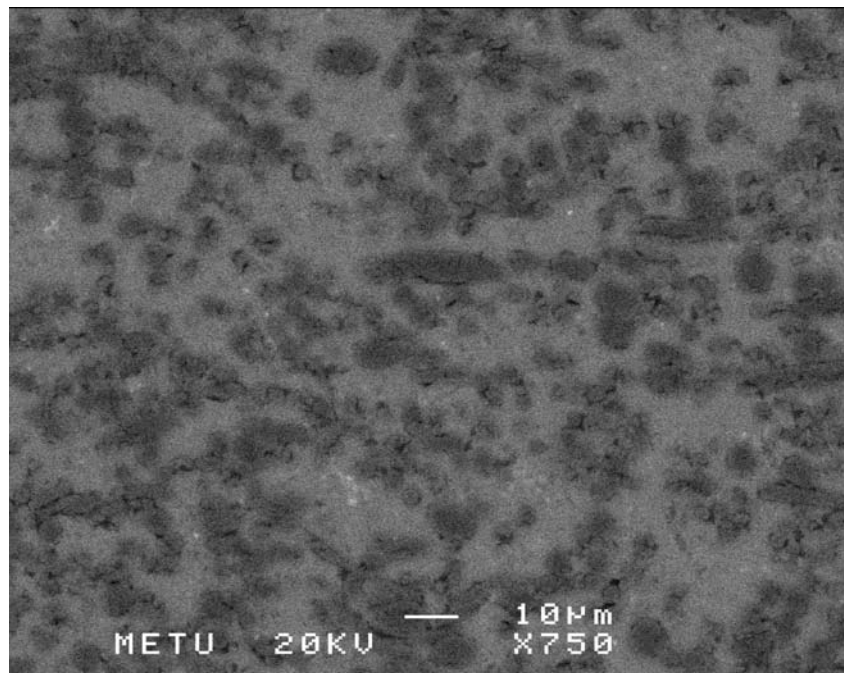
(b)

Figure 4.27 Back scattered SEM image of Saffil fiber reinforced AlSi10Mg0.3 matrix composite cast at 800 °C parallel to the fiber orientation a) 10 vol% b) 30 vol%

In Figure 4.27 micro pores can be seen as black points between the fibers which were inevitable due to the very high capillary forces. There was not a direct relationship between the fiber volume fraction and micro porosity. Micro pores increased much more for higher fiber volume fractions. Because as the fiber volume increased the fiber lengths got smaller and this increased the number of possible sites for micro porosity.

4.7   Metallographic Examination Results

Metallographic examinations were done to reveal the distribution of the alumina fibers and the microstructure of the composite. The surfaces parallel and vertical to the fiber orientation are investigated. The Figures 4.28 to 4.60 show the optical micrographs of aluminum alloy matrix composites and non-reinforced alloy.
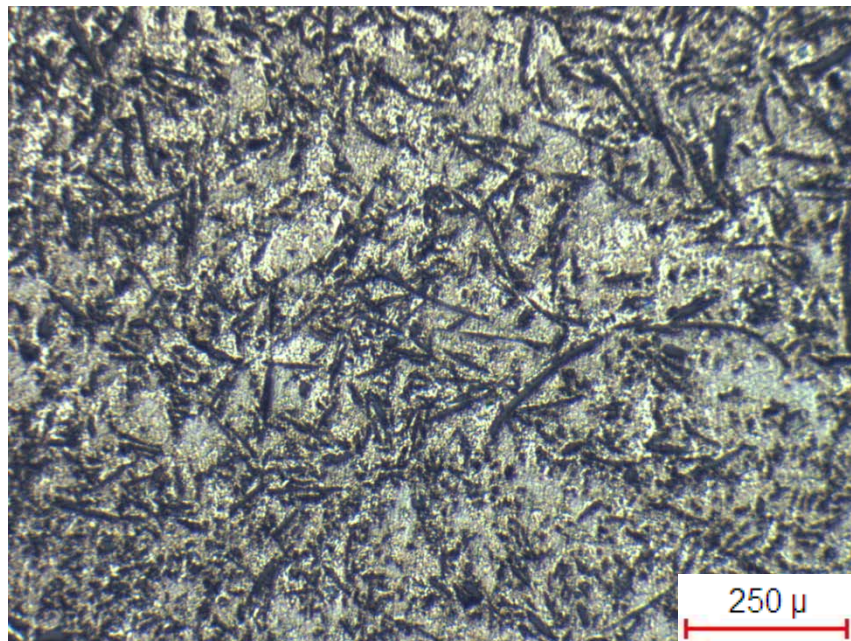
Figure 4.28 Optical micrograph showing 10 vol% alumina fiber reinforced composite vertical to the fiber orientation at 50X magnification.
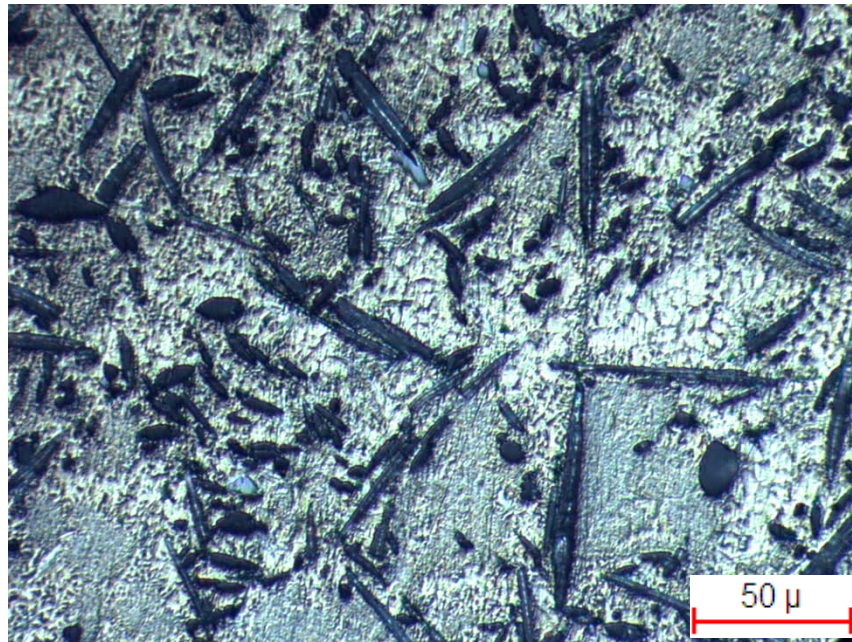
Figure 4.29 Optical micrograph showing 10 vol% alumina fiber reinforced composite vertical to the fiber orientation at 200X magnification.

Figure 4.30 Optical micrograph showing 10 vol% alumina fiber reinforced composite vertical to the fiber orientation at 500X magnification.
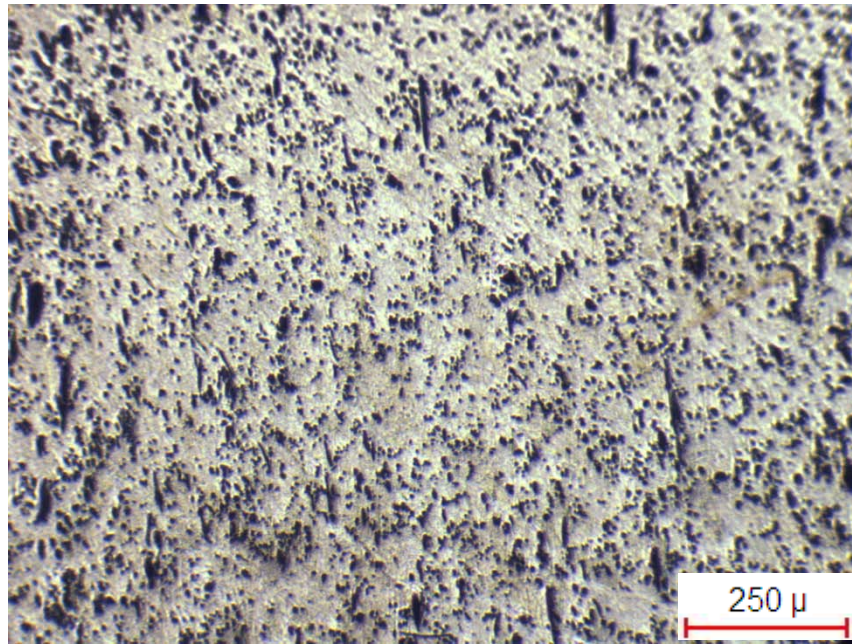
Figure 4.31 Optical micrograph showing 10 vol% alumina fiber reinforced composite parallel to the fiber orientation at 50X magnification.
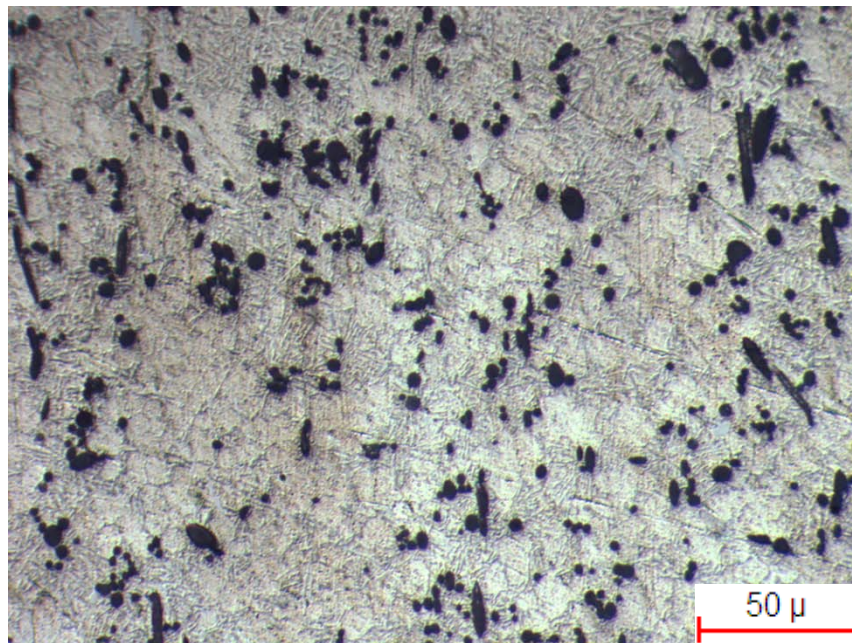
Figure 4.32 Optical micrograph showing 10 vol% alumina fiber reinforced composite parallel to the fiber orientation at 200X magnification.
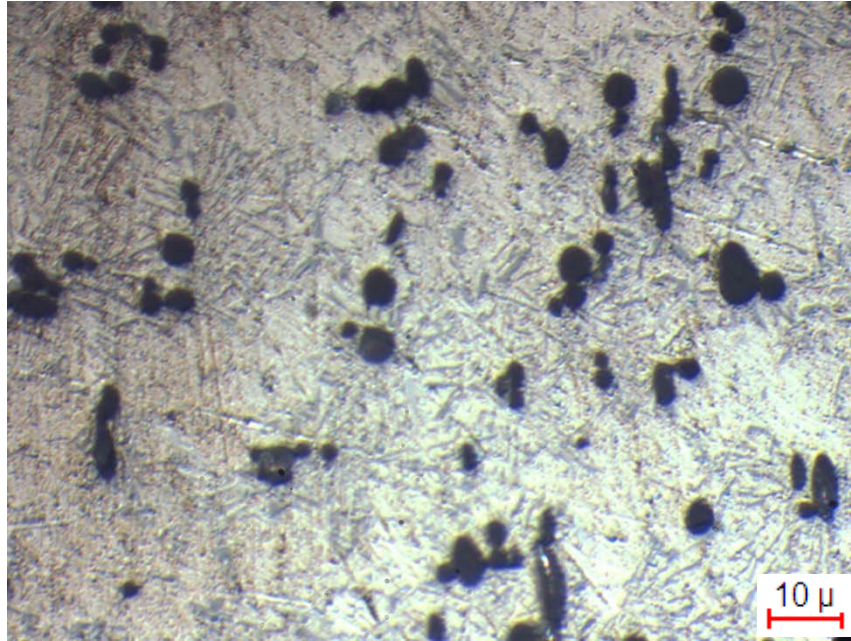
Figure 4.33 Optical micrograph showing 10 vol% alumina fiber reinforced composite parallel to the fiber orientation at 500X magnification.
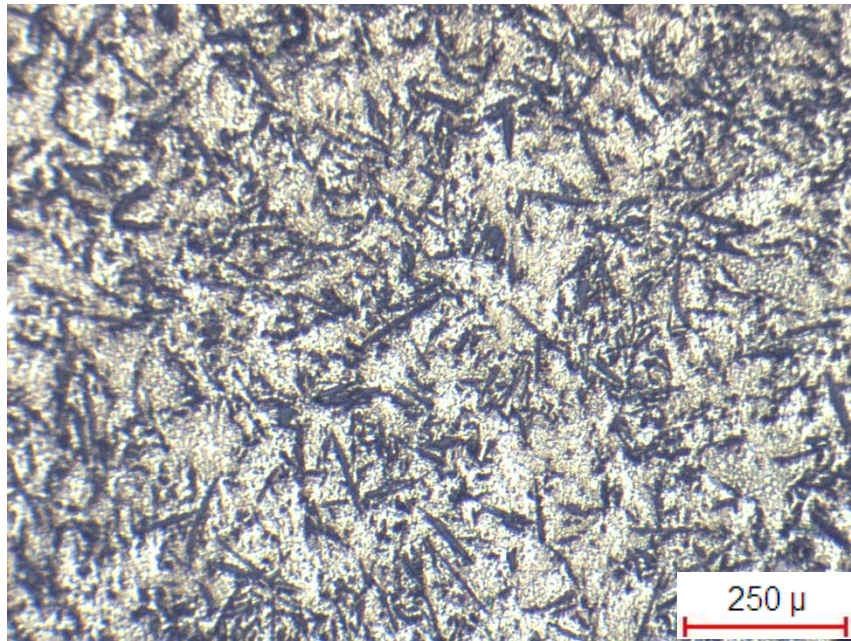
Figure 4.34 Optical micrograph showing 15 vol% alumina fiber reinforced composite vertical to the fiber orientation at 50X magnification.
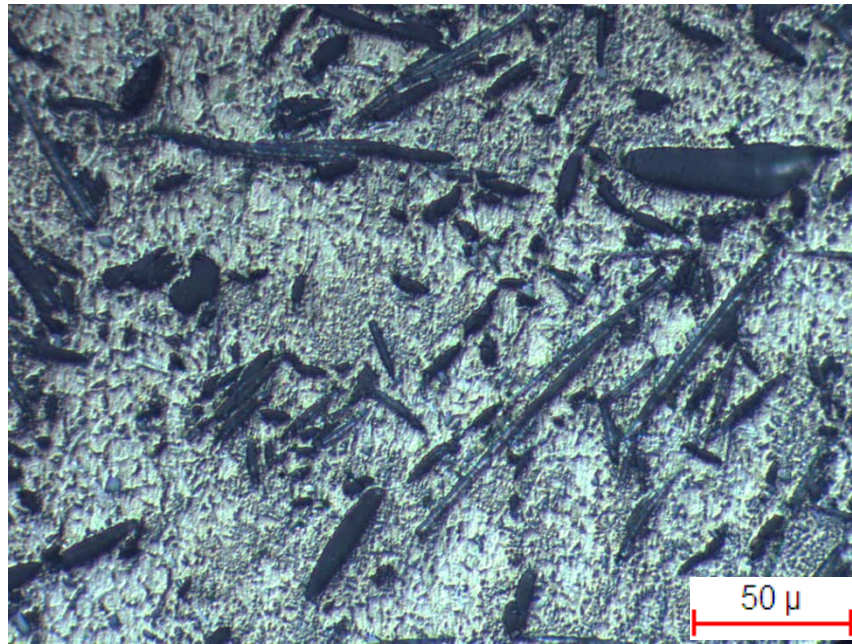
Figure 4.35 Optical micrograph showing 15 vol% alumina fiber reinforced composite vertical to the fiber orientation at 200X magnification.

Figure 4.36 Optical micrograph showing 15 vol% alumina fiber reinforced composite vertical to the fiber orientation at 500X magnification.
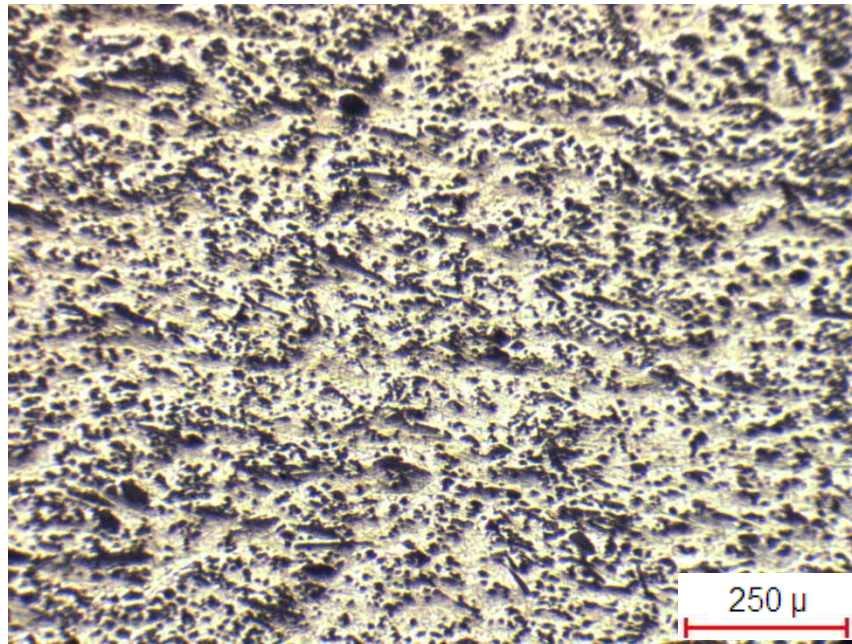
Figure 4.37 Optical micrograph showing 15 vol% alumina fiber reinforced composite parallel to the fiber orientation at 50X magnification.
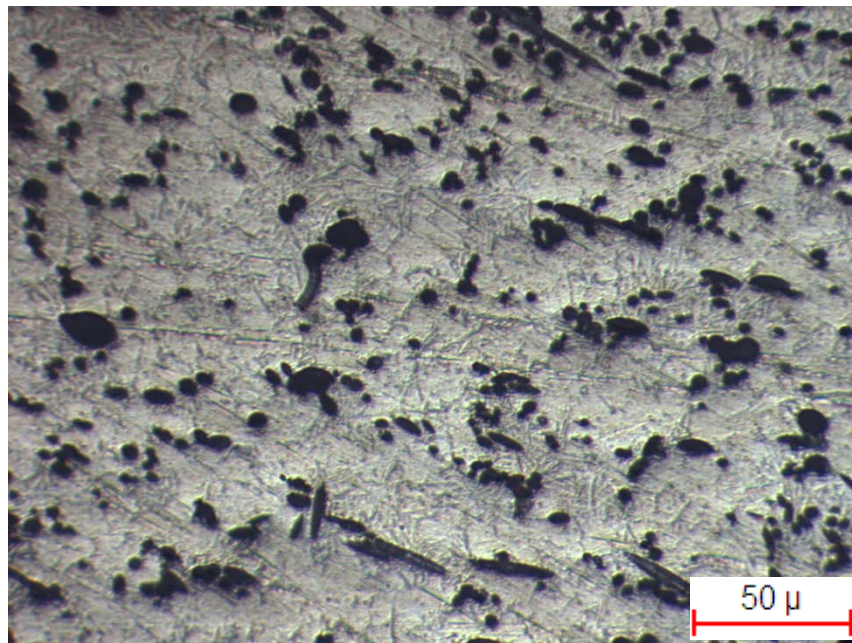
Figure 4.38 Optical micrograph showing 15 vol% alumina fiber reinforced composite parallel to the fiber orientation at 200X magnification.
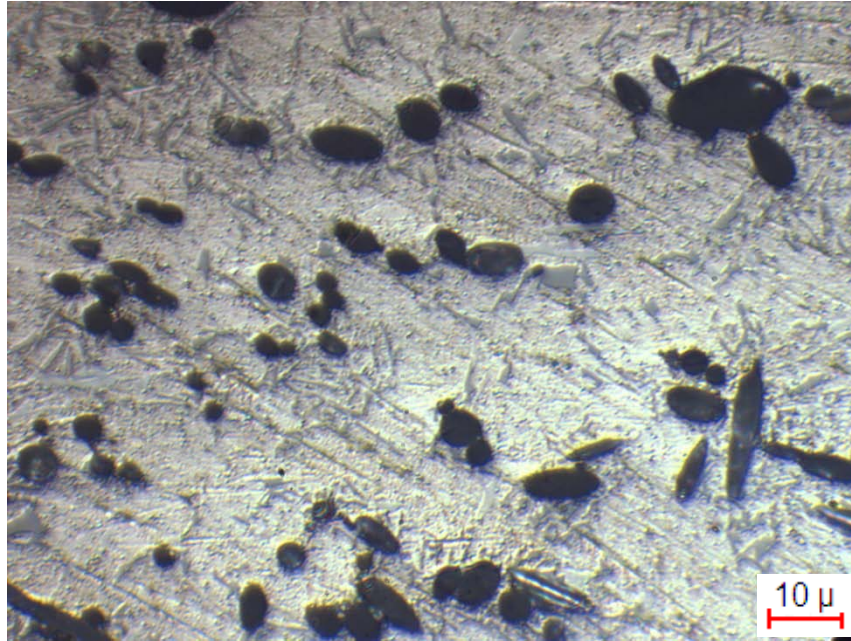
Figure 4.39 Optical micrograph showing 15 vol% alumina fiber reinforced composite parallel to the fiber orientation at 500X magnification.
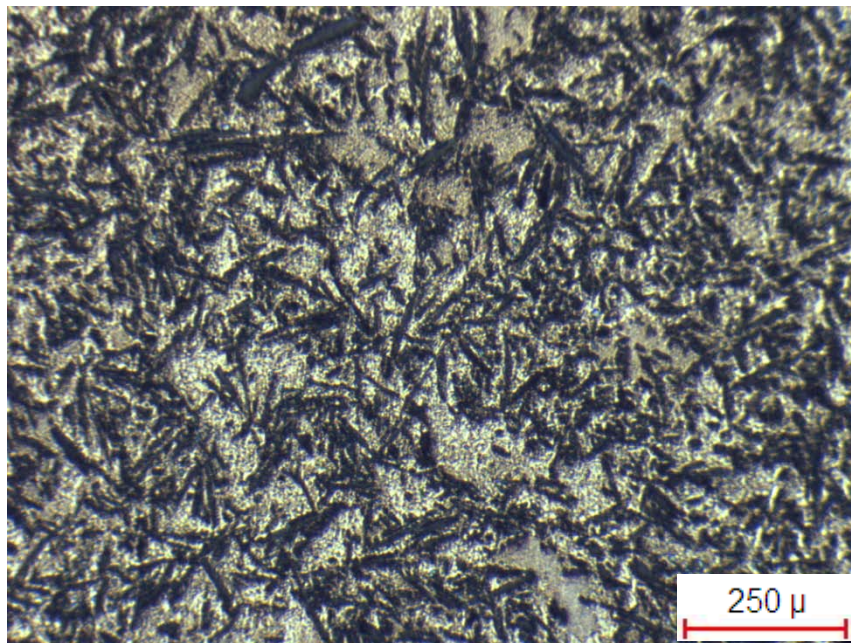
Figure 4.40 Optical micrograph showing 20 vol% alumina fiber reinforced composite vertical to the fiber orientation at 50X magnification.
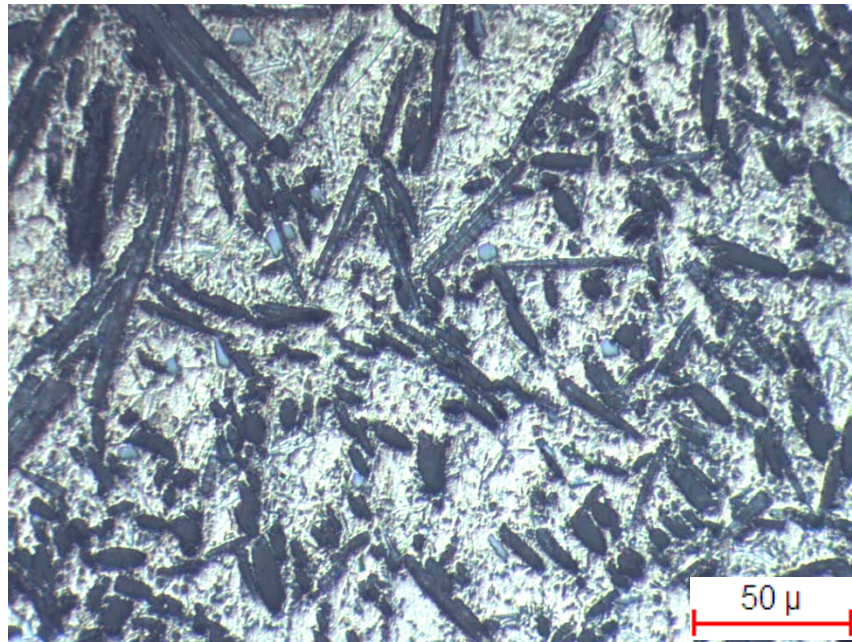
Figure 4.41 Optical micrograph showing 20 vol% alumina fiber reinforced composite vertical to the fiber orientation at 200X magnification.

Figure 4.42 Optical micrograph showing 20 vol% alumina fiber reinforced composite vertical to the fiber orientation at 500X magnification.
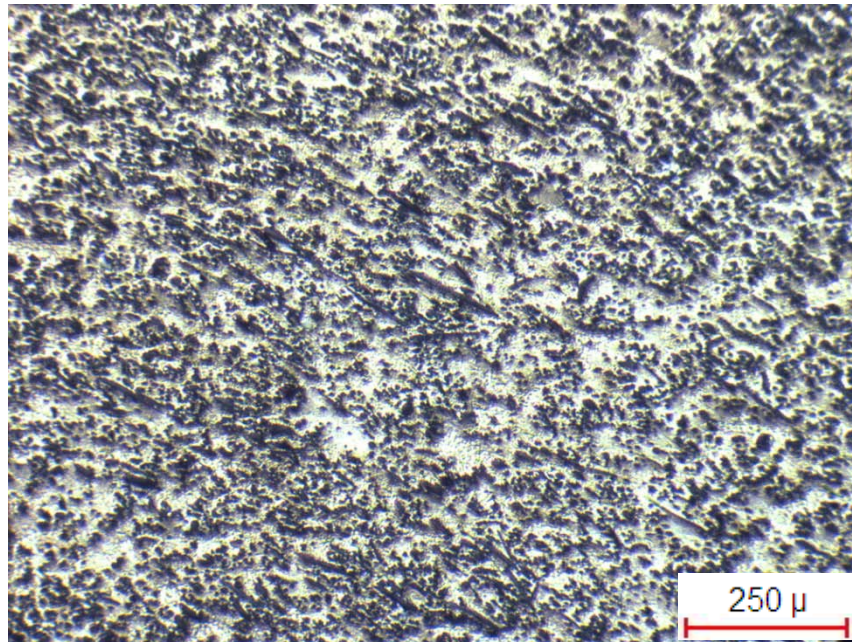
Figure 4.43 Optical micrograph showing 20 vol% alumina fiber reinforced composite parallel to the fiber orientation at 50X magnification.
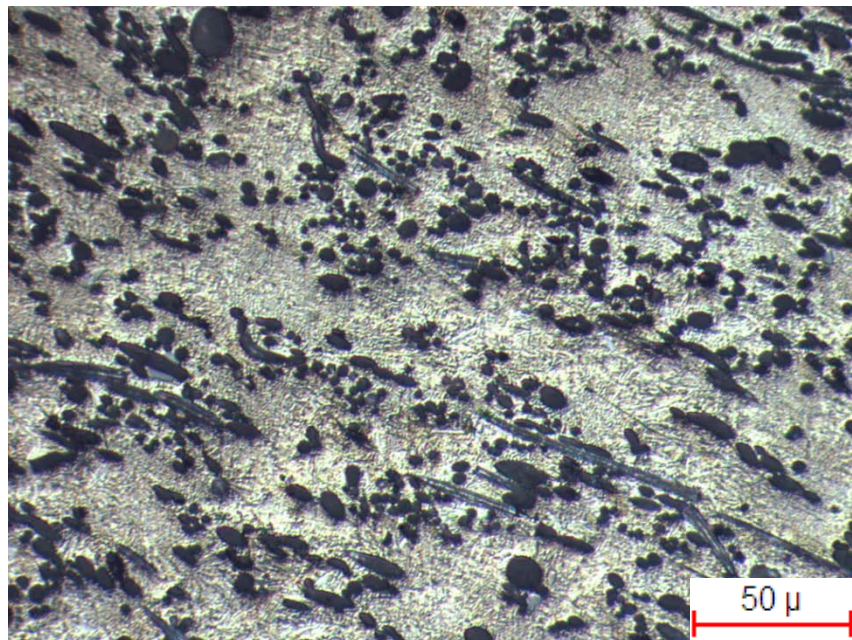
Figure 4.44 Optical micrograph showing 20 vol% alumina fiber reinforced composite parallel to the fiber orientation at 200X magnification.
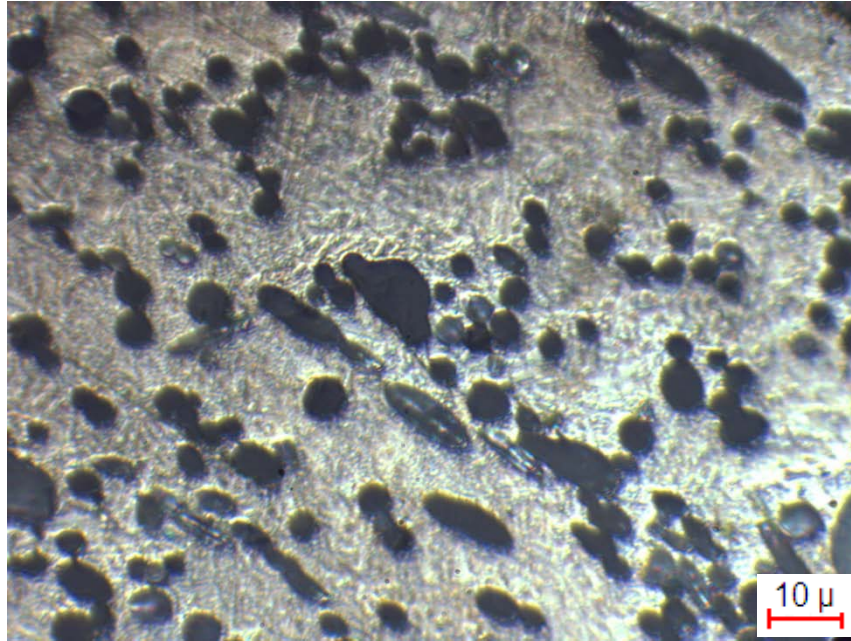
Figure 4.45 Optical micrograph showing 20 vol% alumina fiber reinforced composite parallel to the fiber orientation at 500X magnification.
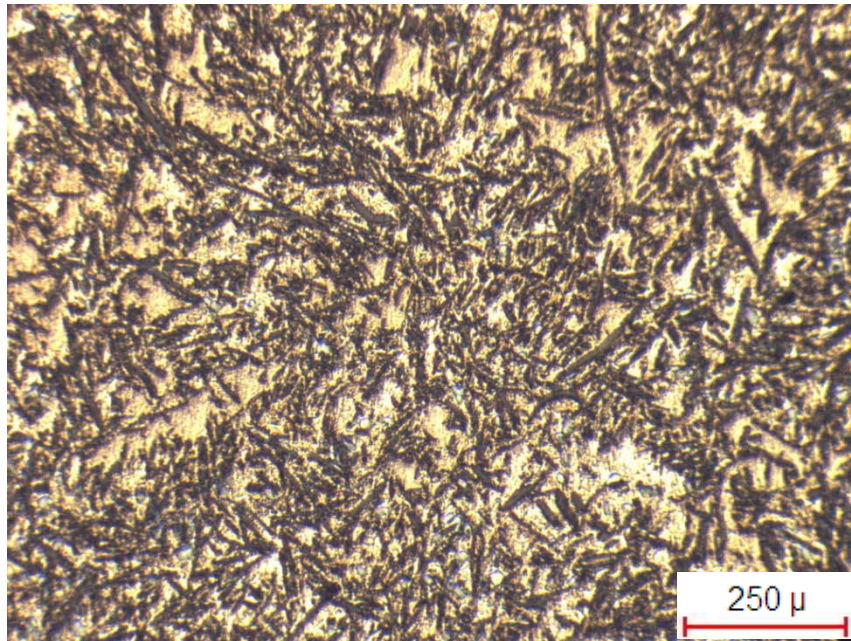
Figure 4.46 Optical micrograph showing 25 vol% alumina fiber reinforced composite vertical to the fiber orientation at 50X magnification.
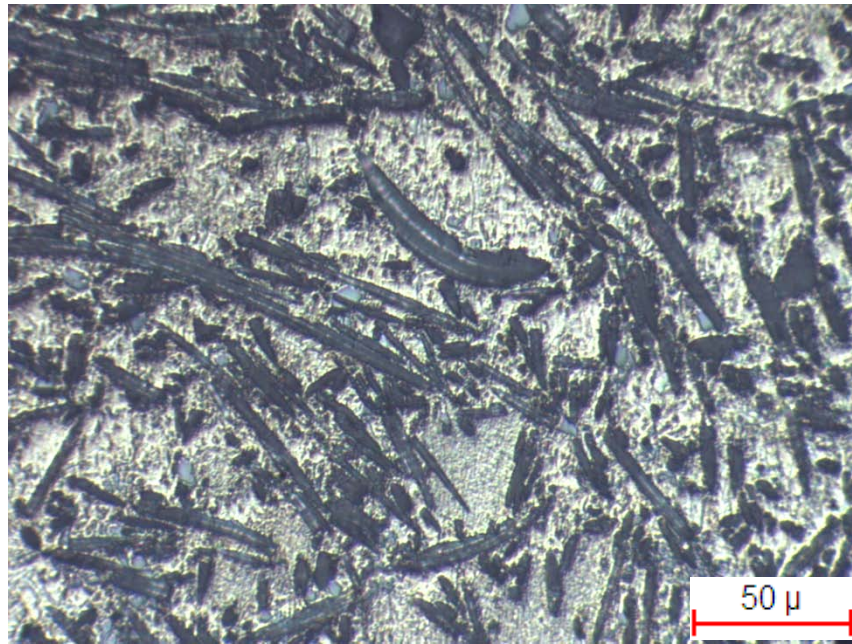
Figure 4.47 Optical micrograph showing 25 vol% alumina fiber reinforced composite vertical to the fiber orientation at 200X magnification.
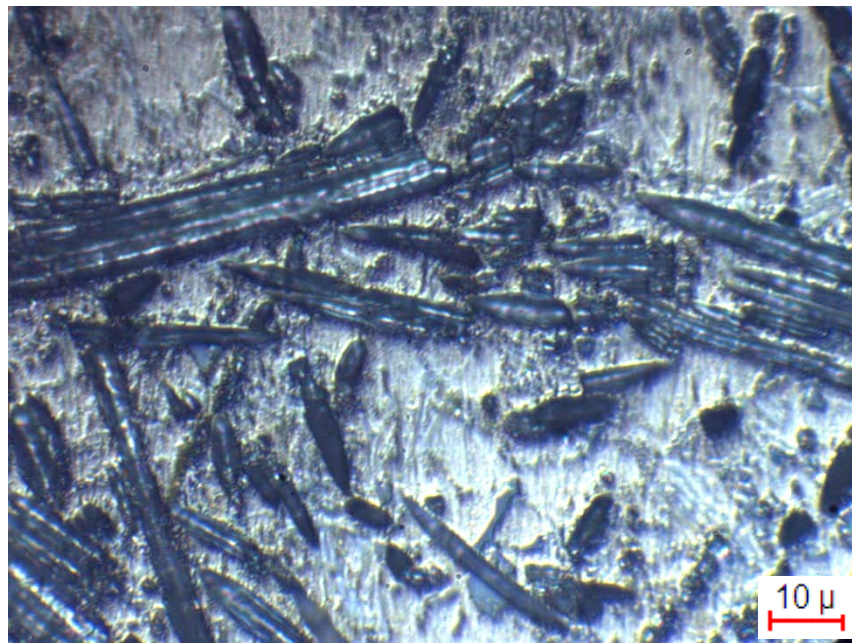
Figure 4.48 Optical micrograph showing 25 vol% alumina fiber reinforced composite vertical to the fiber orientation at 500X magnification.
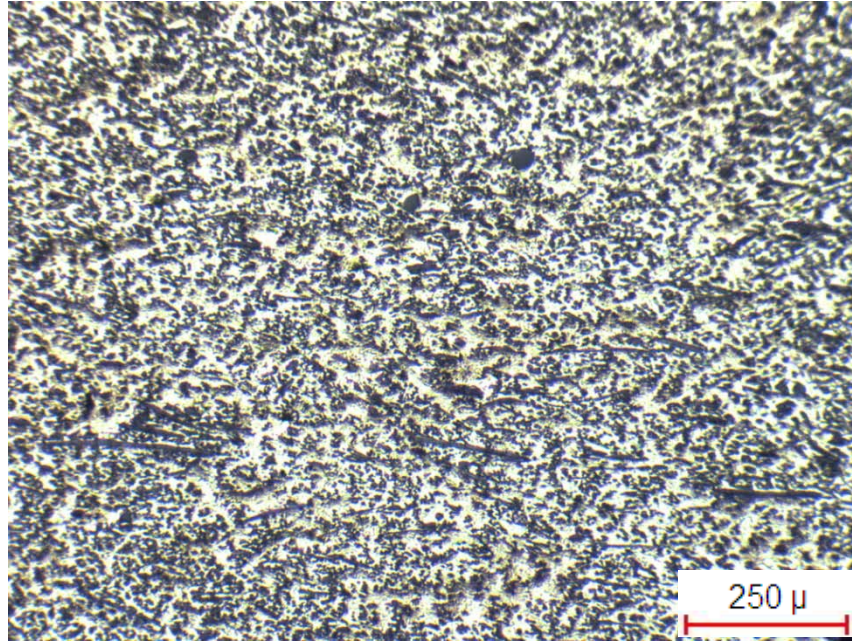
Figure 4.49 Optical micrograph showing 25 vol% alumina fiber reinforced composite parallel to the fiber orientation at 50X magnification.

Figure 4.50 Optical micrograph showing 25 vol% alumina fiber reinforced composite parallel to the fiber orientation at 200X magnification.
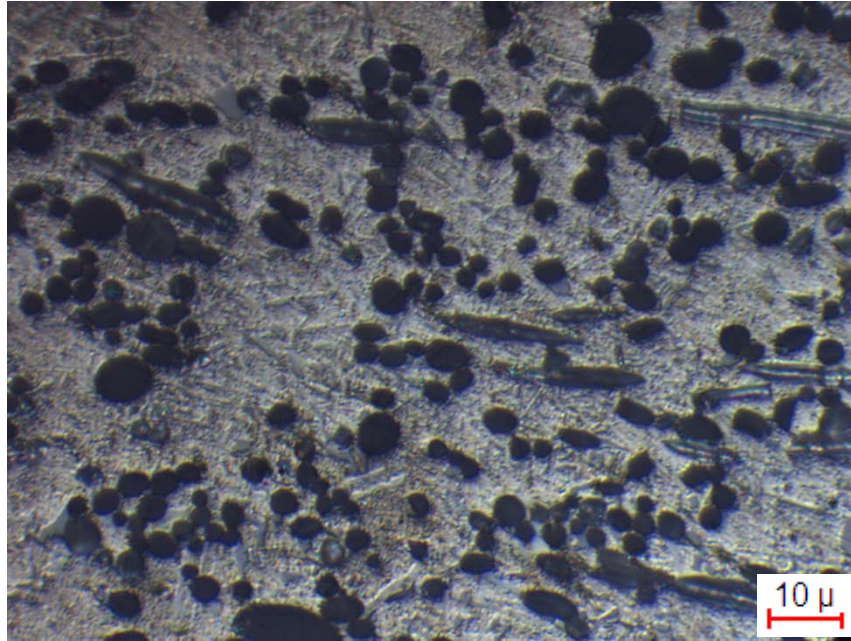
Figure 4.51 Optical micrograph showing 25 vol% alumina fiber reinforced composite parallel to the fiber orientation at 500X magnification.
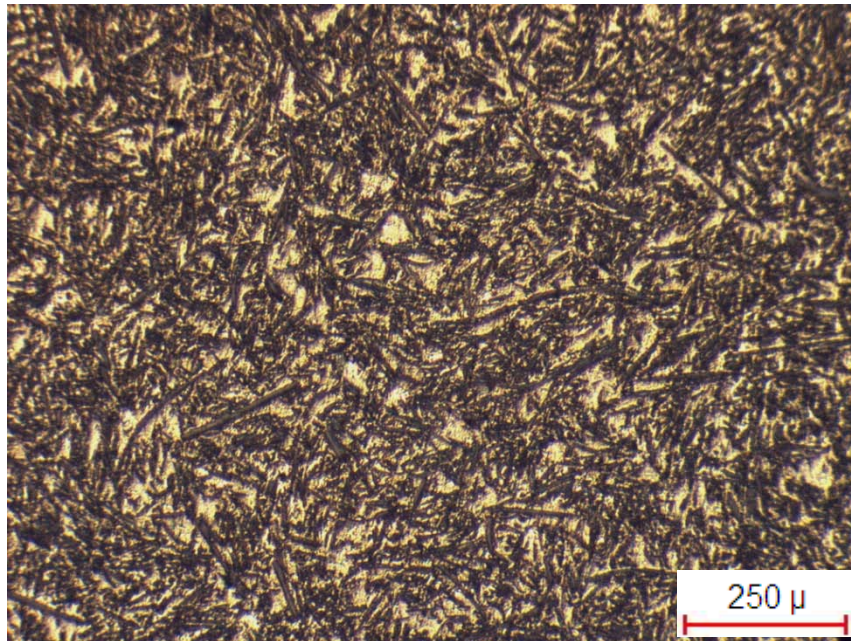
Figure 4.52 Optical micrograph showing 30 vol% alumina fiber reinforced composite vertical to the fiber orientation at 50X magnification.
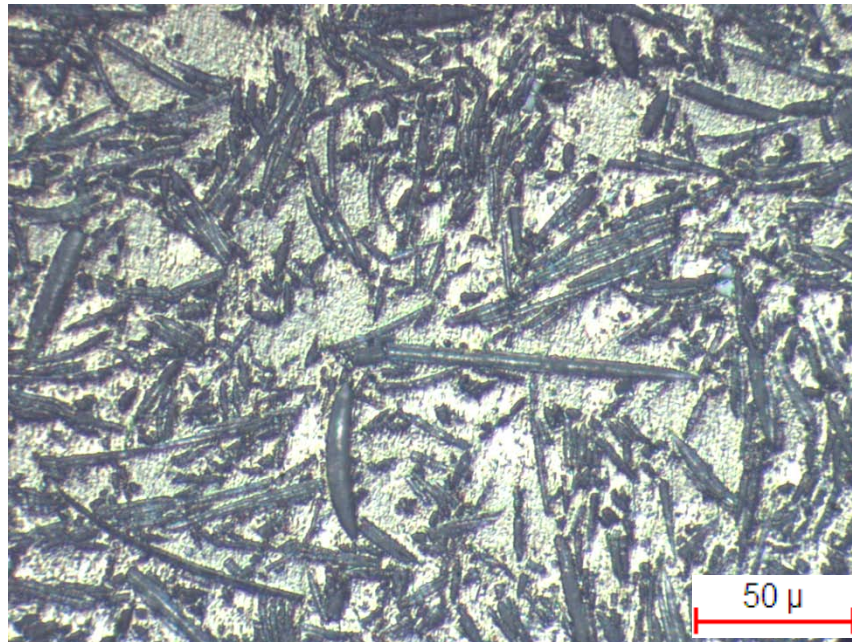
Figure 4.53 Optical micrograph showing 30 vol% alumina fiber reinforced composite vertical to the fiber orientation at 200X magnification.

Figure 4.54 Optical micrograph showing 30 vol% alumina fiber reinforced composite vertical to the fiber orientation at 500X magnification.

85
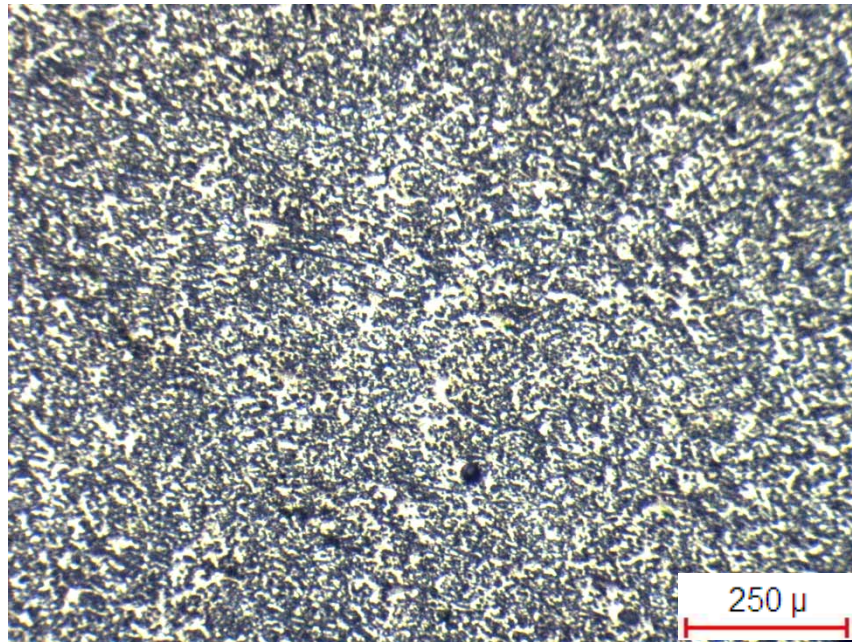
Figure 4.55 Optical micrograph showing 30 vol% alumina fiber reinforced composite parallel to the fiber orientation at 50X magnification.
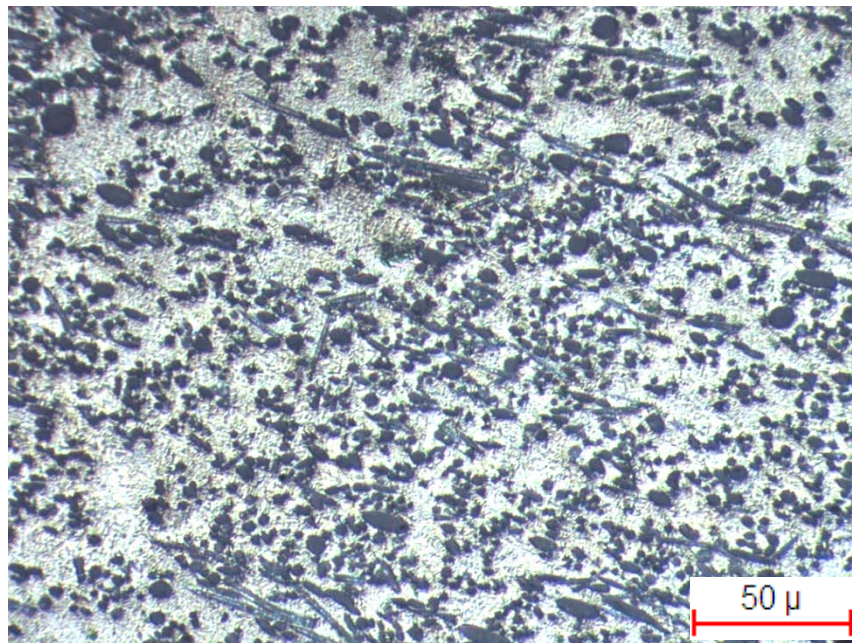
Figure 4.56 Optical micrograph showing 30 vol% alumina fiber reinforced composite parallel to the fiber orientation at 200X magnification.
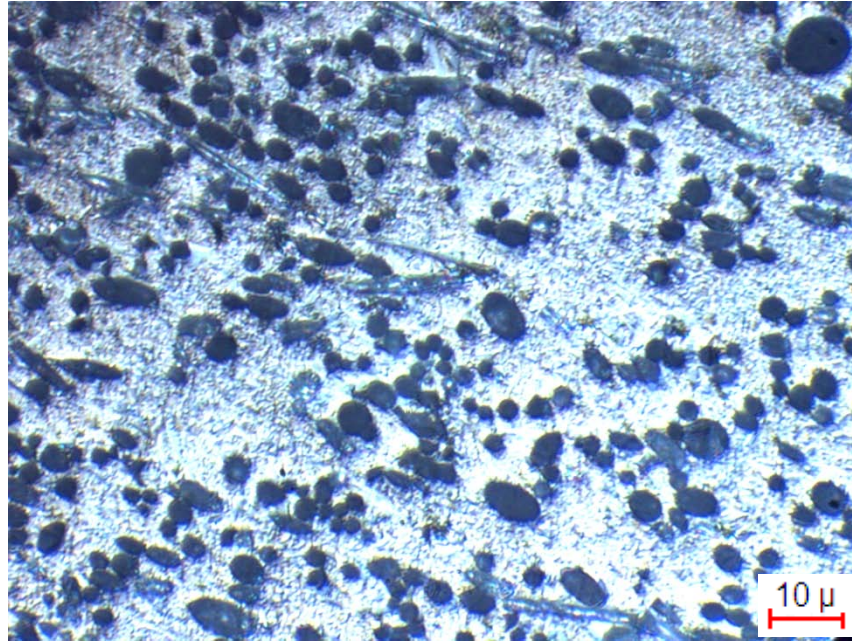
Figure 4.57 Optical micrograph showing 30 vol% alumina fiber reinforced composite parallel to the fiber orientation at 500X magnification.
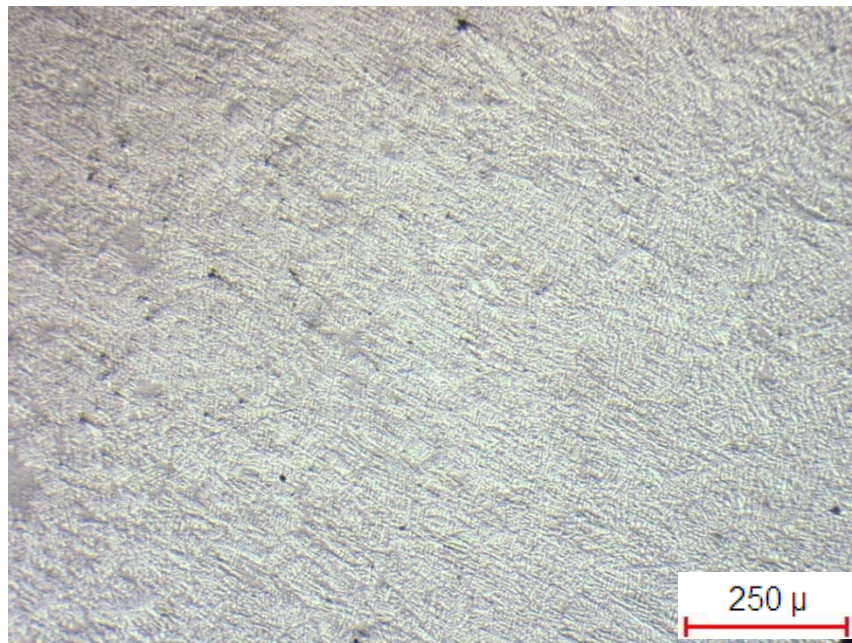
Figure 4.58 Optical micrograph showing non-reinforced alloy at 50X magnification.
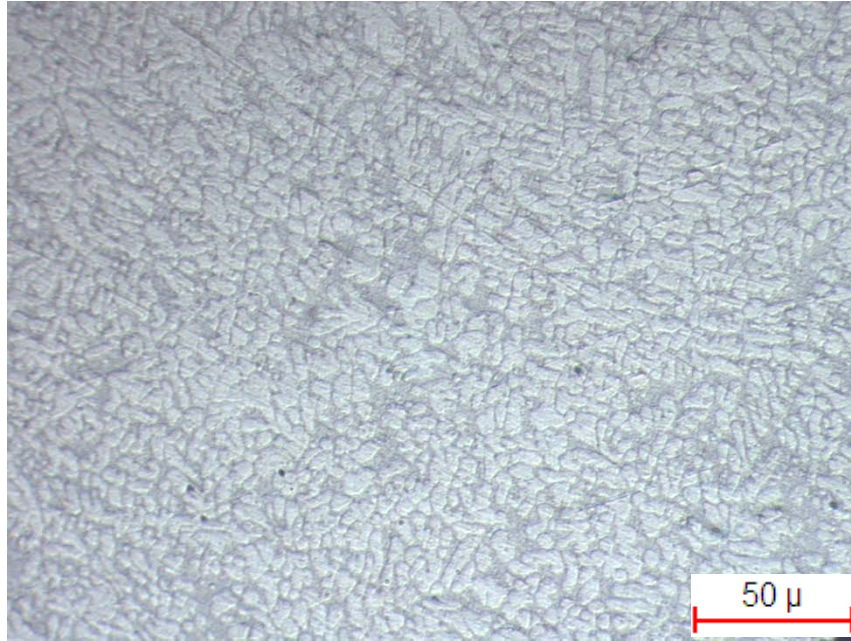
Figure 4.59 Optical micrograph showing non-reinforced alloy at 200X magnification.

Figure 4.60 Optical micrograph showing non-reinforced alloy at 500X magnification.

As observed from the micrographs, the distribution of alumina fibers were more uniform for 20 vol%, 25 vol% and 30 vol% fiber reinforced composites than that of 10 vol% and 15 vol% fiber reinforced ones. In the composites, porosity was not detected under optical microscope. It was seen that the primary dendrite arm size decreased with increasing fiber vol%.

CHAPTER 5

CONCLUSION

The following conclusions can be drawn after investigating the effects of fiber vol%, magnesium content of the matrix alloy and liquid metal infiltration temperature on the mechanical behavior and physical properties of Saffil alumina fiber reinforced aluminum alloy matrix composites, performing hardness tests, three point bending tests, X-ray analysis, image analyzing, SEM analysis and metallographic examinations:

1. Vacuum assisted gas pressure infiltration was not successful under 20 Atm argon gas and 0.05 Torr vacuum level. The isolation between gas pressure and vacuum atmosphere was not proper at 750 °C and higher temperatures which decreased the pressure difference required for infiltration of Saffil alumina fiber preforms.

2. The increase in Saffil alumina fiber addition resulted in an increasing porosity level. There was not observed any distinct effect of casting temperature on closed porosity.

3. There was not seen any distinct effect of magnesium on closed porosity up to 25 fiber vol%. However, the increase in closed porosity for the change in fiber vol% from 25 vol% to 30 vol% was higher for AlSiMg0.3 matrix composites than the AlSiMg1 matrix composites. This was seen as an indication of increased effect of magnesium on wetting of 30 vol% alumina fiber preform.

4. Hardness values increased with increasing Saffil alumina fiber addition. Hardness values taken from direction parallel to the fiber orientation were higher than the values taken from direction vertical to the fiber orientation. It was observed that the increase in magnesium content and the decrease in casting temperature accounted for an increase in hardness values for planes vertical and parallel to the fiber orientation.

5. The flexural strength values decreased to a minimum value at 10 vol% Saffil fiber addition and started to increase with volume fraction of fibers. Fibers hinder the dislocation motion and resulted in a strain hardening. The increased fiber volume also decreased the grain and subgrain size. Effective reinforcement was achieved at 20 vol% Saffil alumina fiber addition where the composites reached non-reinforced alloy strength. Maximum flexural strengths were obtained at 30 vol% fiber addition.

6. As the magnesium content increased the flexural strength decreased and for composites cast at 750 °C flexural strength was higher than the ones cast at 800 °C.

7. The maximum increase in flexural strength was 70 MPa for AlSi10Mg0.3 alloy cast at 800 °C. 15 % increase was gained compared to non-reinforced alloy.

8. X-ray analysis revealed that there is no phase other than alumina and matrix alloys.

9. Image analysis showed that the vol%'s calculated by computer software were close to the theoretical values. The values gathered from the plane parallel to the fiber orientation were slightly higher than the ones taken from the plane vertical to the fiber orientation.

10. SEM study revealed that micro porosity was present especially at the fiber-fiber interconnections and there is a strong fiber-matrix bonding.

11. Optical micrographs showed that with increasing fiber vol% the primary dendrite arm size decreased. There was not any porosity observed during optical microscope examination.

REFERENCES

[1] K. K. Chawla, "Composite materials: Science and engineering", 2nd edition, Springer-Verlag, New York, 1998

[2] D. D. L. Chung, "Composite materials: Functional materials for modern technologies", Springer-Verlag, London, 2003

[3] G. Akovali, "Handbook of composite fabrication", Rapra Technology Ltd., UK, 2001

[4] K. U. Kainer, "Metal matrix composites: Custom-made materials for automotive and aerospace engineering", Wiley-VCH Verlag GmbH & Co. KGaA, Weinheim, 2006

[5] S. Can Kurnaz, "Production of saffil fiber reinforced Zn-Al (ZA 12) based metal matrix composites using infiltration technique and study of their properties", Materials Science & Engineering A, 2002, vol. 346, pp. 108-115

[6] B. R. Henrisken, T.E. Johnsen, "Influence of microstructure of fiber/matrix interface on mechanical properties of Al/SiC composites", Materials Science and Technology, 1990, vol.6, pp. 857-863

[7] H. S. Yılmaz, "Characterization of silicon carbide particulate reinforced squeeze cast Aluminum 7075 matrix composite", METU, 2004

[8] S. K. Chaudhury, "Preparation and thermomechanical properties of stir cast Al-2Mg-11TiO2 (rutile) composite", Bulletin of Material Science, 2004, vol. 27, pp. 517-521

[9] T. S. Srivatstan, I. A. Mohamed, E. J. Lavernia, "Processing techniques for particulate-reinforced metal aluminum matrix composites", Journal of Material Science, 1991, vol. 26, pp. 97-109

[10] T. S. Srivatsan, I. A. Ibrahim, F. A. Mohammed, E.J. Lavernia, M. I. Pech-Canul, R.N. Katz, M. M. Makhlouf, "Optimum parameters for wetting silicon carbide by aluminum alloys", Metallurgical and Materials Transactions A, vol. 31 A, 2000, pp. 565-573

[11] A. Mclean, H. Soda, Q. Xia, A. K. Paramanick, A. Ohno, T. Shimizu, S. A. Gedeon and T. North, "SiC Particulate-reinforced, aluminum matrix composite rods and wires produced by a new continuous casting route", Composites Part A, 1996, Vol. 28, pp. 153-162

[12] M. Taya, R.J. Arsenault, "Metal Matrix Composites", Pergamon Press, 1989, pp. 51-63

[13] M. M. Schwartz, "Composite Materials Handbook", Mc Graw - Hill, New York, 1984

[14] E. Carreño-Morelli, T. Cutard, R. Schaller, C. Bonjour, "Processing and characterization of aluminum-based MMCs produced by gas pressure infiltration", Materials Science & Engineering A, 1998, vol. 251, pp. 48-57

[15] S. Long, Z. Zhang and H. M. Flower, "Characterization of liquid metal infiltration of a chopped fiber preform aided by external pressure—I. Visualization of the flow behaviour of aluminum melt in a fiber perform", Acta Metallurgica et Materialia, 1995, pp. 3489-3498

[16] S. Long, Z. Zhang and H. M. Flower, "Characterization of liquid metal infiltration of a chopped fiber preform aided by external pressure—II. Modelling of liquid metal infiltration process", Acta Metallurgica et Materialia, 1995, pp. 3499-3509

[17] S. Nourbakhsh, F. L. Liang and H. Margolin , "An apparatus for pressure casting of fiber-reinforced high-temperature metal-matrix composites", Journal of Physics, 1998, vol. 21, pp. 898-902

[18] T. W. Clyne and J. F. Mason, "The Squeeze Infiltration Process for Fabrication of Metal Matrix Composites", Metallurgical Transactions, 1987, vol.18 A, pp. 1519-1530

[19] P. A. Karnezis, G. Durrant, B. Cantor, "Microstructure and tensile properties of squeeze cast SiC particulate reinforced Al-7Si alloy", Materials Science and Technology, 1998, vol. 14, pp. 97-107

[20] S. Skolianos, Griourtsidis, Thomas, Xatzifotiou, "Effect of applied pressure on the microstructure and mechanical properties of squeeze cast aluminum AA6061 alloy", Materials Science and Engineering, 1997, vol. 231 A, pp. 17-24

[21] K. Naplocha, A. Janus, J. W. Kaczmar, Z. Samsonowicz, "Technology and mechanical properties of ceramic preforms for composite materials", Journal of Materials Processing Technology, 2000, vol. 106, pp. 119-122

94

[22] H. X. Peng, Z. Fan, D. S. Mudher, J. R. G. Evans, "Microstructures and mechanical properties of engineered short fiber reinforced aluminium matrix composites", Materials Science and Engineering A, 2002

[23] T. Choh, T. Oki, "Wettability of silicon carbide by aluminum and aluminum alloy", Materials Science and Technology, 1987, vol. 3, p. 378

[24] R. Warren and C. H. Andersson, "Silicon carbide fibers and their potential for use in composite materials: Part II", Composites, 1984, Vol. 15, pp. 101-111

[25] K. B Lee, Y. S. Kim, and H. K. Won, "Fabrication of Al- 3 wt% Mg matrix composites reinforced with Al2O3 and SiC particulates by the pressureless infiltration technique", Metallurgical and Materials Transactions A, 1998, Vol. 29, pp. 3087-3095

[26] M. Fishkis, "Interface and fracture surface in Saffil/Al-Cu-Mg metal matrix composites", Journal of Materials Science, 1991, pp. 2651-2661

[27] B. Hallstadt, Z. K. Liu and J. Argen, "Fiber matrix interactions during fabrication of Al2O3 - Mg metal matrix composites", Materials Science and Engineering A, 1990, pp. 135-145

[28] J. C. Lee, J. H. Shim, H. K. Seok, H. I. Lee, "Interfacial reaction and its influence on the mechanical properties of the ASZ short fiber-reinforced Al alloy composite", Journal of Microscopy, 2001, Vol. 201, pp. 291-298

[29] C. Fritze, "Infiltration keramischer Faserformkörper mit Hilfe des Verfahrens des selbstgenerierenden Vakuums ", Ph.D. Thesis, Technische Universität Clausthal, 1997

[30] A. Mortensen, I. Jin, "Solidification processing of metal matrix composites", International Materials Reviews, 1992, Vol. 37, No. 3, pp. 101-128

[31] A. Mortensen, L. J. Masur, J. A. Cornie and M. C. Flemings, "Infiltration of Fibrous Preforms by a Pure Metal: Part I. Theory", Metallurgical Transactions A, 1989, pp. 2535-2547

[32] A. Mortensen and J. A. Cornie, "On the Infiltration of Metal Matrix Composites", Metallurgical Transactions A, 1987, pp. 1160-1163

[33] A. Mortensen and T. Wong, "Infiltration of Fibrous Preforms by a Pure Metal: Part III. Capillary Phenomena", Metallurgical Transactions A, 1990, pp. 2257-2263

[34] A. Matterna, B. Huchler, D. Staudenecker, R. Oberackera, A. Nagel, M.J. Hoffmann, "Preparation of interpenetrating ceramic–metal composites", Journal of the European Ceramic Society, 2004, vol. 24, pp. 3399-3408

[35] J. Bear, Dynamics of Fluids in Porous Media, Elsevier, New York, 1972

[36] Hu Lianxi, Yang Yiwen, Luo Shoujing, Xu Xinying, "Investigation on the kinetics of infiltration of liquid aluminum into an alumina fibrous perform", Journal of Materials Processing Technology, 1999

[37] D. L. McDanels, "Tungsten fiber reinforced copper matrix composites", Metallurgical Transactions, 1965, vol. 223, pp. 636-642

[38] C.M. Friend, "The effect of matrix properties on reinforcement in short alumina fiber – aluminum metal matrix composites", Journal of Materials Science, 1987, Vol 22, pp. 3005–3010

[39] Shahram Amini, S. Javadpour, M. S. Jamshidi, Shahin Amini, "Manufacturing and Property Evaluation of A356/SAFFIL and Hybrid A356/(SiCP+SAFFIL) Composites via Squeeze Casting Process", Proceeding of the Conference of Metallurgists, 2003, Vancouver, Canada

[40] P.K. Rohatgi, R. Asthana, S. Das, "Solidification, structures, and properties of cast metal – ceramic particle composites", International Metallurgical Reviews, 1986, Vol. 31, pp. 115-139

[41] G. E. Totten and D. S. Machkenzie, eds, "Handbook of Aluminum: Physical Metallurgy and Processes", 2003, Taylor and Fracais Group, Florida

[42] H. Akbulut, M. Durman, "Temperature dependent strength analysis of short fiber reinforced Al – Si metal matrix composites", Materials Science and Engineering A, 1999, vol. 262, pp. 214-226

[43] R. Tavangar, L. Weber, A. Mortensen, "Damage evolution in Saffil alumina short – fiber reinforced aluminum during tensile testing", Materials Science and Engineering A, 2005, vol. 395, pp. 27-34

APPENDIX A

DETAILED TABULATION OF MOULD TEMPERATURES

Table A.1 Detailed tabulation of mould temperatures for AlSi10Mg0.3 alloy casting.

Casting No	Upper Mould Temperature (°C)	Lower Mould Temperature (°C)
1 (10 vol% Al_2O_3)	177	199
2 (15 vol% Al_2O_3)	182	205
3 (20 vol% Al_2O_3)	185	198
4 (25 vol% Al_2O_3)	180	199
5 (30 vol% Al_2O_3)	178	201
6 (10 vol% Al_2O_3)	188	195
7 (15 vol% Al_2O_3)	186	197
8 (20 vol% Al_2O_3)	176	190
9 (25 vol% Al_2O_3)	184	196
10 (30 vol% Al_2O_3)	187	193

Table A.2 Detailed tabulation of mould temperatures for AlSi10Mg1 alloy casting.

Casting No	Upper Mould Temperature (°C)	Lower Mould Temperature (°C)
1 (10 vol% Al_2O_3)	195	210
2 (15 vol% Al_2O_3)	176	195
3 (20 vol% Al_2O_3)	187	192
4 (25 vol% Al_2O_3)	186	199
5 (30 vol% Al_2O_3)	179	185
6 (10 vol% Al_2O_3)	185	196
7 (15 vol% Al_2O_3)	188	204
8 (20 vol% Al_2O_3)	176	193
9 (25 vol% Al_2O_3)	192	205
10 (30 vol% Al_2O_3)	178	192

APPENDIX B

DETAILED TABULATION OF DENSITY MEASUREMENT

Table B.1 Variation in densities and porosity values with fiber vol% AlSi10Mg0.3 alloy cast at 750 °C.

Fiber Volume %	0	10	15	20	25	30
M Specimen Air (g)	1.1923	0.7623	1.8299	1.4694	1.1861	1.6731
M Specimen Xylol / Xylol (g)	0.8070	0.5207	1.2507	1.0171	0.8268	1.1696
M Specimen Air / Xylol (g)	1.1950	0.7670	1.8347	1.4753	1.1893	1.6816
ρ theoretical (g/cm^3)	2.6679	2.7991	2.8647	2.9303	2.9959	3.0615
V experimental (cm^3)	0.4506	0.2861	0.6783	0.5322	0.4210	0.5947
ρ experimental (g/cm^3)	2.6458	2.6648	2.6978	2.7611	2.8172	2.8136
P% (Total)	0.8287	4.7983	5.8249	5.7735	5.9659	8.0998
P% (Open)	0.0070	0.0191	0.0082	0.0129	0.0088	0.0166
P% (Closed)	0.8218	4.7792	5.8166	5.7606	5.9570	8.0832

Table B.2 Variation in densities and porosity values with fiber vol% AlSi10Mg0.3 alloy cast at 800 °C.

Fiber Volume %	0	10	15	20	25	30
M Specimen Air (g)	0.6725	1.1000	1.5653	1.4870	1.4496	1.4924
M Specimen Xylol / Xylol (g)	0.4549	0.7549	1.0777	1.0292	1.0103	1.0420
M Specimen Air / Xylol (g)	0.6740	1.1069	1.5695	1.4930	1.4535	1.5000
ρ theoretical (g/cm^3)	2.6679	2.7991	2.8647	2.9303	2.9959	3.0615
V experimental (cm^3)	0.2544	0.4088	0.5712	0.5387	0.5147	0.5319
ρ experimental (g/cm^3)	2.6428	2.6907	2.7404	2.7605	2.8161	2.8057
P% (Total)	0.9410	3.8731	4.3395	5.7949	6.0010	8.3573
P% (Open)	0.0070	0.0196	0.0085	0.0129	0.0088	0.0166
P% (Closed)	0.9340	3.8535	4.3309	5.7820	5.9921	8.3407

Table B.3 Variation in densities and porosity values with fiber vol% AlSi10Mg1 alloy cast at 750 °C.

Fiber Volume %	0	10	15	20	25	30
M Specimen Air (g)	1.9529	1.4992	1.4617	1.4642	1.5646	1.9631
M Specimen Xylol / Xylol (g)	1.3188	1.0242	1.0060	1.0107	1.0874	1.3722
M Specimen Air / Xylol (g)	1.9557	1.5028	1.4660	1.4707	1.5700	1.9740
ρ theoretical (g/cm^3)	2.6603	2.7923	2.8583	2.9242	2.9902	3.0562
V experimental (cm^3)	0.7397	0.5559	0.5343	0.5343	0.5605	0.6990
ρ experimental (g/cm^3)	2.6400	2.6971	2.7359	2.7406	2.7914	2.8086
P% (Total)	0.7601	3.4099	4.2800	6.2799	6.6498	8.1011
P% (Open)	0.0044	0.0075	0.0093	0.0141	0.0112	0.0181
P% (Closed)	0.7557	3.4024	4.2707	6.2658	6.6386	8.0830

Table B.4 Variation in densities and porosity values with fiber vol% AlSi10Mg1 alloy cast at 800 °C.

Fiber Volume %	0	10	15	20	25	30
M Specimen Air (g)	1.4862	1.3238	1.8037	1.3207	1.1515	0.8539
M Specimen Xylol / Xylol (g)	1.0031	0.9037	1.2369	0.9112	0.7988	0.5972
M Specimen Air / Xylol (g)	1.4883	1.3270	1.8090	1.3266	1.1555	0.8587
ρ theoretical (g/cm^3)	2.6603	2.7923	2.8583	2.9242	2.9902	3.0562
V experimental (cm^3)	0.5635	0.4916	0.6645	0.4824	0.4143	0.3037
ρ experimental (g/cm^3)	2.6373	2.6928	2.7144	2.7376	2.7794	2.8118
P% (Total)	0.8638	3.5625	5.0335	6.3818	7.0492	7.9982
P% (Open)	0.0044	0.0075	0.0093	0.0141	0.0111	0.0181
P% (Closed)	0.8594	3.5550	5.0243	6.3676	7.0381	7.9800

APPENDIX C

DETAILED TABULATION OF HARDNESS MEASUREMENT

Table C.1 Hardness test results of AlSi10Mg0.3 composite cast at 750 °C vertical to the fiber orientation measured by Brinell test (62.5 kg and 2.5 mm sphere indenter).

Measurement No:	1	2	3	4	5	Average	Std. Dev.
Al – 0% $Al_2O_3{}_{(f)}$	96	99	99	96	99	97.8	2
Al – 10% $Al_2O_3{}_{(f)}$	107	110	107	112	107	108.6	2
Al – 15% $Al_2O_3{}_{(f)}$	112	115	112	107	112	111.6	3
Al – 20% $Al_2O_3{}_{(f)}$	121	121	121	115	121	119.8	3
Al – 25% $Al_2O_3{}_{(f)}$	138	138	133	138	138	137.0	2
Al – 30% $Al_2O_3{}_{(f)}$	142	142	142	151	151	145.6	5

Table C.2 Hardness test results of AlSi10Mg0.3 composite cast at 750 °C parallel to the fiber orientation measured by Brinell test (62.5 kg and 2.5 mm sphere indenter).

Measurement No:	1	2	3	4	5	Average	Std. Dev.
Al – 0% $Al_2O_3{}_{(f)}$	96	99	99	96	99	97.8	2
Al – 10% $Al_2O_3{}_{(f)}$	112	110	112	110	112	111.2	1
Al – 15% $Al_2O_3{}_{(f)}$	128	128	121	121	125	124.6	4
Al – 20% $Al_2O_3{}_{(f)}$	128	128	125	131	124	127.2	3
Al – 25% $Al_2O_3{}_{(f)}$	142	142	151	151	151	147.4	5
Al – 30% $Al_2O_3{}_{(f)}$	169	174	174	174	174	173.0	2

Table C.3 Hardness test results of AlSi10Mg0.3 composite cast at 800 °C vertical to the fiber orientation measured by Brinell test (62.5 kg and 2.5 mm sphere indenter).

Measurement No:	1	2	3	4	5	Average	Std. Dev.
Al – 0% $Al_2O_{3\,(f)}$	90	96	96	96	93	94.2	3
Al – 10% $Al_2O_{3\,(f)}$	99	99	107	104	104	102.6	4
Al – 15% $Al_2O_{3\,(f)}$	104	104	110	110	110	107.6	3
Al – 20% $Al_2O_{3\,(f)}$	115	121	112	112	124	116.8	5
Al – 25% $Al_2O_{3\,(f)}$	138	135	135	135	138	136.2	2
Al – 30% $Al_2O_{3\,(f)}$	146	141	141	141	146	143.0	3

Table C.4 Hardness test results of AlSi10Mg0.3 composite cast at 800 °C parallel to the fiber orientation measured by Brinell test (62.5 kg and 2.5 mm sphere indenter).

Measurement No:	1	2	3	4	5	Average	Std. Dev.
Al – 0% $Al_2O_{3\,(f)}$	90	96	96	96	93	94.2	3
Al – 10% $Al_2O_{3\,(f)}$	110	104	99	104	107	104.8	4
Al – 15% $Al_2O_{3\,(f)}$	110	121	115	115	125	117.2	6
Al – 20% $Al_2O_{3\,(f)}$	121	128	131	125	125	126.0	4
Al – 25% $Al_2O_{3\,(f)}$	146	146	151	146	146	147.0	2
Al – 30% $Al_2O_{3\,(f)}$	159	159	159	159	159	159.0	0

Table C.5 Hardness test results of AlSi10Mg1 composite cast at 750 °C vertical to the fiber orientation measured by Brinell test (62.5 kg and 2.5 mm sphere indenter).

Measurement No:	1	2	3	4	5	Average	Std. Dev.
Al – 0% $Al_2O_{3\,(f)}$	107	102	107	112	112	108.0	4
Al – 10% $Al_2O_{3\,(f)}$	110	107	110	110	112	109.8	2
Al – 15% $Al_2O_{3\,(f)}$	115	124	116	115	116	117.2	4
Al – 20% $Al_2O_{3\,(f)}$	121	123	123	123	123	122.6	1
Al – 25% $Al_2O_{3\,(f)}$	146	146	146	146	146	146.0	0
Al – 30% $Al_2O_{3\,(f)}$	146	155	155	155	159	154.0	5

Table C.6 Hardness test results of AlSi10Mg1 composite cast at 750 °C parallel to the fiber orientation measured by Brinell test (62.5 kg and 2.5 mm sphere indenter).

Measurement No:	1	2	3	4	5	Average	Std. Dev.
Al – 0% $Al_2O_{3\,(f)}$	107	102	107	112	112	108.0	4
Al – 10% $Al_2O_{3\,(f)}$	118	115	118	110	112	114.6	4
Al – 15% $Al_2O_{3\,(f)}$	128	128	131	133	131	130.2	2
Al – 20% $Al_2O_{3\,(f)}$	138	142	128	138	138	136.8	5
Al – 25% $Al_2O_{3\,(f)}$	164	164	155	159	159	160.2	4
Al – 30% $Al_2O_{3\,(f)}$	179	185	179	179	179	180.2	3

Table C.7 Hardness test results of AlSi10Mg1 composite cast at 800 °C vertical to the fiber orientation measured by Brinell test (62.5 kg and 2.5 mm sphere indenter).

Measurement No:	1	2	3	4	5	Average	Std. Dev.
Al – 0% $Al_2O_{3\,(f)}$	97	107	104	106	104	103.6	4
Al – 10% $Al_2O_{3\,(f)}$	107	110	112	112	110	110.2	2
Al – 15% $Al_2O_{3\,(f)}$	112	115	121	121	115	116.8	4
Al – 20% $Al_2O_{3\,(f)}$	121	124	112	118	124	119.8	5
Al – 25% $Al_2O_{3\,(f)}$	138	142	138	146	146	142.0	4
Al – 30% $Al_2O_{3\,(f)}$	159	155	150	155	159	155.6	4

Table C.8 Hardness test results of AlSi10Mg1 composite cast at 800 °C parallel to the fiber orientation measured by Brinell test (62.5 kg and 2.5 mm sphere indenter).

Measurement No:	1	2	3	4	5	Average	Std. Dev.
Al – 0% $Al_2O_{3\,(f)}$	97	107	104	106	104	103.6	4
Al – 10% $Al_2O_{3\,(f)}$	115	110	115	110	112	112.4	3
Al – 15% $Al_2O_{3\,(f)}$	124	128	128	128	128	127.2	2
Al – 20% $Al_2O_{3\,(f)}$	128	133	124	135	138	131.6	6
Al – 25% $Al_2O_{3\,(f)}$	164	159	159	155	159	159.2	3
Al – 30% $Al_2O_{3\,(f)}$	174	174	169	179	159	171.0	8

APPENDIX D

DETAILED TABULATION OF THREE POINT BENDING TEST RESULTS

Table D.1 Variation in flexural strength values with fiber vol%s AlSi10Mg0.3 alloy cast at 750 °C a) 10 vol% b) 15 vol% c) 20 vol% d) 25 vol% e) 30 vol%.

Specimen No:	b (mm)	d (mm)	L (mm)	F (N)	Flexural Strength (MPa)
1	9.38	6.14	43.00	2239.00	408.39
2	10.36	6.30	43.00	2264.00	355.14
3	11.04	6.40	43.00	2443.50	348.53
Standard Deviation	33			Average	370.69

(a)

Specimen No:	b (mm)	d (mm)	L (mm)	F (N)	Flexural Strength (MPa)
1	11.39	7.23	43.00	2729.00	295.64
2	11.20	4.74	43.00	1929.00	494.44
3	10.42	6.19	43.00	3207.00	517.87
4	11.85	7.36	43.00	2979.00	299.28
Standard Deviation	122			Average	401.81

(b)

Table D.1 (Cont'd)

Specimen No:	b (mm)	d (mm)	L (mm)	F (N)	Flexural Strength (MPa)
1	11.35	6.19	43.00	3491.50	517.84
2	11.26	6.55	43.00	3419.00	456.50
3	11.58	6.57	43.00	3902.00	503.51
Standard Deviation	32			Average	492.62

(c)

Specimen No:	b (mm)	d (mm)	L (mm)	F (N)	Flexural Strength (MPa)
1	10.73	6.97	43.00	3504.00	433.57
2	10.25	6.29	43.00	3491.50	555.32
3	10.98	6.47	43.00	3902.00	547.57
Standard Deviation	68			Average	512.15

(d)

Specimen No:	b (mm)	d (mm)	L (mm)	F (N)	Flexural Strength (MPa)
1	10.76	6.54	43.00	4014.00	562.56
2	10.68	6.55	43.00	3468.00	488.19
3	10.89	6.00	43.00	3603.00	592.78
Standard Deviation	54			Average	547.84

(e)

Table D.2 Variation in flexural strength values with fiber vol%s AlSi10Mg0.3 alloy cast at 800 °C a) 10 vol% b) 15 vol% c) 20 vol% d) 25 vol% e) 30 vol%.

Specimen No:	b (mm)	d (mm)	L (mm)	F (N)	Flexural Strength (MPa)
1	10.78	6.21	40.00	2504.80	361.51
2	10.96	6.40	40.00	2879.00	384.79
3	10.80	6.09	40.00	2854.60	427.60
Standard Deviation	34			Average	391.30

(a)

Specimen No:	b (mm)	d (mm)	L (mm)	F (N)	Flexural Strength (MPa)
1	10.88	6.22	40.00	3219.50	458.91
2	11.15	5.96	40.00	2746.35	416.04
3	11.61	5.65	40.00	2747.50	444.79
Standard Deviation	22			Average	439.92

(b)

Specimen No:	b (mm)	d (mm)	L (mm)	F (N)	Flexural Strength (MPa)
1	10.44	5.58	40.00	2970.50	548.29
2	11.32	6.05	40.00	2964.85	429.34
3	6.23	8.75	40.00	3652.30	459.42
Standard Deviation	62			Average	479.02

(c)

Specimen No:	b (mm)	d (mm)	L (mm)	F (N)	Flexural Strength (MPa)
1	10.85	6.39	40.00	3453.80	467.75
2	11.26	6.35	40.00	3767.00	497.81
3	11.04	6.47	40.00	4222.50	548.21
Standard Deviation	41			Average	504.59

(d)

Table D.2 (Cont'd)

Specimen No:	b (mm)	d (mm)	L (mm)	F (N)	Flexural Strength (MPa)
1	11.29	6.25	40.00	4056.00	551.82
2	8.11	6.16	40.00	2512.05	489.78
3	10.06	6.38	40.00	4059.50	594.82
Standard Deviation	53			Average	545.47

(e)

Table D.3 Variation in flexural strength values with fiber vol%s AlSi10Mg1 alloy cast at 750 °C a) 10 vol% b) 15 vol% c) 20 vol% d) 25 vol% e) 30 vol%.

Specimen No:	b (mm)	d (mm)	L (mm)	F (N)	Flexural Strength (MPa)
1	11.32	6.73	40.00	3146.85	368.26
2	11.54	6.66	40.00	3075.35	360.49
3	11.52	6.11	40.00	3225.35	449.98
Standard Deviation	50			Average	392.91

(a)

Specimen No:	b (mm)	d (mm)	L (mm)	F (N)	Flexural Strength (MPa)
1	11.61	7.01	40.00	4285.00	450.64
2	11.27	7.12	40.00	3480.20	365.49
3	10.99	6.82	40.00	4174.50	489.99
Standard Deviation	64			Average	435.37

(b)

Specimen No:	b (mm)	d (mm)	L (mm)	F (N)	Flexural Strength (MPa)
1	12.00	6.85	40.00	3995.00	425.70
2	11.47	6.42	40.00	4182.50	530.83
3	10.99	6.62	40.00	4010.20	499.58
Standard Deviation	54			Average	485.37

(c)

Table D.3 (Cont'd)

Specimen No:	b (mm)	d (mm)	L (mm)	F (N)	Flexural Strength (MPa)
1	11.68	7.21	40.00	4604.20	454.98
2	11.57	6.22	40.00	4245.00	569.00
3	11.23	6.28	40.00	3533.00	478.63
Standard Deviation	60			Average	500.87

(d)

Specimen No:	b (mm)	d (mm)	L (mm)	F (N)	Flexural Strength (MPa)
1	11.38	7.18	40.00	4713.00	482.01
2	11.74	7.00	40.00	5586.00	582.62
3	11.42	6.98	40.00	4620.50	498.27
Standard Deviation	54			Average	520.97

(e)

Table D.4 Variation in flexural strength values with fiber vol%s AlSi10Mg1 alloy cast at 800 °C a) 10 vol% b) 15 vol% c) 20 vol% d) 25 vol% e) 30 vol%.

Specimen No:	b (mm)	d (mm)	L (mm)	F (N)	Flexural Strength (MPa)
1	11.16	5.96	40.00	2428.50	367.56
2	11.41	7.47	40.00	4411.50	415.73
3	6.03	7.77	40.00	1954.50	322.13
Standard Deviation	47			Average	368.47

(a)

Specimen No:	b (mm)	d (mm)	L (mm)	F (N)	Flexural Strength (MPa)
1	11.52	8.06	40.00	5289.90	424.11
2	9.26	6.66	40.00	2890.50	422.25
3	10.35	6.81	40.00	3451.50	431.44
Standard Deviation	5			Average	425.93

(b)

Table D.4 (Cont'd)

Specimen No:	b (mm)	d (mm)	L (mm)	F (N)	Flexural Strength (MPa)
1	11.01	6.87	40.00	3825.50	441.71
2	11.41	6.99	40.00	3910.90	420.91
3	11.19	6.88	40.00	4408.50	499.38
Standard Deviation	41			Average	454.00

(c)

Specimen No:	b (mm)	d (mm)	L (mm)	F (N)	Flexural Strength (MPa)
1	11.01	6.87	40.00	3825.50	441.71
2	11.41	6.99	40.00	3910.90	420.91
3	11.19	6.88	40.00	4408.50	499.38
Standard Deviation	41			Average	454.00

(d)

Specimen No:	b (mm)	d (mm)	L (mm)	F (N)	Flexural Strength (MPa)
1	11.34	6.63	40.00	4276.80	514.79
2	11.30	6.49	40.00	3955.95	498.69
3	11.06	6.98	40.00	4764.00	530.47
Standard Deviation	16			Average	514.65

(e)

Table D.5 Variation in flexural strength values with magnesium content and temperature a) AlSi10Mg0.3 alloy cast at 750 °C b) AlSi10Mg0.3 alloy cast at 800 °C c) AlSi10Mg1 alloy cast at 750 °C d) AlSi10Mg1 alloy cast at 800 °C.

Specimen No:	b (mm)	d (mm)	L (mm)	F (N)	Flexural Strength (MPa)
1	9.67	5.00	40.00	1783.00	442.52
2	9.78	5.01	40.00	2135.00	521.84
3	9.74	4.90	40.00	1974.00	506.46
4	9.74	5.02	40.00	2139.00	522.87
5	9.78	5.05	40.00	2050.00	493.16
6	9.90	5.20	40.00	2111.00	473.15
7	9.89	5.22	40.00	2269.00	505.18
Standard Deviation	28.77		Average		495.03

(a)

Specimen No:	b (mm)	d (mm)	L (mm)	F (N)	Flexural Strength (MPa)
1	9.91	5.45	40.00	2179.00	444.16
2	9.90	5.20	40.00	2265.50	507.78
3	9.94	5.22	40.00	2120.00	469.63
4	9.92	5.16	40.00	1983.50	450.58
5	9.89	5.12	40.00	2168.00	501.73
6	9.87	5.17	40.00	2165.50	492.51
7	9.90	5.11	40.00	2001.00	464.43
Standard Deviation	25.09		Average		475.83

(b)

Specimen No:	b (mm)	d (mm)	L (mm)	F (N)	Flexural Strength (MPa)
1	9.92	5.15	40.00	2135.50	487.00
2	9.90	5.12	40.00	1792.90	414.51
3	9.93	5.21	40.00	2291.00	509.98
4	9.90	5.15	40.00	2177.00	497.46
Standard Deviation	42.8613		Average		477.24

(c)

Table D.5 (Cont'd)

Specimen No:	b (mm)	d (mm)	L (mm)	F (N)	Flexural Strength (MPa)
1	9.93	5.29	40.00	2056.50	444.04
2	10.00	5.17	40.00	1997.50	448.39
3	9.92	5.19	40.00	2166.50	486.48
4	9.92	5.20	40.00	2229.00	498.59
5	9.92	5.21	40.00	1714.50	382.03
Standard Deviation		45.6372		**Average**	451.91

(d)

Table D.6 Variation in tensile strength values with magnesium content and temperature.

Specimen No:	Alloy – Casting Temperature			
	AlSi10Mg0.3 750 ˚C	AlSi10Mg0.3 800 ˚C	AlSi10Mg1 750 ˚C	AlSi10Mg1 800 ˚C
1	239	203	194	223
2	280	250	238	245
3	275	248	280	188
4	280	302	231	205
Average Tensile Strength (Mpa)	268.5	250.75	235.75	215.25
Standard Deviation	20	40	35	24

APPENDIX E

X-RAY DIFFRACTION CARDS OF PRESENT PHASES

Table E.1 X-Ray details of aluminum.

Al
Aluminum
Ref: Calculated from ICSD using POWD-12++
Ref: Figgins, B.F., Jones, G.O., Riley, D.P., Philos. Mag., 1, 747 (1956)

2θ	Int-v	h	k	l	2θ	Int-v	h	k	l	2θ	Int-v	h	k	l
38.471	100 *	1	1	1	65.095	38	2	2	0	82.433	12	2	2	2
44.719	53	2	0	0	78.226	44	3	1	1					
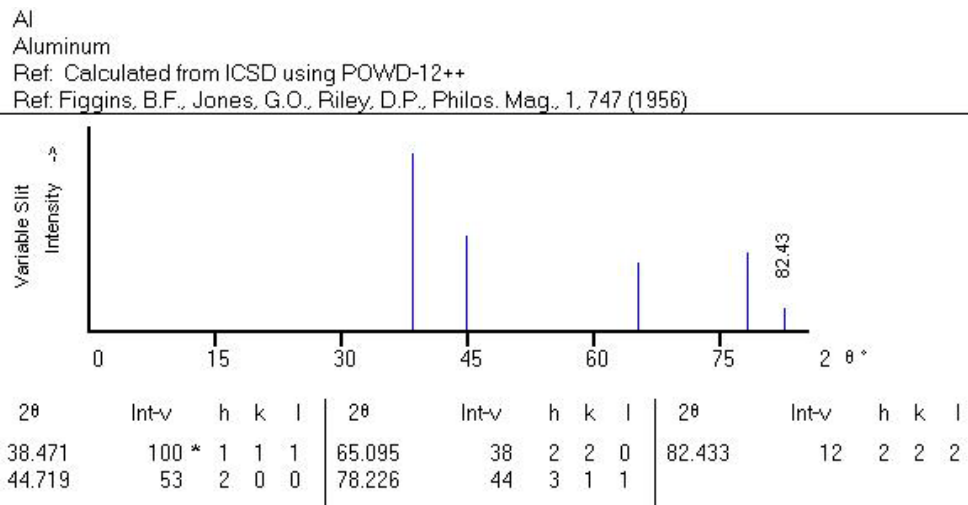
Table E.2 X-Ray details of silicon.

Si
Silicon
Ref: Natl. Bur. Stand. (U.S.) Monogr. 25, 13, 35 (1976)

2θ	Int-v	h	k	l	2θ	Int-v	h	k	l	2θ	Int-v	h	k	l
28.442	100	1	1	1	76.377	28	3	3	1	114.08	24	5	3	1
47.302	90	2	2	0	88.026	34	4	2	2	127.54	29	6	2	0
56.121	57	3	1	1	94.948	18	5	1	1	136.89	11	5	3	3
69.130	14	4	0	0	106.71	10	4	4	0					
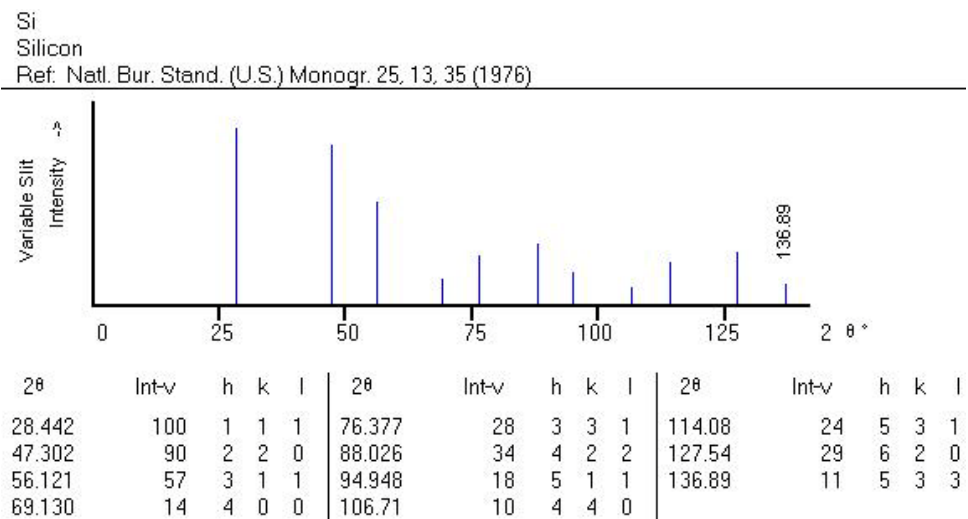
Table E.3 X-Ray details of δ-Al$_2$O$_3$.

δ-Al2 O3
Aluminum Oxide
Ref: Repelin, Y., Husson, E., Mater. Res. Bull., 25, 611 (1990)
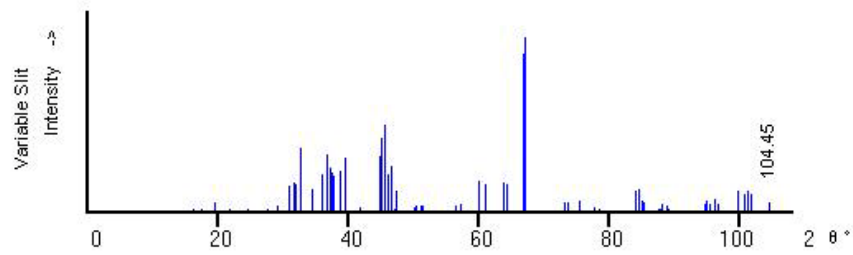
2θ	Int-v	h	k	l	2θ	Int-v	h	k	l	2θ	Int-v	h	k	l
16.201	1	0	1	1	47.060	< 1 [	2	2	3]	84.611	12	2	3	14
17.501	1	0	1	2	47.483	12	2	0	9	85.005	6	0	4	12
19.501	5	0	1	3	50.142	2	0	3	3	85.404	5	1	3	16
21.801	< 0	0	1	4	50.493	3 b	2	0	10	87.609	1	0	5	2
24.641	< 0	0	1	5	51.105	3	0	3	4	87.807	1	0	4	13
27.601	1	0	1	6	51.563	3	1	3	0	87.807	1	0	5	3
29.262	3	1	1	5	51.563	3	2	2	6	88.166	4	2	4	10
31.022	14	0	1	7	56.462	3	1	2	11	88.166	4	2	3	15
31.802	16	0	2	0	57.163	3	2	0	12	88.813	3	0	5	4
32.102	15	0	2	1	60.106	17	2	3	2	89.213	1	1	5	0
32.802	36	0	2	2	61.026	15	1	3	8	94.650	4 b	0	5	8
34.602	12	1	1	7	61.026	15	2	2	10	94.650	4 b	0	4	15
36.003	21	1	2	1	63.886	16	2	2	11	95.067	5	1	5	7
36.763	32	1	2	2	64.406	15	0	2	14	95.599	4 b	3	3	14
37.302	25	0	2	5	66.783	56	0	4	0	95.599	4 b	2	5	0
37.643	22	1	2	3	66.983	90	0	4	1	96.112	7	2	5	2
37.883	20	1	0	9	66.983	90	2	2	12	96.808	4	3	4	9
38.863	22	1	2	4	67.245	100	0	4	2	99.855	11	2	4	14
39.502	31	0	2	6	73.209	4	0	4	7	99.855	11	2	5	6
41.782	2	0	2	7	73.747	4	2	2	14	100.81	10	1	4	16
44.982	31	1	2	7	75.449	6	1	4	7	101.24	11	1	5	10
45.162	42	0	1	11	75.449	6	2	3	11	101.76	10	0	5	11
45.642	49	2	2	0	77.810	2	3	3	7	104.45	4	3	4	12
46.064	21	2	2	1	78.526	< 1	2	3	12					
46.602	26	2	2	2	84.051	11	2	4	8					